



U i T

**THE ARCTIC
UNIVERSITY
OF NORWAY**

Faculty of Science and Technology

Department of Geoscience

The regional Cretaceous development of the southeastern part of the Norwegian Barents Sea- from seismic interpretation

Vegard Heiberg

GEO-3900 Master thesis in Geology

May 2018



Acknowledgments

Da var fem tøffe år på skolebenken plutselig over. Et siste stort arbeid er utført, før man kan påberope seg tittelen som utdannet geolog. Det har vært krevende prosess, men samtidig en veldig lærerik tid.

Masteroppgaven hadde nok ikke kommet i havn, hadde det ikke vært for gode veiledere. Tusen takk for all oppfølging og en særdeles spennende oppgave, hovedveileder Stig-Morten Knutsen og bi-veiledere Iver Martens og Rune Mattingsdal. Takk til Vidar og Torgeir i PGNiG for tips og triks!

Æ vil takke alle flotte klassekamerater for fem fantastiske og lærerike år. Uten dokker, hadde det ikke vært det samme. Spesielt vil æ takke den bunnsolide GEO-gjengen, dokker er rå. Den største takknemlighet går imidlertid til min flotte familie i Harstad. Takk til Mamma og Pappa for gode råd og støtte gjennom alle år. Takk til mine to søstre, Ida og Kaja for all hjelp og motivasjon. En spesiell takk går til flotte Johanne, takk for korrekturlesning, innspill og hjelp underveis.

Abstract

This study sheds new light on the regional Cretaceous development of the southeastern part of the Norwegian Barents Sea. The study area is in the former disputed area between Norway and Russia, which after the agreement on the new borders in 2010 was opened to petroleum activity in 2013. Consequently, the southeastern Barents Sea is still a frontier area with less scientific knowledge, compared to the adjacent onshore/offshore areas of Norway and Russia. Here, seismic interpretation have provided increased geological knowledge about the paleo-environment in Early Cretaceous by the use of new 2D data acquired by the Norwegian Petroleum Directorate (NPD) in 2011/2012. Five seismic sequences (S0-S4) have been defined, and geometry and trajectories for identified seismic clinoforms has been described in order to elucidate the depositional history of the study area. This study revealed a successive displacement of the shelf break southwestwards during Early Cretaceous. Furthermore, shelf-edge clinoforms prograded from the northeast towards the southwest, with the main source of sediments located in a hinterland towards the north/northeast. This source area has been related to the uplift of the northern Barents Shelf in Early Barremian-Early Aptian times caused by magmatic activity, also referred to as the High Arctic Large Igneous Province (HALIP). Cyclic variations in the stratigraphic successions suggested fluctuating sea levels during the Early Cretaceous. Post-depositional doming and faulting events, induced by halokinetic movements have altered the Lower Cretaceous successions in the southeastern Barents Sea.

Vegard Heiberg

The Arctic University of Norway (UiT)

Table of Contents

1	Introduction	1
1.1	Seismic reflection theory	2
1.1.1	Seismic resolution	3
1.1.2	Vertical resolution	5
1.1.3	Horizontal resolution	6
1.2	Sedimentary principles	9
1.2.1	Seismic sequence stratigraphy	9
1.2.2	Seismic sequence analysis	11
1.2.3	Seismic facies	12
1.2.4	Reflection configuration	13
1.2.5	Reflection amplitude	14
1.2.6	Reflection continuity	14
1.2.7	Frequency	14
1.2.8	Clinoforms	16
1.2.9	Trajectories	17
2	Geological background	20
2	Stratigraphic and structural development	21
2.1	Structural development	22
2.1.1	Precambrian	22
2.1.2	Paleozoic	23
2.1.3	Mesozoic	25
2.1.4	Cenozoic	26
2.2	Stratigraphic and depositional environment	27
2.2.1	Paleozoic	28
2.2.2	Mesozoic	28
2.2.3	Cenozoic	30
2.3	Cretaceous Stratigraphic units (Dalland et al., 1988)	31
2.3.1	The Nordvestbanken Group	32
2.3.2	Knurr Formation	32
2.3.3	Kolje Formation	32
2.3.4	Kolmule Formation	32
2.4	Structural elements	33

2.4.1	The Nordkapp Basin.....	34
2.4.2	Tiddlybanken Basin.....	34
2.4.3	Finnmark Platform	35
2.4.4	Bjarmeland Platform	35
2.4.5	Fedynsky High	36
2.4.6	Fault complexes.....	36
3	Database and Seismic data.....	37
3.1	Seismic reflection theory.....	41
3.1.1	Seismic resolution	41
3.1.2	Vertical resolution	42
3.1.3	Horizontal resolution.....	43
3.2	Estimation of clinoform geometry.....	45
4	Results	46
4.1	Seismic well-tie	46
4.2	Intra Cretaceous horizons	46
4.3	Seismic sequence description	53
4.3.1	Sequence 0 (S0).....	53
4.3.2	Sequence 1 (S1).....	57
4.3.3	Sequence 2 (S2).....	60
4.3.4	Sequence 3 (S3).....	63
4.3.5	Sequence 4 (S4).....	66
4.4	Clinoform geometry	69
5	Discussion.....	71
5.1	Timing of deposition	71
5.2	Sequences S0-S4	74
5.2.1	Sequence 0 and 1	74
5.2.2	Sequence 2.....	84
5.2.3	Sequence 3 and 4.....	89
5.3	Post-depositional processes	95
5.3.1	Salt.....	95
5.3.2	Signalhornet Dome.....	98
5.3.3	Faults	100
6	Conclusions	101
7	References	103

1 Introduction

For more than 40 years, Norway and Russia were in political dispute over a 175 000 km² large area in the southeastern Barents Sea. The dispute was related to maritime delimitation, in this context where the offshore border between Russia and Norway should be drawn. However, on 15th September 2010, the foreign ministers of the two Arctic nations signed an agreement on where the geographic offshore boarder between their countries should be. During the spring of 2011, the agreement was ratified by the two parliaments and took affect from the 7th of July 2011 (Hammersvik & Ersdal, 2015). The Norwegian Parliament opened the area to petroleum activity in 2013. Consequently, the southeastern Barents Sea remained an unexplored area with considerable lack of geological knowledge compared the adjacent Norwegian and Russian onshore/offshore areas. This study attempts to provide new and valuable geological information of the former “grey zone “by a regional seismic interpretation of this area.

The objective with this study is to map, describe and interpret the regional depositional system that dominated in the Barents Sea southeast during the Early Cretaceous epoch. This study presents five (S0-S4) seismic sequences bounded by high amplitude seismic horizons. The seismic sequences are described by following the reflection configuration suggested by Mitchum et al. (1977) & Veeken (2007). The study emphasizes seismic clinoforms, which are prominent in the study area. The location of the shelf break and sediment source has also been in focus.

In the next sections, background theory used in this study is presented. Beginning with seismic reflection theory, followed by sedimentary principles.

1.1 Seismic reflection theory

The basic concept in all seismic methods is the controlled generation of elastic waves generated by a seismic source in order to obtain an image of the subsurface (Kearey et al., 2002). The observed arrival time of the waves reflected from interfaces in the subsurface, is termed reflectors. Seismic waves are defined as pulses of strain energy, which has the ability to propagate in solids and fluids (Schuck & Lange, 2007). Seismic reflection surveying is the most widely used geophysical technique since the 1930s. The predominant applications of the seismic reflection method are hydrocarbon exploration and academically research in order obtain detailed images of the subsurface, and reveal stratigraphic and structural features (Kearey et al., 2002; Reynolds, 2011).

In order for a seismic wave to be reflected back to the surface, there has to be a crossing surface interface in the depth, in which there is a contrast in the acoustic impedance between the adjacent/overlying layers. The acoustic properties of a rock is defined by its acoustic impedance, represented by the letter, Z . The acoustic impedance (Z) is the product of density (ρ) and velocity (V):

$$Z = \rho * V$$

The amplitude of a given reflected wave at a boundary is described by the reflection coefficient. For normal and low angles ($< 20^\circ$) of incidence, the equation for the reflection coefficient is given by (Reynolds, 2011):

$$R = (Z_2 - Z_1) / (Z_2 + Z_1)$$

The reflection coefficient is denoted R , whilst the Z represents the acoustic impedance for two separate contrasting layers. Respectively, the Z_1 represents the acoustic impedance of the overlying layer across an interface, whereas Z_2 marks the underlying unit. Furthermore, the reflection coefficient describes the strength of a reflection generated at a specific boundary between two layers. As observed from the equation, the reflection coefficient can be positive or negative, depending upon whether “softer” rocks, overlie “harder” rocks, or the other way around (Kearey et al., 2002; Reynolds, 2011).

1.1.1 Seismic resolution

Seismic waves travel downwards through the subsurface and is reflected back to the receivers when the waves hit an interface, with sufficient acoustic impedance contrast. These acoustic contrasts need to be great enough in order to be detected. The potential for being detected relies mainly on the seismic acquisition method and the processing procedure of the seismic data (Kearey et al., 2002). The resolution, at which these acoustic impedance contrasts can be detected, has both vertical and horizontal aspects (Brown, 1999). Seismic resolution has been defined as the ability to distinguish between separate points or objects, such as sedimentary sequences in seismic sections (Kearey et al., 2002). In other words, a measure of how large a particular object needs to be in order to be detected in seismic sections.

Resolution is significantly influenced by the methods of data collection and processing, however, the resolving seismic image is determined by the relationship between wavelength, velocity and frequency (Brown, 1999; Kearey et al., 2002), and is given by the equation:

$$\lambda = \frac{v}{f}$$

The wavelength and the frequency are respectively denoted λ and f , and the velocity is represented by the letter v . As sound waves travel deeper into the subsurface, the frequency of the soundwaves will decrease, while the velocity and wavelengths increase. The latter is due to more compacted sediments deeper down, which enables the sound wave to travel faster through them. The high frequencies are reflected from relatively shallow reflectors, while the low frequency surveys enable deeper seismic imaging. This means that with increasing depth, the resolution of the seismic will be poorer. Figure 1-1 illustrates the relationship between the physical parameters (wavelength, frequency and velocity) and depth.

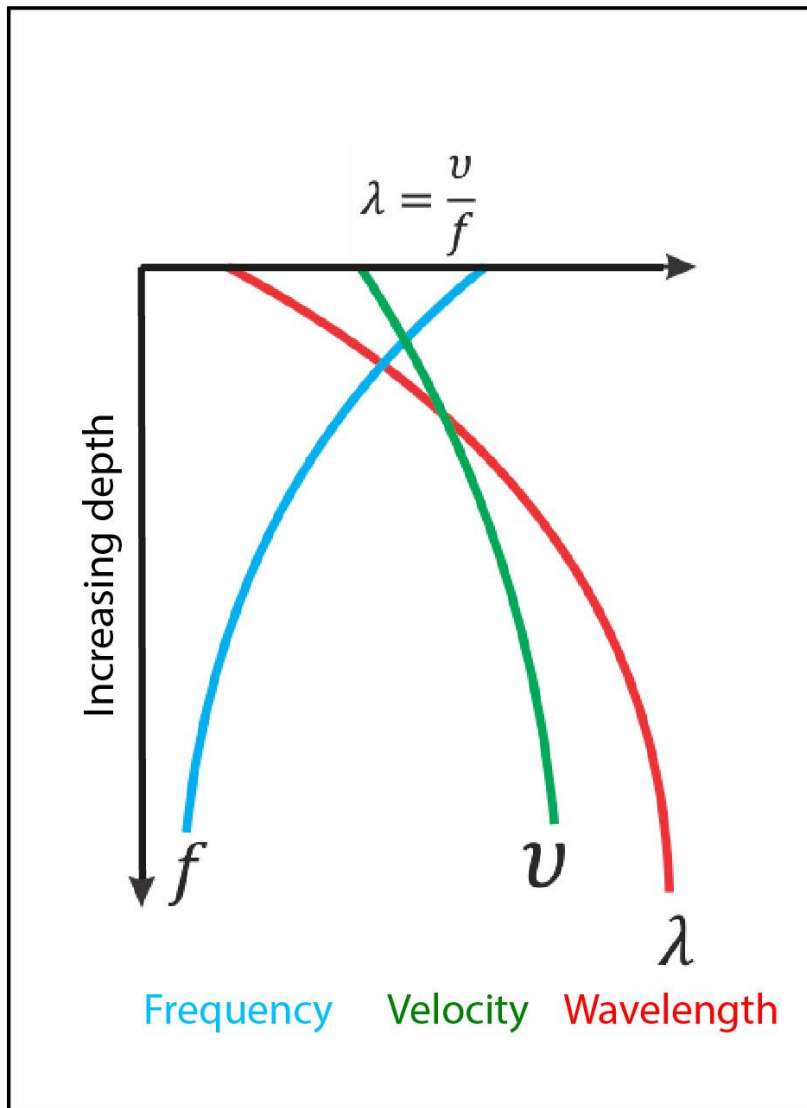


Figure 1-1. The relationship between frequency, velocity and wavelength as seismic waves travel downwards through the subsurface. Notice that the wavelength increases with depth, while the frequency decreases. This relationship contributes to the reduced seismic resolution of data. Figure modified from Brown (1999).

1.1.2 Vertical resolution

Vertical resolution normally refers to the $\frac{1}{4}$ of a wavelength. The vertical resolution is a measure of how individual, closely spaced reflectors can be separated in the seismic data (Kearey et al., 2002). It is determined by the pulse length on the recorded seismic section. As energy travels downwards, a decrease in frequency is common, which is due to the absorption of energy within sediments. Additionally, sediments normally show a trend of higher compaction with depth. The natural process of burial of sediments explains this. When moving into deeper layers, the sediments become gradually more buried, which increases the weight of the overlying sediments. The absorption of energy in combination with the increasing compaction, is the main reasons of decreasing vertical resolutions with depths (Kearey et al., 2002).

Brown (1999) demonstrates that vertical resolution has two limits, respectably the limit of visibility and the limit of separability. Common for both, is that they result from interaction of the wavelets from adjacent reflecting interfaces.

Theoretically, the limit of separability is defined as one-quarter of a wavelength, which corresponds to half a period in the time-domain. In practice it represents the bed thickness, which best corresponds to the closest separation of two wavelets of a given bandwidth. Reflected waves from an interface will be separated in time as long as the time thickness of a certain layer in the subsurface is equal to or larger than the half of the seismic wave's period. Based on this principle, identification of the top and bottom boundaries of layers can be observed in seismic data, as long as their thickness exceeds half of the wavelength to the seismic wave. In situations where layers have vertical extent which do not exceed half of a wavelength, the amplitude will progressively be attenuated by destructive interference until the limit of visibility is reached. This occur when the seismic signal becomes obscured by the unwanted noise. However, the limit of visibility is affected by several factors and depends on how the acoustic contrast of a specified geological layer is characterized relative to the embedding material. In addition to this, random and systematic noise may affect the limit of visibility and shape of the seismic wavelet (Brown, 1999). Vertical resolution is given in metres, by the following equation, where the wavelength is denoted λ :

$$Vr = \frac{\lambda}{4}$$

1.1.3 Horizontal resolution

The soundwave generated by a seismic source propagate as the distance from the shoot point increases. This means that the seismic soundwave travels spherically in three dimensions and spreads out as it reaches deeper down into the subsurface. The spherical spreading of energy is the main concept used when considering horizontal resolution in seismic data (Figure 1-2). Furthermore, the detector spacing of a seismic survey also affects the horizontal resolution (Kearey et al., 2002). Reflections is a result from the interaction of a reflection boundary in combination with a seismic wavefront (Brown, 1999). Due to the wave propagation, the seismic wavefront do not only affect a single point at the interface. Instead, it affects a considerable area of the reflector surface. The part covered by the seismic signal is produced from a circular zone, due to the spherical spreading of energy, and the extend of this zone is termed the Fresnel zone (Brown, 1999). This zone represents the area on the reflector, where the seismic wave is reflected at an interface, and returned to the receivers within a half-cycle after the onset of the reflection. The radius of the Fresnel zone determines the horizontal resolution of unmigrated (stacked) seismic sections (Brown, 1999; Kearey et al., 2002). The magnitude of the Fresnel zone (unmigrated) can be approximated from the equation:

$$rf = \frac{v}{2} \sqrt{\frac{t}{f}}$$

Where,

rf = the radius of the Fresnel zone (m)

v = average propagating speed of the incident wave (m/s)

t = two-way travel time in seconds (TWT)

f = frequency (Hz)

The equation above states that the radius of the Fresnel Zone increases with depth, velocity and lower frequencies (Figure 1-3). Therefore, the horizontal resolution decreases with increased depths, velocities and lower frequencies. Features in the subsurface with a lateral extend which exceed the Fresnel zone will be visible in seismic sections.

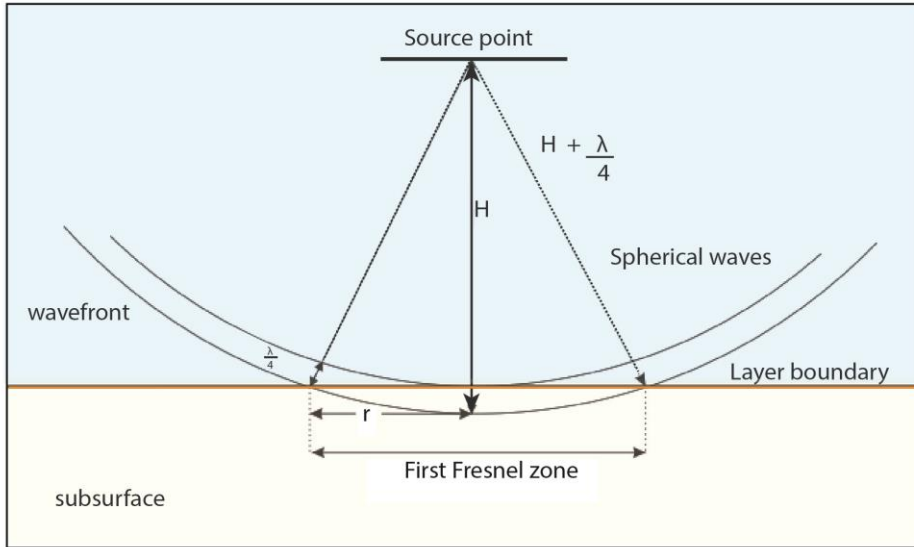


Figure 1-2. Illustration of the first Fresnel zone. Figure modified after Reynolds (2011).

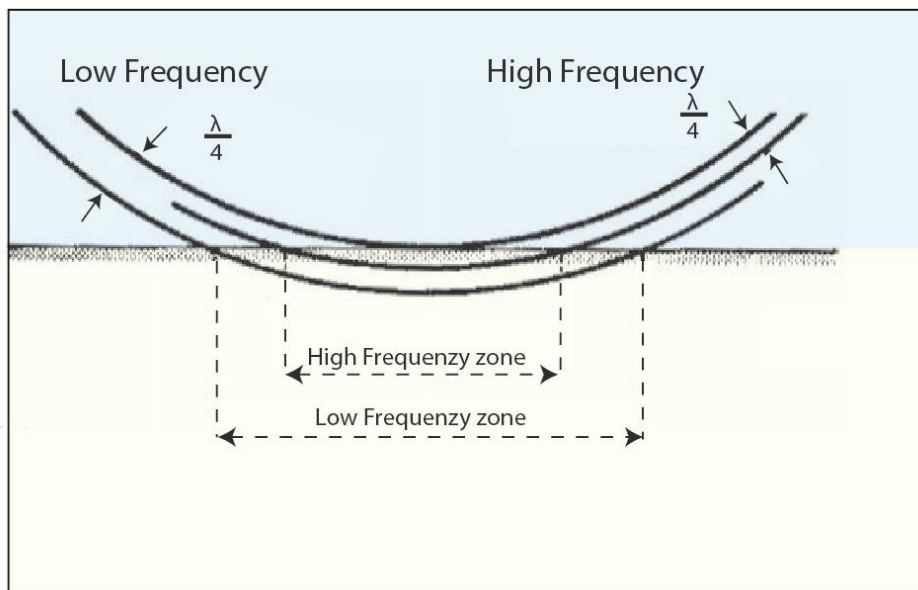


Figure 1-3. Illustration of the Fresnel zone for respectably high and low frequencies. Notice that the Fresnel zone is larger for low frequency components compared to the high frequency components. Figure modified after Sheriff (1985).

In order to improve the horizontal resolution, seismic migration is often applied during the processing of seismic data (Figure 1-4). The migration process includes three distinct functions. The first one is performed by reposition of reflections, which are out of phase because of

dipping interfaces. The second step involves focusing the energy spread over a Fresnel zone. The third process collapses diffraction patterns from point and edges in the subsurface (Brown, 1999). In two-dimensional data, the migration process only collapses the Fresnel zone in the inline direction. Because of this, two-dimensional data is often acquired with the orientation of strike and dip of major features in mind, which minimizes the effect of the third dimension. However, it can never be eliminated (Brown, 1999).

For calculating the radius of the post-migration 2D Fresnel zone, the following equation is applied:

$$rf = \frac{v}{4f}$$

Where,

rf = the radius of the Fresnel zone (m)

v = average propagating speed of the incident wave (m/s)

f = frequency (Hz)

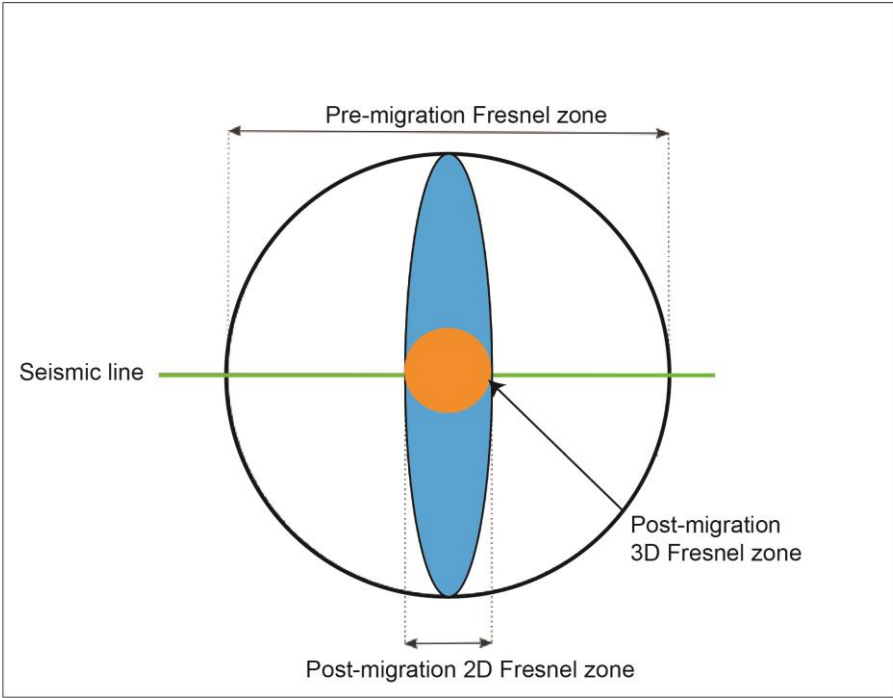


Figure 1-4. Illustration of the Fresnel zone before and after migration. The orange circle located in the middle, shows that the Fresnel zone could be reduced down to a small circle in three-dimensional data. The light blue ellipse represents how the Fresnel zone can be collapsed in two-dimensional data. Here, the reduction is restricted to the inline direction. Figure modified from Brown (1999).

1.2 Sedimentary principles

Sedimentary facies represent stratigraphic units with specified, individual, characteristics that reflect the dominating conditions under which it was formed. Describing the characteristics of sedimentary facies, include documentation of sedimentary structures, dimensions, grain size/shape, color and biogenic content of the sedimentary rock (Nichols, 2009). The term “lithofacies” is used if the description is confined to the physical and chemical aspects of transport and deposition of the sedimentary unit (Nichols, 2009). The facies concept does not only apply to the description of stratigraphical units, but also forms the basis for facies analysis, which is a scientific approach to the interpretation of sedimentary strata. Facies analysis can therefore be used to reconstruct paleo-environments (Nichols, 2009).

1.2.1 Seismic sequence stratigraphy

Sequence stratigraphy is considered to be one of the latest conceptual revolutions in the field of sedimentary geology (Catuneanu et al., 2008). Seismic stratigraphy was defined by Mitchum et al. (1977) in the study of stratigraphy and depositional facies as interpreted from seismic data. The application of this seismic technique is to group seismic reflections into packages that correspond to chronostratigraphically constrained genetic depositional intervals (Vail, 1987). These intervals are called depositional sequences and are further subdivided into system tracts, which comprise predictable stratal patterns and lithofacies, hence provide an opportunity to establish a chronostratigraphic correlation framework based on physical criteria (Vail, 1987). Depositional sequences are chronostratigraphically significant, because they represent a geological time interval of deposition bounded by the ages of the sequence boundaries (Mitchum et al., 1977). Stratal stacking pattern respond to the interplay of changes in rates of sedimentation and base level, hence reflects combinations of depositional events. This includes progradation, retrogradation, aggradation and downcutting (Catuneanu et al., 2008). Every stratal stacking pattern defines a particular generic type of deposit (i.e., transgressive, regressive or forced regressive). Each of them, with a characteristic geometry and facies preservation style, are generic deposits from an environmental perspective and can therefore be identified in different depositional settings (Catuneanu et al., 2008).

Vail (1987) argues that four major variables control the variations in stratal patterns and lithofacies. The first is tectonic subsidence, which creates the space where sediments may deposit. Sequence stratigraphy emphasizes the importance of the space within a basin for sediment to be deposited and the amount of sediment supplied. In order for sediments from either marine or non-marine sources to be deposited, there has to be available space to store it in: this is termed accommodation space (Figure 1-5) (Coe et al., 2003). The second variable is eustatic change of sea level, which highly influences the stratal patterns and the distribution of lithofacies. The third variable refers to the amount of sediments deposited in a basin, which affects paleowater depth. The fourth variable is climate, which holds a major control over the type of sediments that dominate in a specific area. For example, humid conditions and temperature are important climatic factors for the distribution of carbonates and evaporates (Vail, 1987).

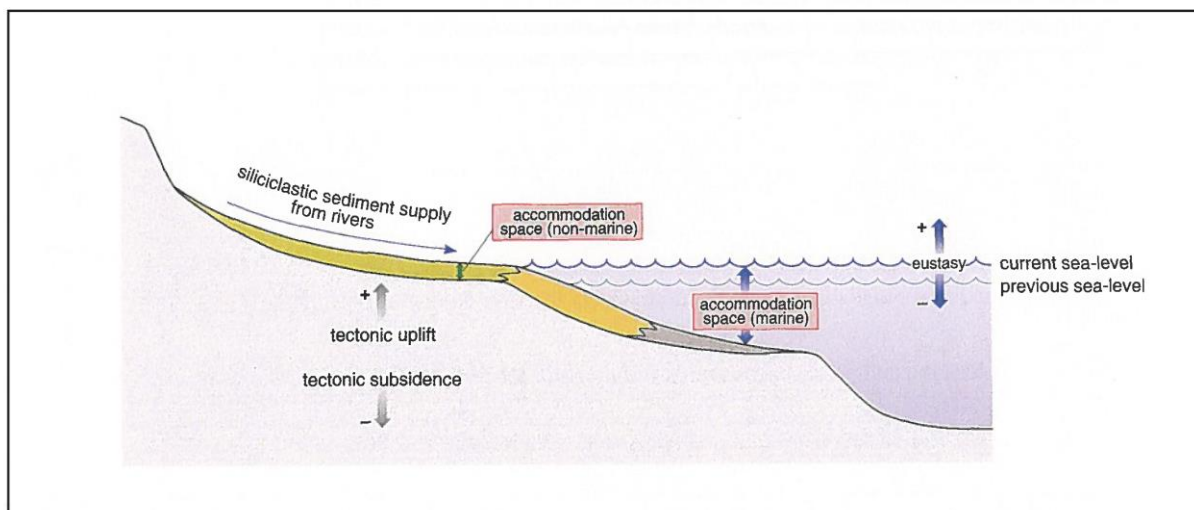


Figure 1-5. Illustration of Sediment accommodation space and its relationship to eustatic sea level, tectonic uplift and subsidence. Marine accommodation space is created during a rise in relative sea level and has been partially filled with sediment (yellow and dark-grey color), whereas the non-marine accommodation space created during the rise in relative sea level has been filled to maximum with sediment (yellowish-green color). Figure and caption from Coe et al. (2003).

1.2.2 Seismic sequence analysis

In seismic sequence analysis, the main objective is to interpret depositional sequences and system tracts on seismic sections by identifying discontinuities on the basis of reflection terminations (Mitchum et al., 1977; Vail, 1987). Figure 1-10 shows stratigraphic reflection terminations, in an idealized seismic sequence. Stratal terminations are defined by the geometric relationship between strata and the stratigraphic surface against which they terminate (Catuneanu, 2006). Four stratal terminations can be used in order to identify sequence stratigraphic surfaces. The following section, defines the main types of stratal terminations. They are respectively described by truncation, toplap, onlap and downlap.

Truncation

Termination of strata against an overlying erosional surface. Truncation implies that the reflection is cut by an unconformity. In some cases, top lap may develop into a truncation (Catuneanu, 2006).

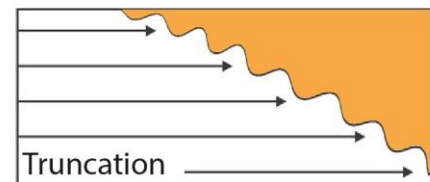


Figure 1-6. Schematic illustration of truncation. Modified from Veeken (2007).

Toplap

Terminations of inclined strata (clinoforms) against an overlying surface, characterized by a lower angle. Toplap is a result of nondeposition (sedimentary bypass) with minor erosional events (Catuneanu, 2006). Many depositional boundaries marked by toplap are found to be rather local in extent. Due to this, toplap is often complex to correlate regionally (Mitchum et al., 1977).

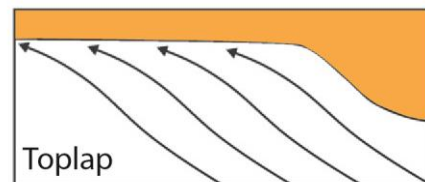


Figure 1-7. Schematic illustration of toplap. Modified from Veeken (2007).

Onlap

Termination of low-angle strata against a steeper stratigraphic surface. The younger strata progressively overstep each other (Veeken, 2007).

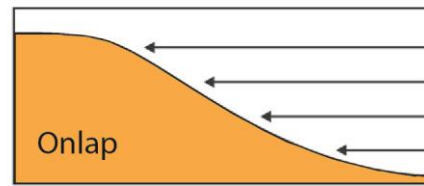


Figure 1-8. Schematic illustration of onlap. Modified from Veeken (2007).

Downlap

Termination of inclined strata against a lower-angle surface. Downlap occur commonly at the base of prograding clinoforms, in both shallow-marine and deep-marine environments. Downlap most often reflects a change from marine (or lacustrine) slope deposition to deeper marine condensation or nondeposition (Catuneanu, 2006).

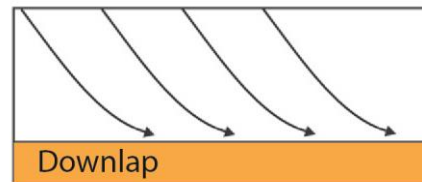


Figure 1-9. Schematic illustration of downlap. Modified from Veeken (2007).

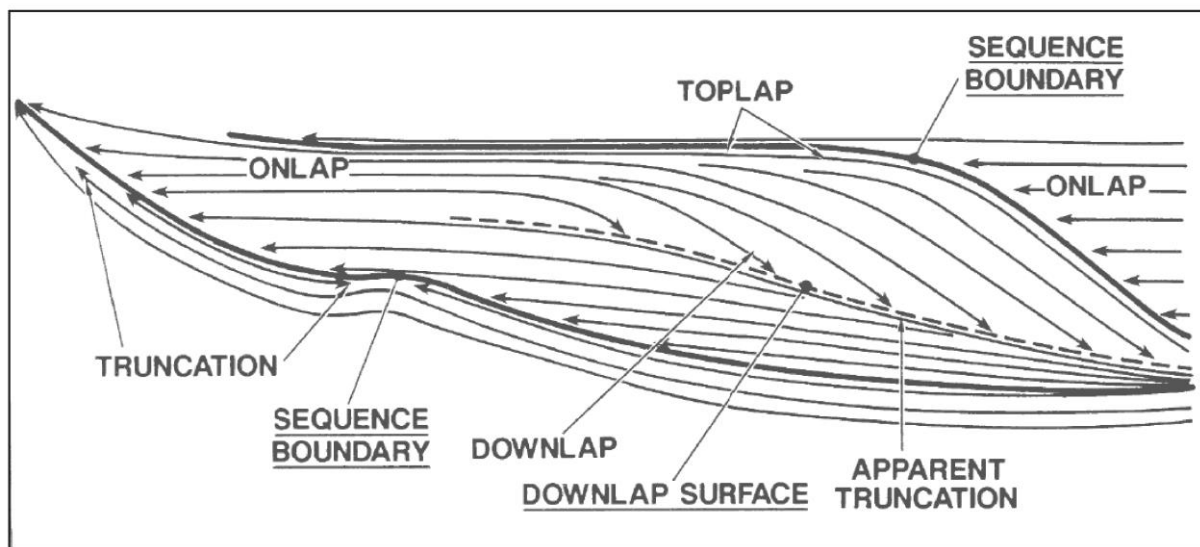


Figure 1-10. Idealized seismic sequence showing the main reflection terminations used in sequence stratigraphy classification. Figure is modified after (Vail, 1987).

1.2.3 Seismic facies

Seismic facies was defined by Mitchum et al. (1977) as the description and geological interpretation of seismic reflection parameters, including configuration, continuity, amplitude and interval velocity. Seismic facies is of significant importance, because they provide

considerable information about the geology in the subsurface. Among these parameters, seismic reflection configuration is most important and therefore used extensively in seismic interpretation.

1.2.4 Reflection configuration

Reflection configuration reveals the gross stratification patterns within seismic data and is directly related to sedimentary processes and therefore also the environment of deposition (Mitchum et al., 1977; Veeken, 2007). Several principle reflection configurations can be recognized, and each of them are described and interpreted in terms of depositional environment and lithofacies distribution (Veeken, 2007). In the following section, an overview of the main types of reflection geometry are presented (Table 1-1).

Parallel and subparallel reflection configuration

The parallel to subparallel configuration is a result of uniform, stable, sedimentation conditions. It may occur in several external forms, but occur most common in sheet, sheet drape and fill units (Mitchum et al., 1977). Subdivisions of parallel configuration are based on variations in seismic parameters, like for example amplitude and continuity (Veeken, 2007).

Divergent reflection configuration

The divergent reflection configuration shows a lateral thickening of sediments and therefore indicates asymmetrical sedimentation. The divergent configuration is typically wedge-shaped and the characteristic geometry can be explained by lateral variations in sedimentation rates, subsidence and/or burial effects (Veeken, 2007). The wedge-shape of the deposits may indicate syn-depositional conditions.

Chaotic reflection configuration

Chaotic reflection configurations are represented by discontinuous and discordant reflections, suggesting a disordered arrangement of reflection surfaces (Mitchum et al., 1977). Chaotic reflections is often characterized with variance in amplitude and frequency (Veeken, 2007). Mitchum et al. (1977) discuss two principle methods for the presence of chaotic reflections. They may either be interpreted as strata deposited in a variable environment characterized by high-energy settings, or deposited as initially continuous strata, which later have been affected by deformation processes.

Reflection-free configuration

Reflection free zones in seismic sections, coincidence with areas where acoustic impedance contrast are weak or lacking (Veeken, 2007). Several lithologies can appear reflection-free, for example igneous masses, salt features or thick homogenous shales or sandstones (Mitchum et al., 1977).

1.2.5 Reflection amplitude

The reflection amplitude provides information of the velocity and density contrast of individual interfaces and their spacing (Mitchum et al., 1977). Reflections characterized with high amplitude (Table 1-1), generally points to vertical alternation of contrasting lithologies, while reflections characterized with a low amplitude indicates lithologies of more similar properties on both sides of the interface (Veeken, 2007). It is often used to predict lateral bedding changes and hydrocarbon occurrences.


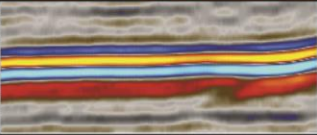


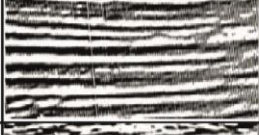
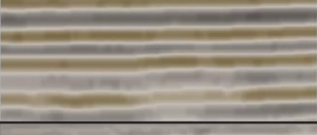



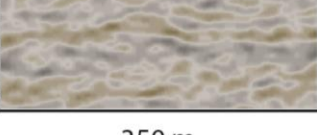
1.2.6 Reflection continuity

Reflection continuity provides information on energy conditions that have affected the deposits (Veeken, 2007). Reflection continuity is often associated with continuity of stratal deposits. A high continuity suggests a great lateral extend and uniform deposits, deposited under the same sedimentary conditions (Table 1-1). Discontinues reflections occur in depositional environments characterized by rapid changes in energy conditions (Mitchum et al., 1977; Veeken, 2007).

1.2.7 Frequency

Frequency is a characteristic feature describing the nature of a seismic pulse, but can also relate to geological factors such as the spacing of reflectors or lateral changes in interval velocity, as associated with gas occurrences (Kearey et al., 2002; Veeken, 2007).

Table 1-1. Comparison of seismic facies in the dataset used for this study, after (Veeken, 2007)

Seismic facies	Reflection geometry	Reflection amplitude	Seismic facies after (Veeken 2006)	Seismic facies from survey NPD 1201
Example 1	Parallel continuous	High amplitude		
Example 2	Parallel continuous	Medium amplitude		
Example 3	Parallel continuous	low amplitude		
Example 4	Subparallel discontinuous	low-medium amplitude		
Example 5	Chaotic	low amplitude		

350 m

1.2.8 Clinoforms

The term clinoform was originally defined by Rich (1951) to represent the inclined surface (foreset) formed between the wave base and the bottom of a water body. Today, the term include the entire sigmoid profile from the topset, foreset and bottomset (Steel & Olsen, 2002; Helland-Hansen & Hampson, 2009). This thesis focuses primary on larger-scale clinoforms (Figure 1-11), which reflect sediment transport into basinal waters, which are deep enough to produce brake-of-slope characteristics of shelf-margins.

Prograding slope systems in standing bodies of water have varying shapes and angles, which are controlled by several factors. These factors include (among others), the sedimentation rate and quantity of sediment input, the composition of the deposited material, the salinity of the water, water depth, energy level (of the depositional environment), and the relative sea level (Steel & Olsen, 2002; Veeken, 2007). The subsidence rate may be crucial in order to create accommodation space where sediments can deposit.

Clinofoms reflect basinward-fining and accretionary units that progressively built out from shallow, basin-margin areas to deeper water (Steel & Olsen, 2002). In addition, clinoforms can allow time lines to be visualized, since they represent regressive-to-transgressive building blocks in stratigraphic successions (Steel & Olsen, 2002). Clinofoms can form at different scales, usually on the size of deltas/shorefaces (tens of meters) or of shelf margins (hundreds of meters) (Steel & Olsen, 2002; Helland-Hansen & Hampson, 2009).

Shelf-margin (also termed shelf-slope-basin) clinoforms, record the advance of a shelf margin. The successive migration of deltas and shoreline across the shelf is the main mechanism by which a shelf-margin accrete (Johannessen & Steel, 2005). Although, storms may influence the sediment transport on shelves by eroding sediments that aggrade above the shelf equilibrium profile (Grundvåg et al., 2017). Storm eroded sediments, where mud dominates, can be transported across a low-gradient sloping shelf under the combined influence of gravity and storm waves (Grundvåg et al., 2017). The dimension of clinoforms varies. Shelf-margin slopes commonly display slopes that varies between 2 to 7 degrees (Steel & Olsen, 2002; Johannessen & Steel, 2005). Slopes with high amount of coarse material, often tend to be steeper compared to slopes containing more muddy sediments (Johannessen & Steel, 2005). Sand-prone slopes is often the result of channelized slopes or when it support sandy, shelf-edge-attached aprons, in

situations where the sediment flux from the shelf break is high (Johannessen & Steel, 2005). Although, during times of low-stand it is likely that the slope occasionally is sand-prone.

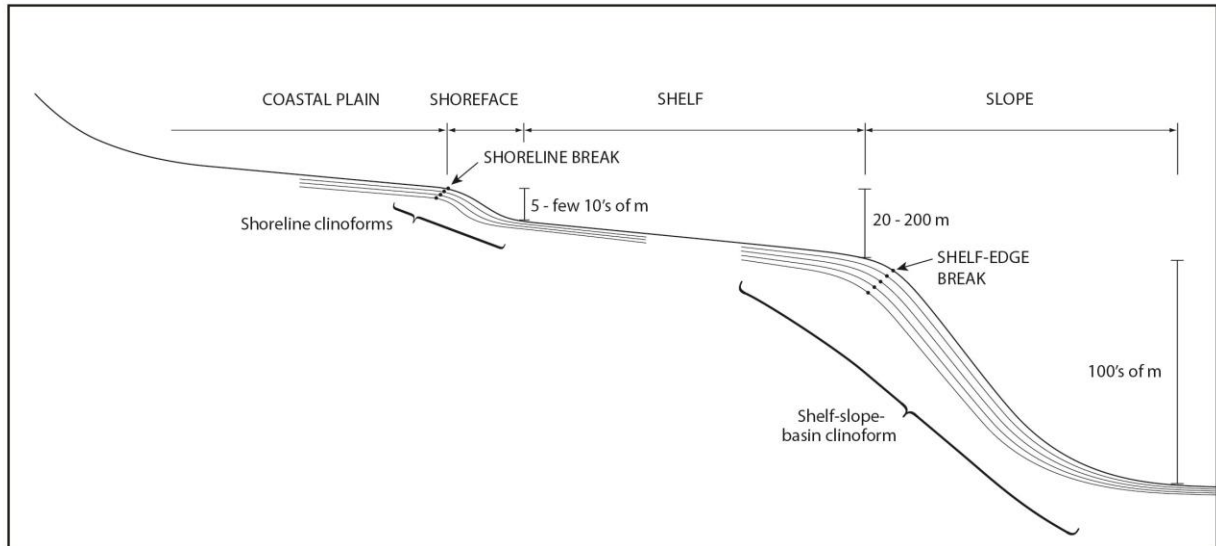


Figure 1-11. Topographic profile showing scale of shelf-edge clinoforms identified in this study. Figure modified from Helland-Hansen and Hampson (2009).

1.2.9 Trajectories

A shelf-edge trajectory is the pathway taken by the shelf during the development of series of accreting clinoforms (Johannessen & Steel, 2005). It is of significant importance, since trajectory analysis provides a unique opportunity to investigate migration of shelf-edge through time. The physical features are often expressed by a break-in-slope (Figure 1-12), which enable suitable mapping of lateral and vertical shifts in depositional systems (Helland-Hansen & Hampson, 2009). More importantly, the shelf break represents an area where significant changes in depositional processes and products occur. The shelf break separates the shelf from slope, where processes such as mass gravity dominate causing resedimentation, bypass and channelling. In contrast, the shelf is dominated by the already mentioned processes like successive migration of deltas and shorelines, in addition to tides and waves (Helland-Hansen & Hampson, 2009).

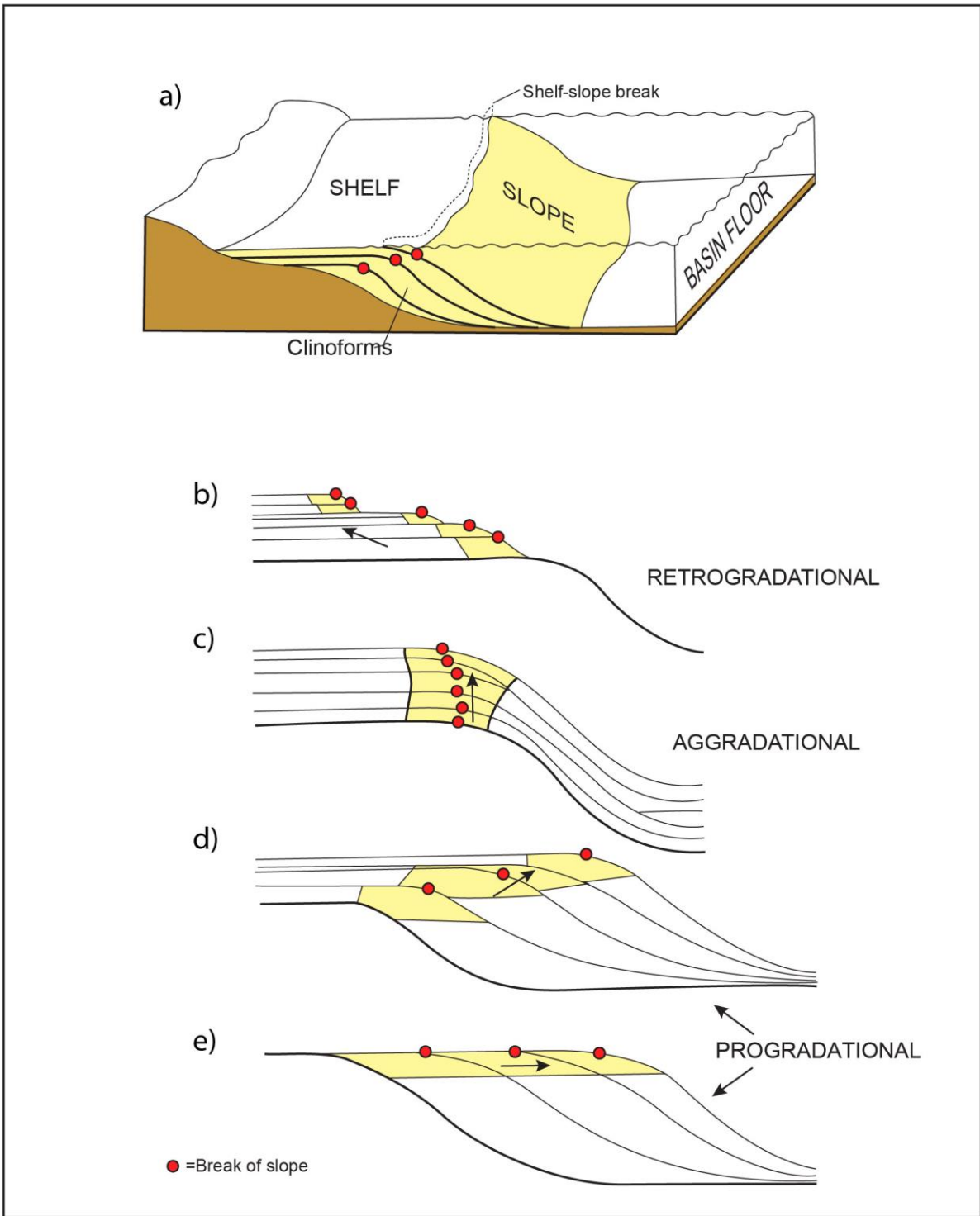


Figure 1-12. a) Sedimentary prism built out from a basin margin, with internal clinoforms and the shelf-slope-basin floor morphology displayed. b-e) Illustration of how shelf-edge break can vary between retrogradational, aggradational and progradational through time. Note that d) shows ascending trajectories and e) shows flat trajectories. Figure modified from Steel and Olsen (2002).

The trajectory of the shelf break is a function of bathymetry, sediment supply, eustatic sea level changes and subsidence (Helland-Hansen & Hampson, 2009). As clinoforms accrete, the trajectory can vary in its inclination or gradient (Johannessen & Steel, 2005). Based on this, trajectories can be subdivided into ascending, flat or descending subgroups (Helland-Hansen & Hampson, 2009).

The ascending trajectory geometry indicates a long-term rise in relative sea level (Johannessen & Steel, 2005; Helland-Hansen & Hampson, 2009). The ascending geometry is the result of sediments being stored on the shelf break, because the volume of sediments delivered out to the shelf were not sufficient to overcome the rise in relative sea level (Helland-Hansen & Hampson, 2009; Helland-Hansen et al., 2012). This results in less sediments being partitioned into the deep water, while more sediments accumulates at the contemporary shelf and coastal plain (Johannessen & Steel, 2005).

Flat and descending shelf-edge trajectories in contrast, represent a long-term relative sea level with a stable or falling trend (Helland-Hansen & Hampson, 2009). The lowstand regime across the shelf allow delivery of sediments across the shelf, which eventually can result in channelized deposits on the slope and the basin floor (Steel & Olsen, 2002).

2 Geological background

The Barents Sea has been defined as an epicontinental sea which is bounded by young passive continental margins in the north and west (Faleide et al., 1984). Novaya Zemlya forms the eastern boundary, which extends southwards to the Kola Peninsula and the Norwegian coast, and thereby defines the southern boundary (Faleide et al., 1984). The northern boundary is marked by Franz Josef Land. The Svalbard Archipelago defines the northwestern corner of the Barents Shelf. The Barents Sea covers the north-western corner of the Eurasian continental shelf, and comprises an area of approximately 1.2 million km² (Rønnevik et al., 1982). The water depth in the Barents Sea is relatively shallow, with an average depth of approximately 300m (Rønnevik et al., 1982).

The southern Barents Sea is characterized by a marked difference in time, trend and magnitude between the tectonic and stratigraphic development around the western margin, and the eastern platform (NPD, 2014b). The boundary which separates east and west, is defined by the dominant north-south to northeast-southwestern trending Ringvassøy-Loppa and Bjørnøyrenna Fault complexes. In the southeastern parts of the Barents Sea (Figure 2-1) , successions are dominated by thick Upper Paleozoic and Mesozoic sequences, with faults trending generally in east-west to northwest-southeast directions (NPD, 2014b). In the western part of the Barents Sea shelf, younger tectonism throughout Late Mesozoic and Cenozoic times resulted in deposition of thick packages of Cretaceous, Paleogene and Neogene sediments in the Harstad, Tromsø and Bjørnøya Basins (Worsley, 2008). Fault patterns dominating in the western regions, are respectively orientated northeast-southwest (NPD, 2014b). The regional trend concerning structural elements in the Barents Sea shows major basins west of Novaya Zemlya. This is the South Barents Basin, North Barents Basin and the offshore part of the Timan-Pechora Basin, passing westwards into smaller basins, highs and platforms (Henriksen et al., 2011). The North and South Barents Basins, which belongs to the Russian sector of the Barents Sea, formed in the foredeep zone to the Novaya Zemlya tectonic belt directly in the northwestern prolongation of the onshore Pechora Basin (Smelror et al., 2009). The depressed basins (sag) terminate further west in the Barents Sea, in areas where sedimentary strata rises towards the subsurface in Svalbard and others platforms located in the western part of the Barents Sea (Smelror et al., 2009).

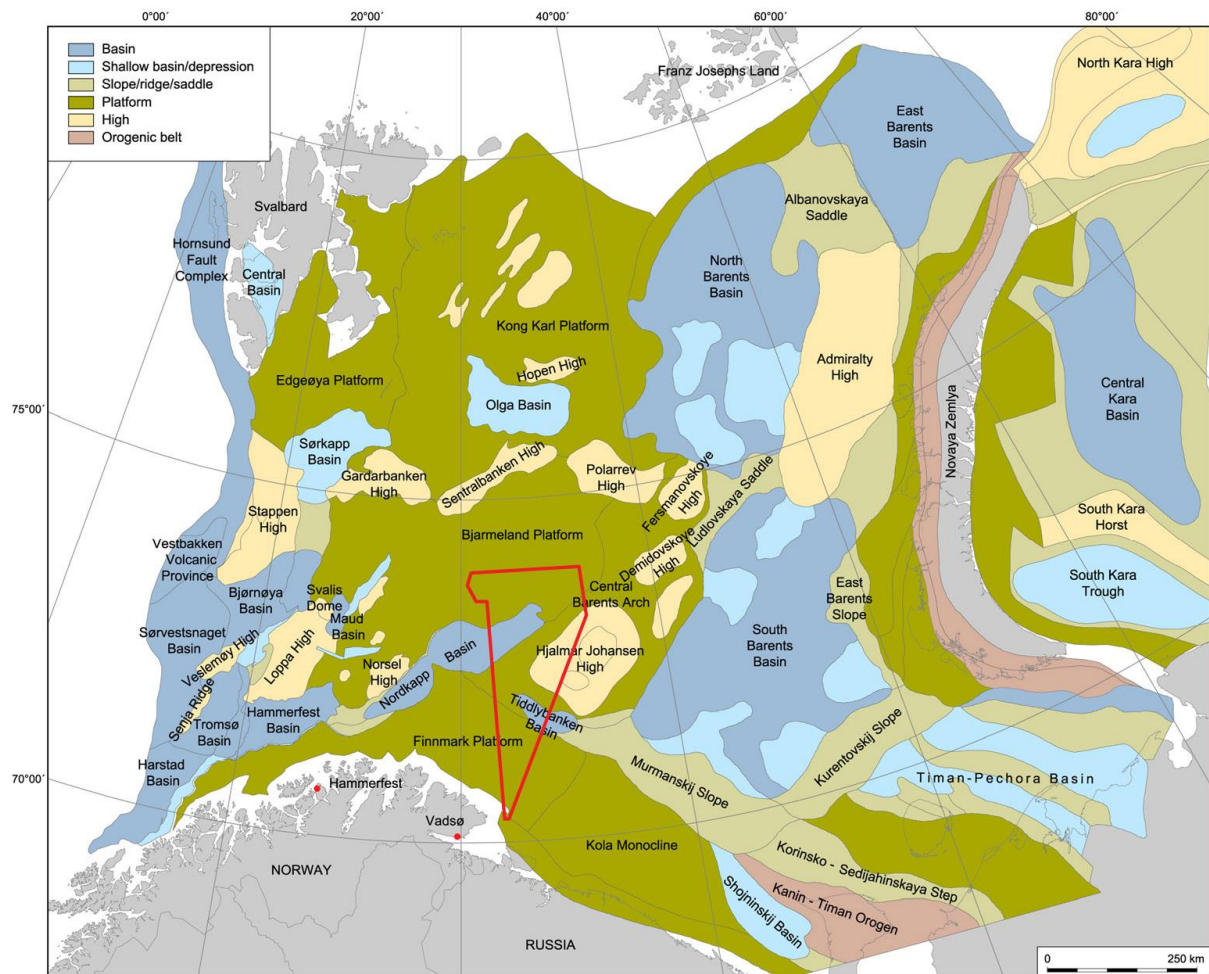


Figure 2-1 Structural elements of the greater Barents Sea. Study area is shown as red polygon. North is upwards in the figure. Figure modified from Henriksen et al. (2011).

2. Stratigraphic and structural development

The stratigraphic and structural development of the Barents Sea has been studied and presented by numerous authors (Worsley, 2008; Smelror et al., 2009; Henriksen et al., 2011; Faleide et al., 2015). The geology of the Barents Sea area is characterized by a complex combination of large-scale tectonic processes, fluctuating climatic conditions and varying depositional conditions. The tectonic development in the Barents Sea is locally still debatable, but the main outline is relatively well established up to Paleoproterozoic times (Gernigon et al., 2014). The Svalbard Archipelago, forming the subaerially exposed northwestern margin of the Barents Shelf, displays a comprehensive geological overview of the Barents Sea region. It is located in

a favorable position, south of the polar Euramerican Basin and east of the Norwegian-Greenland Sea, which enables recognition of main features controlling the development of the Barents Sea (Worsley, 2008). The Svalbard Archipelago is acknowledged as an important source for correlation between the western and the eastern provinces in the Barents Sea.

2.1 Structural development

The Barents Sea and the Kara Sea (located in Russian sector) have repeatedly been influenced by major tectonic phases, involving multiple orogenies with episodes of subsidence and young continental breakups (Klitzke et al., 2014). In particular, three orogenic events influenced the Barents Shelf. This is respectively the Timanian, Caledonian and Uralian orogenic events. In addition to these three tectonic events, the Barents Shelf has also been influenced by Proto-Atlantic rifting episodes in the west, the opening of the Euramerican Basin in north, and the break-up which eventually resulted in opening of the northern North Atlantic ocean in the west (Smelror et al., 2009). Furthermore, the Barents Sea region was subjected to different magnitudes of uplift and erosion, during the period from Early Cretaceous to Holocene (Marin et al., 2016). The following sections describe the main tectonic events during the structural development of the Barents Sea, with focus on the southeastern parts. It follows a chronological order based on geological eras.

2.1.1 Precambrian

The first tectonic episode which involved plate accretion, was the Timanian Orogeny that occurred in the latest Precambrian (Klitzke et al., 2014). The Timanian Orogen developed as a fold-and-thrust belt along the northeastern passive margin of Baltica and the southeastern Barents Sea (Gernigon et al., 2014). The type area for the Timanide Orogen is restricted to the Timan Range of the Northwestern part of Russia, which separates the East European Craton (Baltica) from the Pechora Basin and Polar Urals (Gee & Pease, 2004). The Timan range, is a present day topographic high which provides proof for this collisional event (Klitzke et al., 2014). The Timanian Orogen exceeds over a distance of 3000 km, and can be tracked from the southern Ural Mountains of Kazakhstan to the Varanger Peninsula of northern Norway, flanking towards the eastern margin of the older craton (Gee & Pease, 2004). From the Timan Range, the orogen reaches northeastwards, overlaid by a thick Phanerozoic succession of the Pechora Basin and the Barents Shelf. The same orogen reappears in the Polar Ural Mountain

and continues further northwards through Pai Khoi and up to Novaya Zemlya (Gee & Pease, 2004). It is characterized by dominantly northwest-trending structures (Rippington et al., 2015). Due to the extent and the complexity of the Timanian Orogeny, it influenced a vast region of the northwestern Russia and thereby the southeastern part of the Barents Sea.

2.1.2 Paleozoic

The second tectonic event, which influenced and disturbed the evolution of complex, mosaic platform areas and basins in the Barents Sea, was respectively the Caledonian Orogeny. This episode culminated approximately 400 Ma, during the Middle Ordovician and reached a climax in Silurian times. The Caledonian Orogeny resulted in a collision between the Laurentian (Greenland, North America) and Baltican (Scandinavia, western Russia) plates into the Laurasian continent and marked the closure for the Iapetus Ocean (Smelror et al., 2009; Gernigon et al., 2014). The Iapetus Ocean is considered to represent an analog to the present northeast Atlantic, which occupied a similar position (Dorè, 1995). The Caledonian Orogeny influence is well documented on the western Barents margin and Svalbard, where north-south striking bedrocks are exposed (Smelror et al., 2009). The most accepted explanation for the origin of the Caledonian Orogeny onshore northern Norway, has been regarded to have formed during two major orogenic phases, respectively; the Finnmarkian (Late Cambrian) and Scandian phases (Mid-Silurian-Devonian) (Ritzmann & Faleide, 2007). The basement of the present day Barents Sea is suggested to have formed during the Silurian period (Smelror et al., 2009).

Late Paleozoic times in the Barents Sea region were characterized by crustal extension. The most pronounced event is represented by a 300 km wide rift zone that extended approximately 600 km northeast (Smelror et al., 2009). It was established as a direct continuation of the northeast Atlantic rift between Greenland and Norway in the middle Carboniferous. Because of this massive rifting episode, Late Paleozoic structures represent a fan-shaped array of northeast-southwest-trending horst and graben geometries along the Caledonian basement (Glørstad-Clark et al., 2010).

The third major tectonic phase, which influenced the evolution of the southeastern Barents Sea and the Kara Region, is related to the development of the Uralian Ocean. An ocean which formed along the eastern margin of Baltica as a result of Ordovician rifting (Petrov et al., 2008). During the Carboniferous, the progressive closure of the Uralian Ocean led to continental

collision between Baltica and Kazakhstan, which resulted in the formation of the Ural Mountains south of Pay-Khoy (Smelror et al., 2009). According to Smelror et al. (2009) the Uralian Orogeny can be divided into two different tectonic phases. The first collisional phase occurred in the timeframe from Early Carboniferous to the Late Permian, followed by the second orogenic phase in between the Late Permian and Triassic times. The final closure of the Uralian Ocean was caused by an inferred collision of the Yamal-Gydan Plate and an Island arc bordering the Novaya Zemlya marginal basins (Petrov et al., 2008; Smelror et al., 2009). This theory is supported by seismic data showing evidence of folding within the eastern part of the South Kara basin during Carboniferous and Permian times (Smelror et al., 2009). During this period, carbonate platforms which originally were formed in the subsequent Pragian-Emsian phase (Early Devon), was gradually folded and thrust (Petrov et al., 2008). This deformation process, caused a progressive filling of the Novaya Zemlya foredeep, with terrigenous material derived mainly from the growing Kara Thrust belt (Smelror et al., 2009). At the same time, major reefs formed along the margin of sediment-starved deep-water troughs within the Barents plate (Petrov et al., 2008). The late Early Permian is characterized by a dramatic change in the

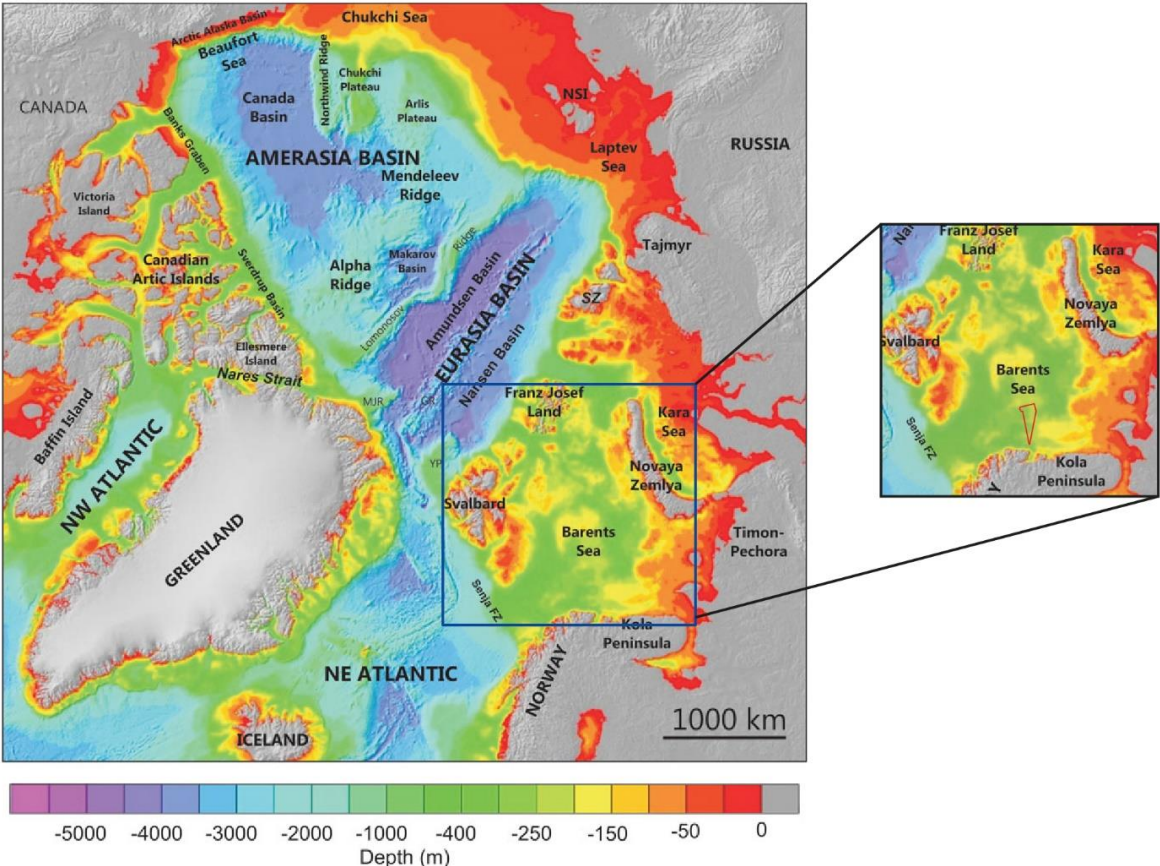


Figure 2-2. Bathymetric map showing the regional setting of the Barents Sea, and the study area (red polygon) in relation to the other basins of the Arctic region. Figure modified from Corfu et al. (2013).

marine circulation pattern, with the growth of a marine seaway which developed around Baltica and the western shelf margins (Smelror et al., 2009). The new marine seaway progressively opened a connection between Norway and Greenland, resulting in an abrupt change in oceanic circulation, as cool dense water flowed across the Barents Shelf (Henriksen et al., 2011). During this period, the western shelf of the Barents Sea experienced low-energy shelf conditions and basinal environments, which contained rich siliceous sponge-fauna strata (Henriksen et al., 2011). In contrast to the eastern Barents Shelf, which represented shallow marine, slope and deep basinal facies (Henriksen et al., 2011).

2.1.3 Mesozoic

At the beginning of Triassic time, landmasses were concentrated into a single continent (Pangaea) which was located around the equator, with continental areas extending towards the poles. The Barents Sea Basins were located at this time, approximately at 50° N to 55° N (Ryseth, 2014). In general, the Triassic period is explained as a tectonically quiet period in the Barents Sea region, especially in the western part. Here, passive regional subsidence accompanied by minor movements are recognized on the Bjarmeland and Finnmark Platforms (Henriksen et al., 2011). Further to the east, the East Barents Mega Basin located between the North Barents Basin and the South Barents Basin, experienced extension and rapid subsidence (Johansen et al., 1992). Rapid subsidence continued from Late Permian throughout the Triassic, which resulted in deposition of thick sequences of clastic sediments in the North and South Barents Basins (Ritzmann & Faleide, 2009). The Uralian highland to the east acted as an important sediment source, together with sediments shed into the Barents Sea from the Baltic shield (Faleide et al., 2015).

Fragmentation of the supercontinent Pangea that formed new continental masses and sedimentary basins, began in the Early Cretaceous. The high Arctic underwent several stages of rifting, sedimentation and magmatism in connection with the sea-floor spreading between the Canada and Makarov Basins in the Arctic Ocean (Dorè, 1995; Corfu et al., 2013; Marin et al., 2016). This tectonic event resulted in the opening of the Amerasian Basin (Figure 2-2).

Cretaceous magmatic activity is considered to have been one of the main stages for the evolution of the High Arctic Large Igneous Province (HALIP) (Corfu et al., 2013). The magmatic activity covered a massive area, and evidence of its existence have been found on Svalbard, Franz Josef Land and adjacent shelf areas (Nejbert et al., 2011). Maher (2001) also

suggested that the HALIP province could have influenced the Canadian Arctic Archipelago and the northern Greenland. Recent published studies from Polteau et al. (2015) demonstrates the presence of Cretaceous igneous rocks in the Northeast and the Southeast Barents Basin as well. The center of the HALIP and its influence on the tectonic evolution in the region are still subjects to scientific debate. Furthermore, it has been suggested that the HALIP was emplaced during two phases, respectively at 130 and 90 Ma, which coincide with the opening of the Arctic Ocean (Corfu et al., 2013).

The extensional regime in Early Cretaceous caused uplift and later tilting of the northern parts of the Barents Sea region. It has been suggested that an interaction between a mantle plume and the lithosphere was the main mechanism causing the uplift (Polteau et al., 2015). The subsequent uplift, which was most prominent in the northeastern part of the Barents Sea region, resulted in changes of the sedimentary depositional patterns during the Barremian and Early Aptian times. Marine shelves dominated the central and western parts of the Barents Sea. The uplifted areas contributed to the generation of prograding sediments from the elevated areas in the northeast, towards subsiding basins in the west where they were deposited (i.e. Harstad, Tromsø and Bjørnøya basins) (Smelror et al., 2009; Henriksen et al., 2011; Gernigon et al., 2014).

2.1.4 Cenozoic

The pronounced uplift and erosion of the Barents Shelf during the Cenozoic, has been studied and extensively presented by numerous authors (Vorren et al., 1991; Richardsen et al., 1993; Faleide et al., 1996; Worsley, 2008; Smelror et al., 2009). The Cenozoic evolution of the Barents Sea is closely linked to the opening of the Norwegian-Greenland Sea in Eocene/Oligocene, with significant shearing along the Senja Fracture Zone. The Paleogene is characterized by tectonic activity along the western shelf margins, prior to the final opening of the Norwegian-Greenland Sea (Worsley, 2008; Henriksen et al., 2011). It has been suggested that uplift and erosion during Cenozoic resulted in the removal of between 1400-1600 meters of Cretaceous and Paleogene strata from the southeastern Barents Shelf (Rippington et al., 2015). Cenozoic strata are present particularly in the western Barents Sea, but show a less widespread sedimentary distribution pattern compared to older sedimentary strata, such as the Cretaceous strata.

2.2 Stratigraphic and depositional environment

The term “top basement” refers to the horizon at which the sedimentary strata is separated from the underlying crystalline bedrock, hence representing the base of the basins. Sedimentary rocks usually reflect weak magnetization, while bedrocks commonly show a stronger magnetization. The use of magnetic anomalies can therefore be applied to estimate the depth of the basement (Smelror et al., 2009).

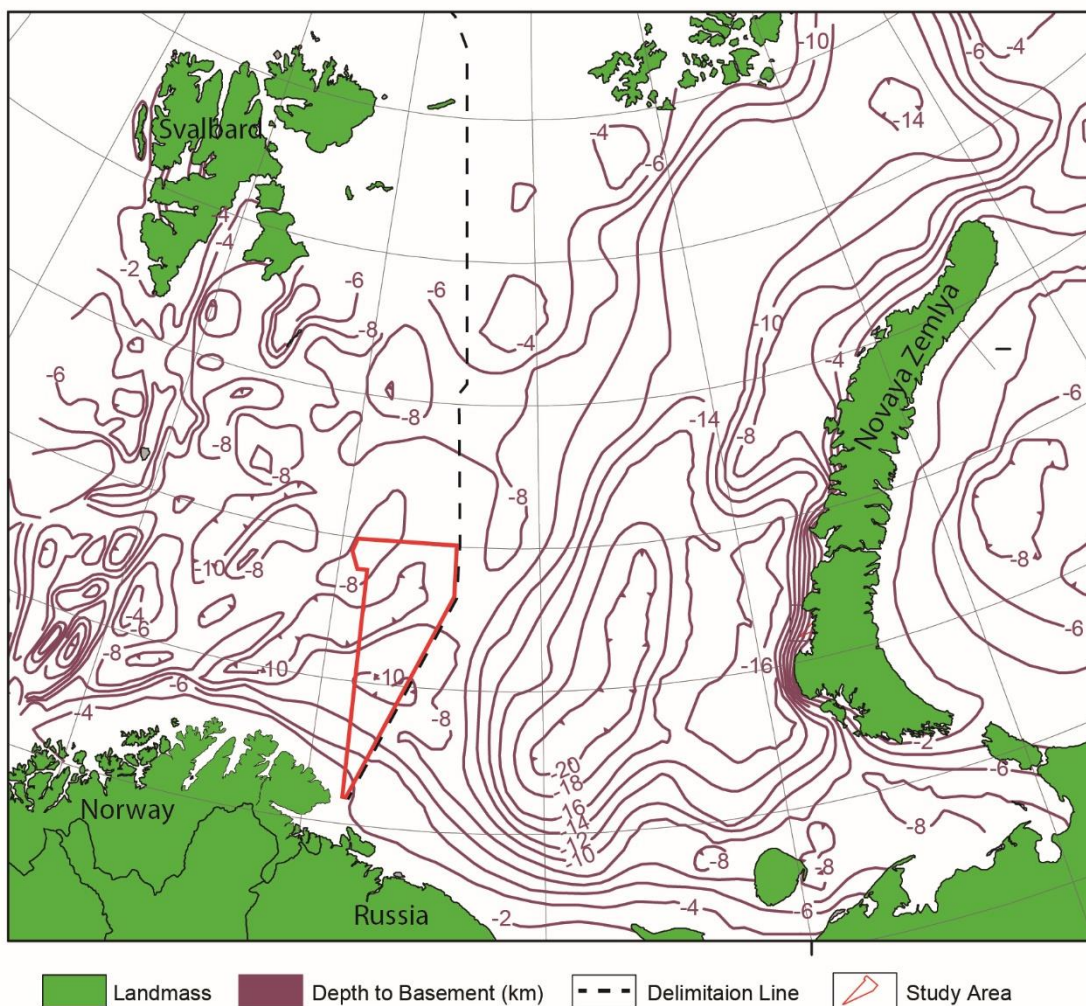


Figure 2-3. Depth to basement map showing the depth the top basement. The figure displays variations in sedimentary thicknesses particularly between the western and eastern Barents Sea. Figure modified after Smelror et al. (2009).

The thickness of sedimentary strata down to basement rocks are shown in Figure 2-3. It indicates variation in thicknesses across the Barents Shelf. In particular, the contrast between the western Barents Sea (Norway) and eastern Barents Sea (Russia) is significant. The eastern part of the Barents Sea is dominated by two mega-scale basins, respectively the North and South

Barents Basin. The top basement horizon is located at 20 km depth. In the western part of the Barents Sea, the top basement has a depth of up to 14 km, hence reflecting series of narrow basins (Smelror et al., 2009). Sediments found in basins located in the southern and eastern Barents Sea has been deposited during three stages. The oldest sediments represent sedimentary strata deposited during the Caledonian Orogen. The second sedimentary sequence corresponds to Devonian time, which again are overlaid by a third sedimentary sequence of Carboniferous-lower Permian strata (Smelror et al., 2009).

2.2.1 Paleozoic

During the Late Ordovician to Middle Devonian a general transgression took place, which resulted in generation of a thick (200-1000 m) Silurian-Devonian carbonate unit in the Pechora region (Henriksen et al., 2011). Later on, during the Middle Devonian, the depositional environment changed, from carbonates towards shallower marine siliciclastic deposits. This was most likely sourced by erosion of local highs in the region (Henriksen et al., 2011). Another shift occurred in Late Devonian time, when Carbonate platforms were re-established in the Timan-Pechora region. The eastern Barents Sea, western and southern part of Novaya Zemlya together with the Timan-Pechora region, acted as a major depocenter for sediments prograding from the western part of the Barents Sea (Henriksen et al., 2011). The Caledonian Orogen which covered most of the western part was gradually eroded, which resulted in development of delta systems that prograded in an eastward direction (Henriksen et al., 2011).

2.2.2 Mesozoic

Triassic and Jurassic

The Triassic succession in the Barents Sea was deposited during a relative quiet tectonic phase, compared to large-scale basin forming processes in Late Paleozoic and Late Mesozoic times (Glørstad-Clark et al., 2010). Marine conditions prevailed in the Late Permian and Early Triassic times (Faleide et al., 2015). In Early Triassic, a regional deep-water basin covered most of the Barents Sea. The time was characterized by strong subsidence within the South Barents Basin, whereas a more tectonically quiescent, shallow-water, siliciclastic marine shelf dominated on the western parts in the Barents Sea. The Early Triassic depositions of sediments is assumed to have been influenced by erosion of the Ural Mountains in the east/southeast. The Ural Mountains were uplifted in the east, and sediments prograded into the western Barents Sea

siliciclastic marine shelf (Smelror et al., 2009). This is suggested based on the west and northwest prograding Triassic deposits identified both in the Russian and Norwegian Barents Sea (Smelror et al., 2009).

The Nordkapp Basin appeared as a shallow marine shelf, with alternations of being a dry land with vast alluvial plains (Ramberg et al., 2008). The Middle Triassic strata is characterized by a shift into more continental regimes, exemplified with northward and westward prograding deltaic systems, which continued to infill sediments in regional basins (Faleide et al., 2015). The infill of restricted basins was mostly prevailing in the eastern Barents Sea, whereas the western parts of the shelf was dominated by near-shore and continental environments (Smelror et al., 2009). The basins comprised anoxic environments. In this period, organic-rich mudstones were deposited within the Nordkapp Basin as the basin was a marine embayment almost cut off from the open sea (Ramberg et al., 2008). The late Triassic ended with a regression, due to continuing uplift and erosion in the east (Smelror et al., 2009). This resulted in shoreline movement back to the southern and eastern borders of the Southeast Barents Basin (Faleide et al., 2015).

The Barents Sea region experienced a shift from a regression, towards a marine transgression in the Late Jurassic, which led to shallow marine environments that dominated most of the Barents Sea (Smelror et al., 2009; Klett & Pitman, 2011). The transgression reached its maximum in the middle Jurassic, and shallow-marine sediments such as sandstones, siltstones, and organic-rich muds were deposited as the Stø Formation within the Hammerfest, Nordkapp and Bjørnøya Basins (Smelror et al., 2009). The Late Jurassic transgression reached its maximum in the latest Jurassic, where fine-grained clay sediments were deposited in open marine environments in the southeastern Pechora area. The Jurassic Hekkingen Formation consists of organic-rich material which represents an open-marine environment, with anoxic bottom-water conditions (Smelror et al., 2009).

Cretaceous

In the earliest Cretaceous, an overall regression, which began in the latest Jurassic, continued (Smelror et al., 2009). At the same time, the northern part of the Barents Sea region was uplifted and tilted gently. This uplift was a result of breakup and sea-floor spreading associated with the opening of the Amerasian Basin in the Arctic Ocean, which was accompanied by extensive

magmatism (Marin et al., 2016). The magmatism caused the formation of sills and dykes, and have been identified as dolerites on Svalbard (Faleide et al., 2015). The uplift was most prominent in the northeastern part of the Barents Sea region, while simultaneous marine shelves dominated in the central and western parts. These uplifted areas, contributed to the generation of sediments prograding from the elevated areas in the northeast, towards subsiding basins in the west where they were deposited (i.e. Harstad, Tromsø and Bjørnøya Basins) (Smelror et al., 2009; Henriksen et al., 2011). During this time, the sediment supply was dominated by fine-grained, clastic material, which gave rise of up to 700-meter thick successions of basinal shales that have some organically enriched intervals. The fine-grained clastic material was consisting of shales and claystone, with interbeds of silt, limestones and dolomite (Faleide et al., 2015). Platform areas were dominated by thinner successions, with carbonates being the most prominent (Worsley, 2008). Throughout the Late Cretaceous, significant subsidence persisted (Henriksen et al., 2011). The Upper Cretaceous successions is more or less absent within the Barents Sea (Faleide et al., 2015). The maximum regression was reached during the late Albian time, which was followed by a new transgression (Smelror et al., 2009).

2.2.3 Cenozoic

The Cenozoic sediment deposition in the Barents Sea was confined to the westernmost basins, due to the tectonic events linked to the Atlantic opening and general uplift (Smelror et al., 2009). The eastern and northern parts of the Barents Sea were uplifted (Smelror et al., 2009). During the late Cenozoic, parts of the Barents Sea was subsided and buried. The uplifted areas derived thick successions of clastic sediments towards the shelf (Faleide et al., 2015). The latest Cenozoic sediments are mostly absent within the Barents Sea, due to low rate of sedimentation in addition to strong glacial erosion which removed thick successions (Smelror et al., 2009). The base of the Quaternary deposit is recognized as an erosional boundary, the so-called Upper Regional Unconformity (URU), which separates the glacial sediments from pre-glacial Paleogene and older sediments (Richardsen et al., 1993). Much of the Cenozoic strata which originally was deposited on elevated highs, i.e. the Finnmark and Bjarmeland Platforms, has been eroded below the base of the Quaternary (Smelror et al., 2009; Henriksen et al., 2011).

2.3 Cretaceous Stratigraphic units (Dalland et al., 1988)

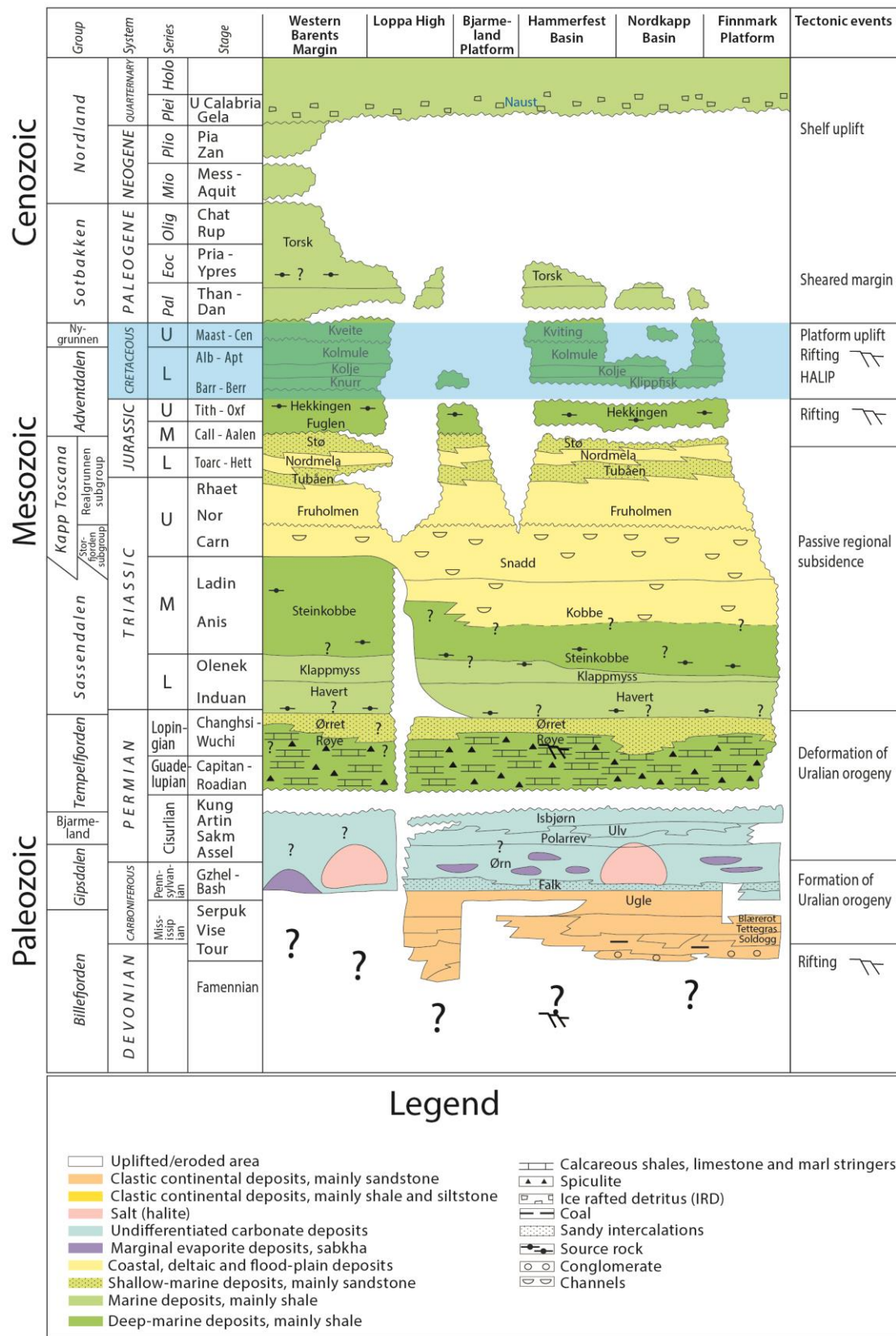


Figure 2-4. Lithostratigraphic diagram with formation and group names. The Cretaceous system is highlighted in blue color. Figure modified after NPD (2014a).

2.3.1 The Nordvestbanken Group

Nordvestbanken Group is the lithostratigraphic unit corresponding to the Upper Cretaceous sequence in the Barents Sea. The Nordvestbanken group corresponds to Valanginian to Cenomanian age, and is subdivided into the Knurr, Kolje and Kolmule Formations.

2.3.2 Knurr Formation

The Knurr Formation represents Ryazanian/Valangian to Early Barremian age. This formation consists of dark claystone, with thin limestone and dolomite interbeds. Thin sandstone also occur locally in the lower parts, whereas red claystone generally occur in the upper parts of the formation. The formation was deposited in an open and generally distal environment, with local restricted bottom conditions.

2.3.3 Kolje Formation

The Kolje Formation represents Early Barremian to late Barremian/Early Aptian age. This formation consists of dark grey shale and claystone, with interbeds of limestone and dolomite. The upper part of the formation has thin interbeds of siltstone and sandstone. The formation was deposited in distal, open marine environment with good water circulation, but episodes of restricted water circulation occurred.

2.3.4 Kolmule Formation

The Kolmule Formation represents Aptian to mid-Cenomanian age. This formation consists of green claystone and shale, with more silty parts and limestone/dolomite strings. The formation was deposited in an open marine environment.

2.4 Structural elements

Five regional elements define the structural framework in the Barents Sea southeast (Figure 2-5). In the southern part in the study area, the Finnmark Platform abuts the Norwegian coast with strata dipping northwards (NPD, 2013). In the northern part of the study area, the Bjarmeland Platform show strata dipping in the opposite direction, respectively southwards (NPD, 2013). In-between the two major platforms, the Nordkapp Basin developed as a deep subsidence basin, which contains large quantities of salt diapirs. In addition to the Nordkapp Basin, the Tiddlybanken Basin which forms a corresponding salt basin located further southeast in the study area (NPD, 2013). The last structural elements, which also represent the eastern elevated high, is the Fedynsky High.

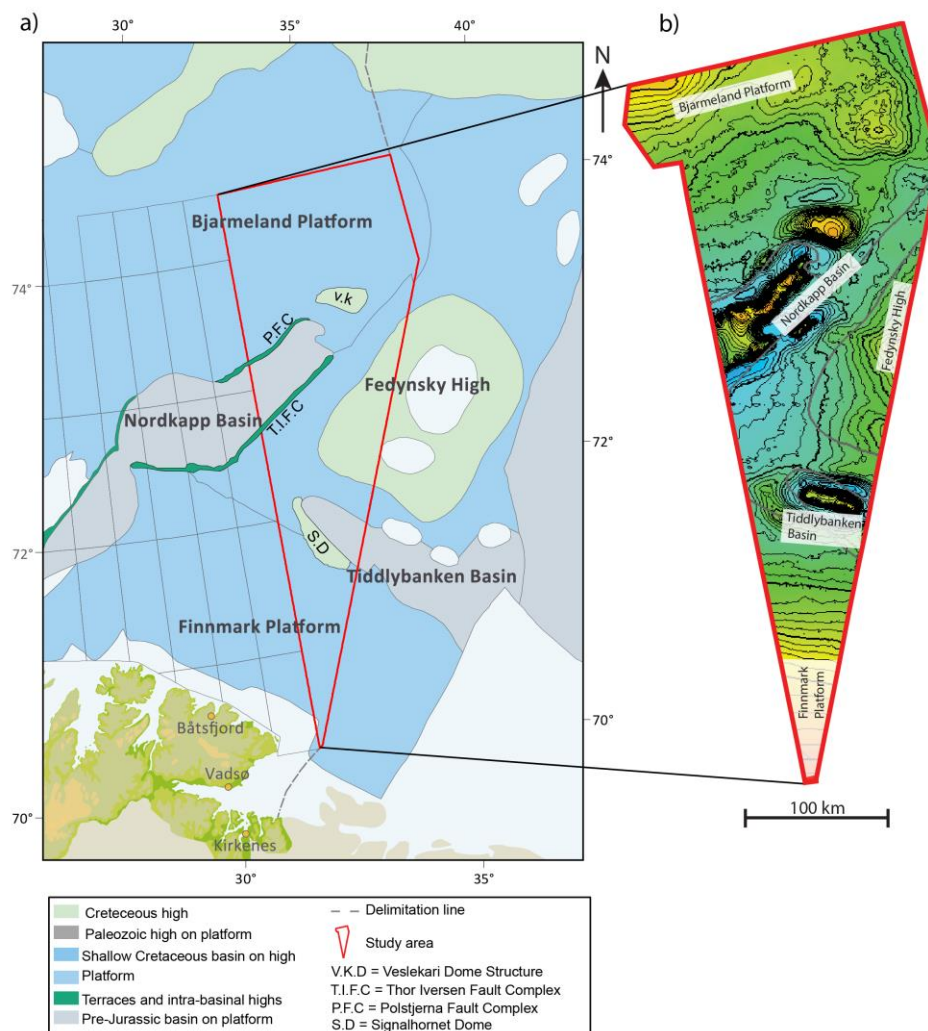


Figure 2-5. a) Overview map showing the structural framework in the Barents Sea southeast. b) Highlighted BCU surface, showing the five structural elements. Note salt diapirs within the Nordkapp and Tiddlybanken Basins. PFC=Polstjerna Fault Complex. T.I.F.C=Thor Iversen Fault Complex. V.K.=Veslekari Dome. S.D.=Signalhornet Dome. Figure modified from NPD (2013).

2.4.1 The Nordkapp Basin

The Nordkapp Basin is an elongated, fault-controlled (northeast-southwest) basin located in the southern part of the Barents Sea (Figure 2-5) (Larssen et al., 2002). The basin is bounded by the Bjarmeland Platform to the north and the Finnmark Platform to the south (Larssen et al., 2002). The size of the basin is approximately 300 km, and it is divided into two sub-basins (Bugge et al., 2002). The Nordkapp Basin is a salt-filled basin that formed as a Late Devonian-Early Carboniferous deep, subsidence basin (Gabrielsen et al., 1992; Bugge et al., 2002). The Tiddlybanken Basin is suggested to form a corresponding subsidence basin (NPD, 2013).

The initial sediment fill in the Nordkapp Basin has been suggested to represent coaly, alluvial, siliciclastic material which correspond to the Billefjorden Group (Bugge et al., 2002). Repeated rift episodes in the Carboniferous, associated with a climatic shift towards arid condition led to deposition of evaporates and conglomerates, which respectively can be correlated to the Ebbadalen Formation on Svalbard (Bugge et al., 2002). The overlying unit is of Permian age, and consists mainly of cool-water carbonates, siliciclastic and minor amount of cherts (Bugge et al., 2002).

The thickness variation in the Triassic successions in the Nordkapp Basin, indicate increased subsidence during the Spathian and Anisian age. It has been suggested that salt movements, which occurred due to initial diapirism and lateral flow to salt pillows, caused this (Bugge et al., 2002; NPD, 2013). The salt movements occurred in several rounds during the Triassic and Paleogene periods (NPD, 2013). However, perhaps the most pronounced episode which also is responsible for the present-day geometry of the salt, occurred during the Paleogene period (Bugge et al., 2002).

2.4.2 Tiddlybanken Basin

Tiddlybanken Basin is a subsidence basin located northeast of the Finnmark Platform, at 72°05' N, 32°40' E (Figure 2-5). The basin geometry and history is relatively unexplored, and as of present day, knowledge regarding its origin is limited. However, based on the present knowledge it is reasonable to assume that the basin have undergone more or less the same development as the Nordkapp Basin due to the presence of large amount of salt (Gabrielsen et al., 1990b). The presence of salt in the Tiddlybanken and the Nordkapp Basins, contributes to an overall elevated seabed compared the surrounding areas, hence a positive relief (NPD, 2013).

2.4.3 Finnmark Platform

The Finnmark Platform covers a large area extending from west Finnmark along the Varanger Peninsula and into the Russian sector (Figure 2-5) (NPD, 2013). The platform is bounded to the south by the outcrop of the Caledonides of the Norwegian mainland. The Troms-Finnmark Fault Complex and the Nordkapp Basin respectively define the western and northwestern boundaries (Gabrielsen et al., 1990a; Gabrielsen et al., 1990b). To the north, there is a sharp increase in depositional paleo-slope, where platform carbonates pass laterally into lowstand evaporates and deep-water facies of the Nordkapp Basin (Ehrenberg et al., 1998). The Finnmark Platform represents a structural element, which started to develop as a stable platform in Late Carboniferous time, and has been stable since the Late Paleozoic. The platform is assumed to be underlain by Paleozoic and Precambrian basement, probably affected by the Caledonian Orogeny (Gabrielsen et al., 1990b). In Late Carboniferous through Permian times, The Barents Sea was part of a vast province of carbonate-dominated deposition. The type area of this province was from the Canadian Arctic to the northern Russia. The Finnmark Platform is a segment of this province (Ehrenberg et al., 1998).

2.4.4 Bjarmeland Platform

The Bjarmeland Platform represents an area between the Hammerfest and Nordkapp Basins in the southern Barents Sea (Figure 2-5). The Sentralbanken and Gardarbanken Highs defines the northern boundary of the platform. The Fingerdjupet Subbasin and the Loppa High defines the western termination (Gabrielsen et al., 1990b). The Bjarmeland Platform was formed during the Late Carboniferous and Permian, and has been tectonically stable since the Late Paleozoic. The underlying basement is assumed to consist of Paleozoic and Precambrian rocks (Gabrielsen et al., 1990b). Subsequent Paleogene tectonism tilted the Paleozoic and Mesozoic sequences southwards; resulting in unconsolidated Pleistocene sediments overlying successively older rocks to the north (NPD, 2014b). Towards the south and west, the Bjarmeland Platform is divided into minor highs and sub-basins mainly influenced by salt tectonics (NPD, 2014b). In general, the Bjarmeland Platform is characterized by relatively few structures. However, the Platform extends into the northern part of the Barents Sea southeast, where a large structure has been undisturbed, resulting in a more or less intact sedimentary succession from the Permian to the Upper Jurassic succession (NPD, 2013).

2.4.5 Fedynsky High

The western flank of the Fedynsky High is located in the eastern part of the study area (Figure 2-5), with its bulk in Russian waters (NPD, 2013). The Fedynsky High is an inverted basin with a complex geological history. The highest point on the dome is located in the Norwegian sector. The continuation eastwards is more uncertain due to lack of data (NPD, 2013). Seismic investigation shows that the basement is orientated in a standing position on both sides of the basin, which give rise to gravitational and magnetic anomalies on the structure. The structural high is orientated in the same manner as the Tiddlybanken Basin, extending westwards towards the Nordkapp Basin (NPD, 2013). The seismic also reveals the presence of a deep graben that cuts into the Carboniferous and Permian successions on the Norwegian side. In addition, the Fedynsky High is characterized by extensive erosion. In fact, the entire sedimentary package above the base of Cretaceous (BCU) has been eroded (NPD, 2013).

2.4.6 Fault complexes

The Thor Iversen Fault Complex

The Thor Iversen Fault Complex is a prolongation of the Troms-Finnmark and Måsøy Fault Complexes and represents a regional deformation zone in the Barents Sea (Brønner et al., 2009). The Fault Complex has an overall east-west orientation, composed of faults with significant dip-slip components (Gabrielsen et al., 1990b). The fault complex, is suggested to have formed in Early Carboniferous with reactivations during Mesozoic and Cenozoic times (Gabrielsen et al., 1990b). The east-west offshore fault trend is suggested to exploit the Caledonian structural heritage (Brønner et al., 2009). The fault complex is located along the southeastern border of the Nordkapp Basin (Figure 2-5).

The Polstjerna Fault Complex

The Polstjerna Fault Complex represents the structural separation between the Bjarmeland Platform and the northeastern part of the Nordkapp Basin (Figure 2-5). The Polstjerna Fault Complex has an overall east/northeast-west/southwest orientation, composed of faults with significant dip-slip components (Mattingsdal et al., 2015). The fault complex is suggested to have formed during Middle Triassic to Cretaceous times, possibly related to halokinetic movements (Mattingsdal et al., 2015).

3 Database and Seismic data

The seismic interpretation of this study has been done in the Schlumberger software Petrel, 2016 version. Figures have been generated by the use of the graphic illustration programs Adobe Illustrator and Corel Draw. This study uses extensive two-dimensional seismic surveys; dataset NPD1201 and NPD-BA 11. The Norwegian Petroleum Directorate (NPD) acquired the seismic data during the summer season of 2011 (11 500 kilometers) and 2012 (6800 kilometers). Two-dimensional data was also acquired by the NPD back in the period 1974-1982, at the previous Norwegian-Russian boundary, where the two countries had common and overlapping interest. However, the quality of this data was variable. The coverage was low, and the data was collected in unsystematic orientations (NPD, 2013). The new seismic datasets are geologically located at the boundary between the Nordkapp Basin to the west, the Finnmark Platform to the south and the Fedynsky High and Tiddlybanken Basin to the east. The study area (Figure 3-1) comprises an area of approximately 12000km², with a total 2D-inline length of 500km orientated from north to south. The two seismic datasets comprises respectively of 41 and 57 inlines (Figure 3-2, Table 3-2).

In addition to the 2D-seismic data used within the study, a well located outside the study area was occasionally used. The main purpose of the well was to identify the Base Cretaceous Unit (BCU). The well is located on the Norsel High in the southeastern part of the Bjarmeland Platform area close to the southwestern margin of the Nordkapp Basin. The exploration well was drilled in 1987, as a wildcat exploration well by Statoil, with the purpose of reaching Lower Jurassic/Upper Triassic sandstones (NPD, 2011). The BARE-02 dataset was used in order to track the BCU from the well into the study area. Furthermore, no wells drilled within the study area were available or used for this study.

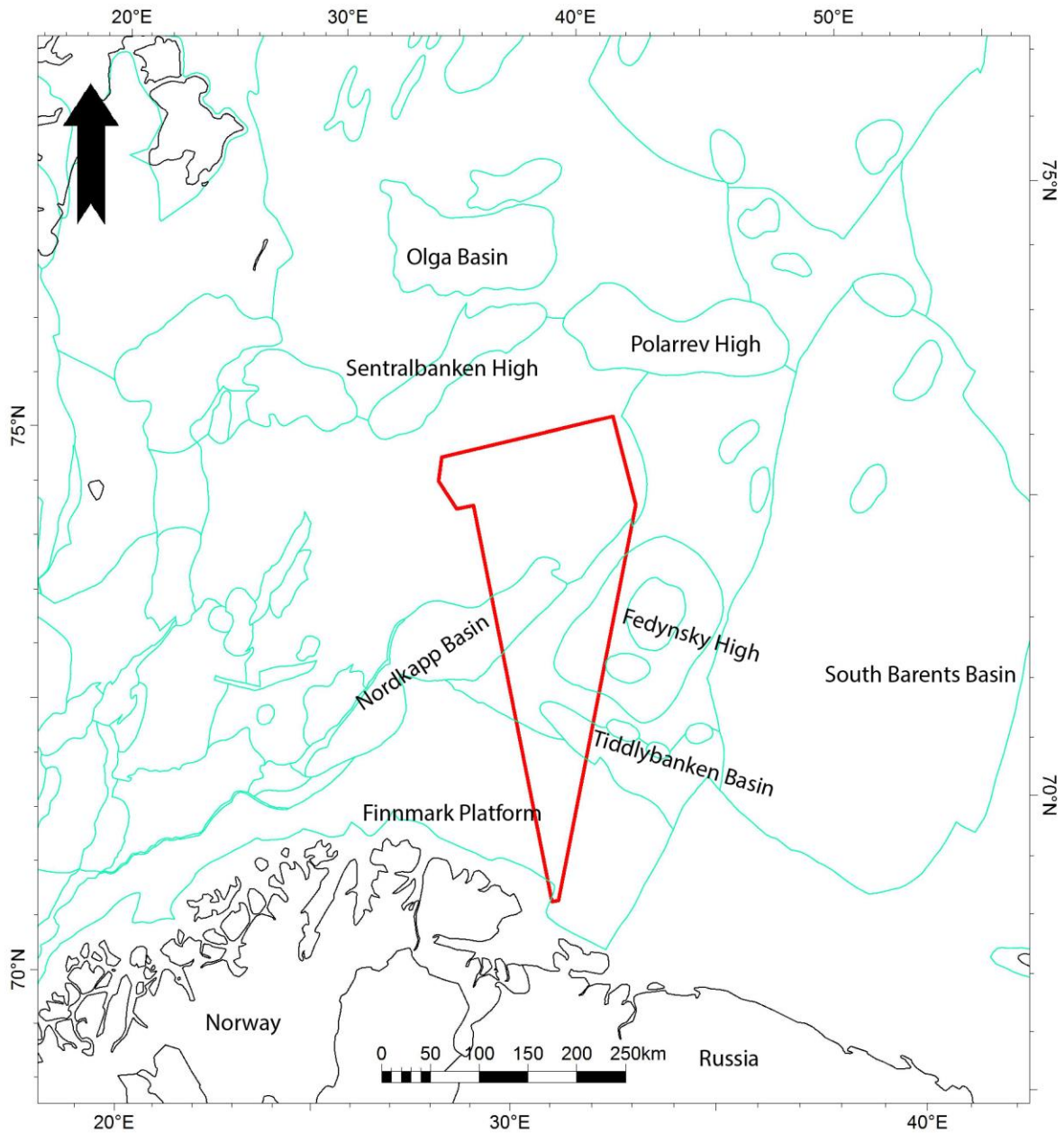


Figure 3-1. Location of the 2D-datasets, showed as red polygon. Selected structural elements are included as well.

General information regarding the two seismic datasets are listed respectively in Table 3-1, while technical information is described in Table 3-2. The seismic dataset collected in 2011, termed NPD- BA-11, was acquired by the use of Geostreamer technology, while the NPD 1201 was acquired by the use of conventional survey methods.

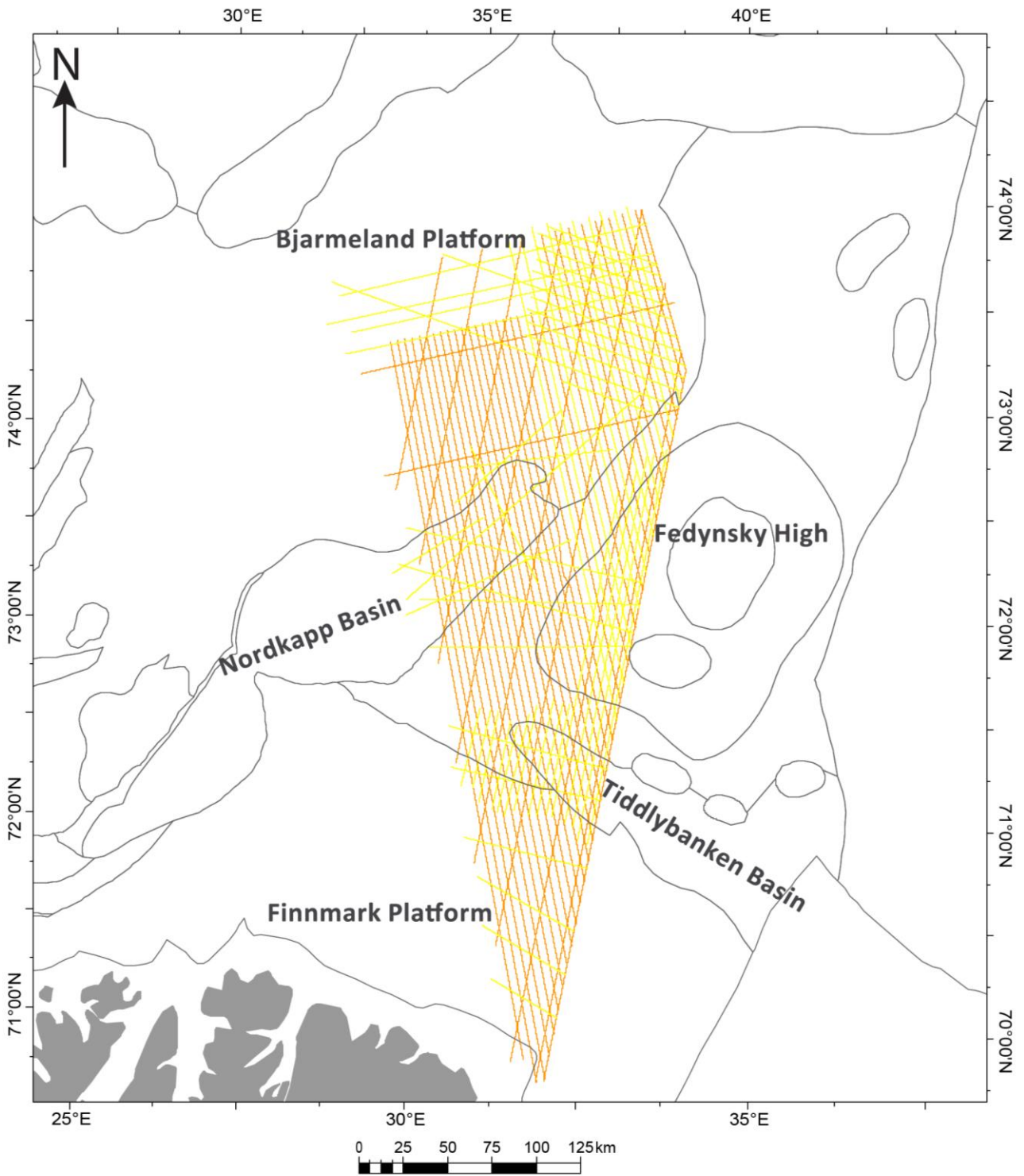


Figure 3-2. Data coverage of the two datasets used in the study. Orange lines represents NPD-BA-11. Yellow lines represents NPD 1201.

Table 3-1. Table showing information of the seismic surveys NPD BA-11 and NPD 1201.

Seismic survey information table					
Survey	Subtype	Company responsible	Acquisition company	Geodetic datum	Projection
NPD BA-11	2D	NPD	PGS Geophysical AS	ED50	35
NPD 1201	2D	NPD	Dolphin AS	ED50	35

Table 3-2. Table showing information regarding frequency, sample interval, number of inlines and polarities for each seismic survey used in the study.

Seismic survey	Dominant Frequency	Sample interval	Number of lines	Polarity
NPD BA-11	25 Hz	4	41	Zero phase
ND 1201	25 Hz	4	57	Zero phase

3.1 Seismic reflection theory

Based on the SEG standard for polarity (Veeken, 2007), the survey is processed to a zero-phase signal with normal polarity (Figure 3-3a). The distance between each trace (line interval) was found in Petrel, by the wiggle display (Figure 3-3) and is approximately 25m. Zero-phase pulses is a product of wavelet processing often used in seismic mapping. It consists of a central peak and two side lobes (troughs) with the opposite sign and lesser amplitude. The boundary is located at the central peak, and not at the wavelet onset as in the case for minimum-phase signals (Brown, 1999).

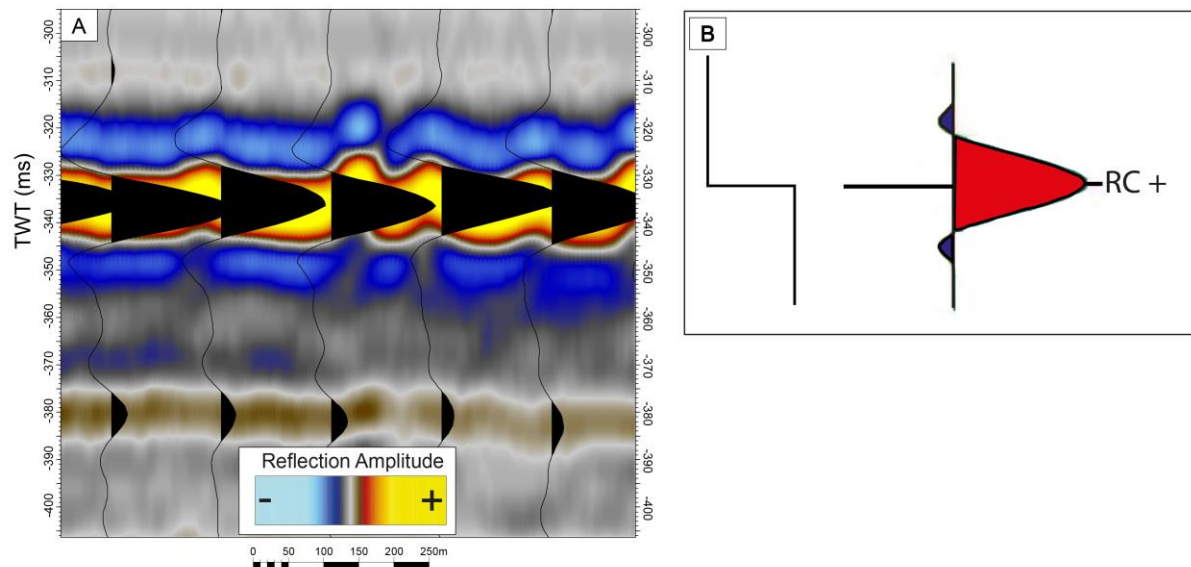


Figure 3-3. Seismic intersection window displaying the seafloor wiggle reflection in the NPD-1201 dataset. B) Simplified model of the seismic trace based on a zero phase signal with normal polarity (SEG polarity). Notice that in this thesis positive amplitudes are yellow, while negative amplitudes are displayed in blue.

3.1.1 Seismic resolution

Both the vertical and horizontal resolution for the dataset have been calculated, in order to determine what the data is expected to show in depth. The resolution determines how large objects need to be, in order to be detected/observed in the seismic.

3.1.2 Vertical resolution

Vertical resolution is given by the following equation:

$$Vr = \frac{\lambda}{4}$$

In order to provide an estimation of the vertical resolution for the seismic data used in this study, both frequency and acoustic velocity values were necessary. The wavelength is given by the formula of velocity divided by frequency;

$$\lambda = \frac{v}{F}$$

Due to the lack of well-data within the study area, the true velocity of the layers was not obtained. Instead, an assumption of increasing velocity with depth was done, which is normally the case within the earth's lithosphere (Kearey et al., 2002). The velocity values were picked with respect to the recorded interval velocity of the Lower Cretaceous identified by Richardsen et al. (1993). Richardsen et al. (1993) suggested an interval velocity of approximately 2800m/s for the Kolmule Formation in the Lower Cretaceous. Therefore, two velocities, 2500m/s and 3500m/s, were used to calculate the wavelength in this study.

The frequencies for each of the sequences can be identified in Petrel. A cropped seismic section for each sequence was obtained by use of the "virtual cropped volume". Further on, the spectral analysis informal tool was used to determine the dominating frequencies within each sequence (Figure 3-4). The dominating frequencies used is a mean value, of the dominating frequency peaks for each sequence, and is summarized in Table 3-3.

3.1.3 Horizontal resolution

In order to calculate the horizontal resolution of the data within the study, the velocity, two-way-traveltime and frequency were necessary. The corresponding frequency and velocity properties used for calculating the vertical resolution were used (Table 3-3). The horizontal resolution was calculated as the radius of the Fresnel zone, hence, features in the subsurface with a lateral extend which exceeds the Fresnel zone will be visible in seismic sections. The following equation was used to calculate the radius of the unmigrated Fresnel zone:

$$rf = \frac{v}{2} \sqrt{\frac{t}{f}}$$

Where,

rf = the radius of the Fresnel zone (m)

v = average propagating speed of the incident wave (m/s)

t = two-way travel time in seconds (TWT)

f = frequency (Hz)

The calculated results is presented in Table 3-3.

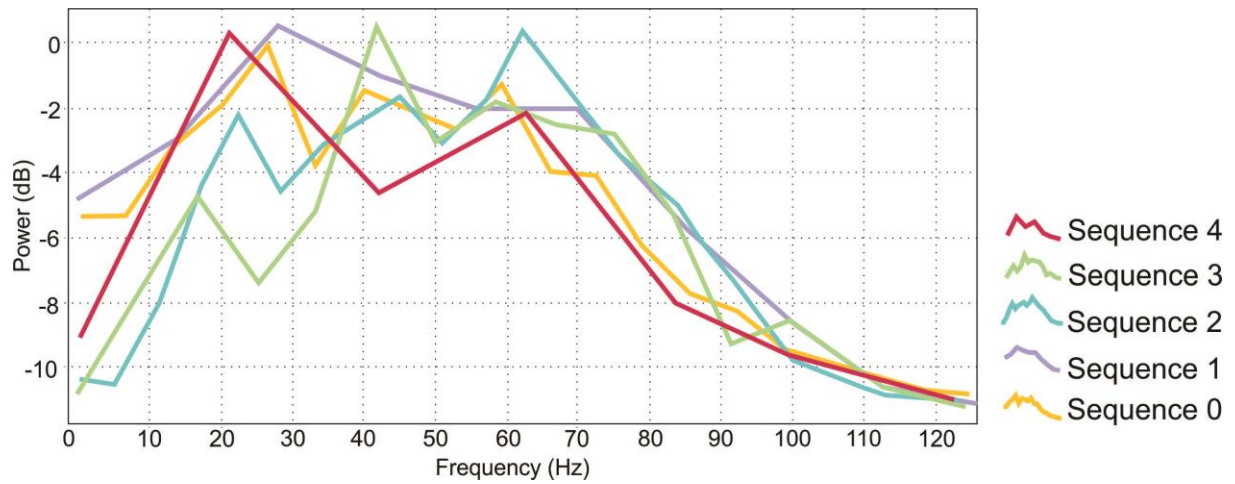


Figure 3-4. The frequency spectra for each sequence shown in Hertz. The dominating frequencies have been identified as a mean value of the given peaks for each sequence.

Table 3-3. Calculated resolutions and wavelengths for the different sequences identified in the dataset.

Sequence	Velocity	Frequency	Wavelength (v/f)	Vertical resolution	Horizontal resolution
S4	2500 m/s	52.5 Hz	47.61m	11.90m	385m
S3	2500 m/s	51.0 Hz	49.01m	12.25m	437m
S2	3500 m/s	50.5 Hz	69.30m	17.32m	665m
S1	3500 m/s	41.5 Hz	84.33m	21.08m	805m
S0	3500 m/s	32.0 Hz	109.37m	27.34m	988m

The calculated values in Table 3-3 shows a dominating pattern of decreasing frequencies with depth, increasing wavelengths with depth, and a poorer vertical and horizontal resolution with depth (increase in meters). The calculated values is merely an approximation to the real resolutions, and represent only one outcome of many possible solutions. Nevertheless, it demonstrates how the dominating frequencies and velocities within layers affect the resolution with increasing depths (Figure 1-1).

3.2 Estimation of clinoform geometry

Pythagoras' Theorem describes the mathematical relation between three sides of a right-angled triangle (Geldand & Saul, 2001). The theorem is used to investigate the geometrical parameters of clinoform foresets (Figure 3-5). It is possible to find an unknown angle, given the lengths of two sides. The seismic velocity has been estimated, as previously discussed, since no seismic velocity can be determined due to the lack of well data within the study area. The chosen interval velocities were respectively 2500 ms (TWT) and 3500 ms (TWT). The distance x (Figure 3-5) is determined by the use of "measure tool" in the Petrel software. An overview of clinoform geometry identified in the survey is presented in Table 4-1.

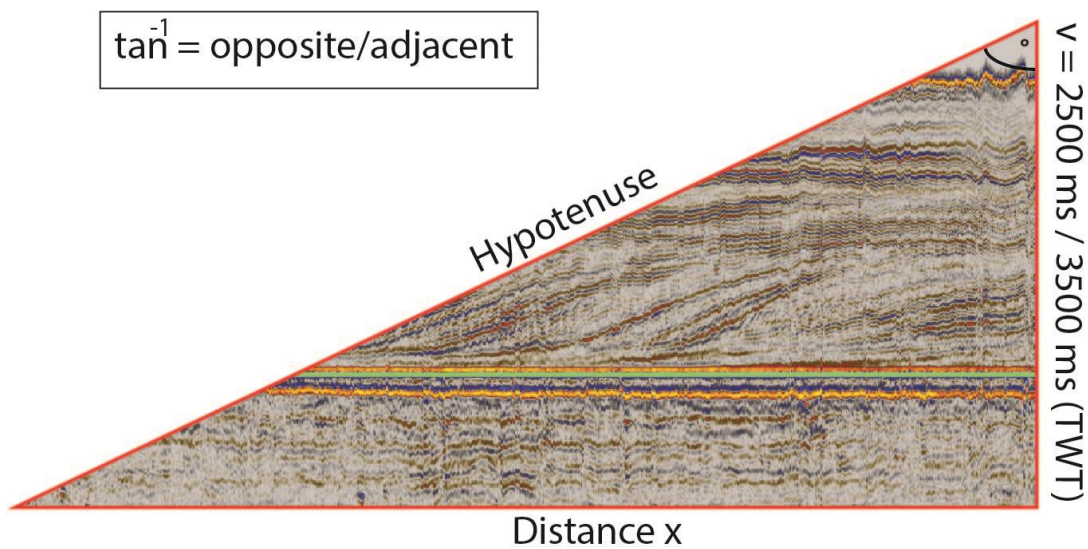


Figure 3-5. Simplified illustration showing Pythagoras's Theorem applied in seismic interpretation.

4 Results

The results are presented in a chronological order, beginning with seismic well tie. This is followed by a presentation of the intra Cretaceous horizons, which forms the basis for the interpretation of sequences within the Cretaceous package. Afterwards, the result chapter describe five sequences, which are explained in detail. Emphasize is given to the clinoforms located in the different sequences. Lastly, the estimated clinoform geometries are presented.

4.1 Seismic well-tie

The Cretaceous package has correlated well 7226/11-1, which is located at the Norsel High, outside the study area. The Hekkingen Formation is interpreted by using the stratigraphic boundaries of well tops from the NPD. Figure 4-1 show the seismic tie from well 7226/11-1, following the dataset BARE-02 northeast and into the survey area.

4.2 Intra Cretaceous horizons

The extent and volume of the Cretaceous package in the southeastern Barents Sea has been investigated based on six different horizons covering specified areas in the survey area (Figure 4-2). The horizons are selected based on amplitude characterization, horizon continuity and where clinoforms are identified in the study area.

To establish a chronostratigraphic framework, five sequences (S0-S4) bounded by the medium- to high amplitude seismic markers were defined. These seismic markers may represent possible flooding surfaces (K0-K4). Flooding surfaces are considered as good markers, because of the lateral continuity (Marin et al., 2016). These seismic markers delimit the Cretaceous package into seismic subunits that possibly can be related to changes in depositional environment. Clinoforms is extensively used to understand the filling and development of basins. The geometry of clinoforms present within the sequences can provide information about sea level fluctuations, process regimes, grain size and sediment supply. By combining the provided information, a reconstruction of original depositional environment can be done (Marin et al., 2016).

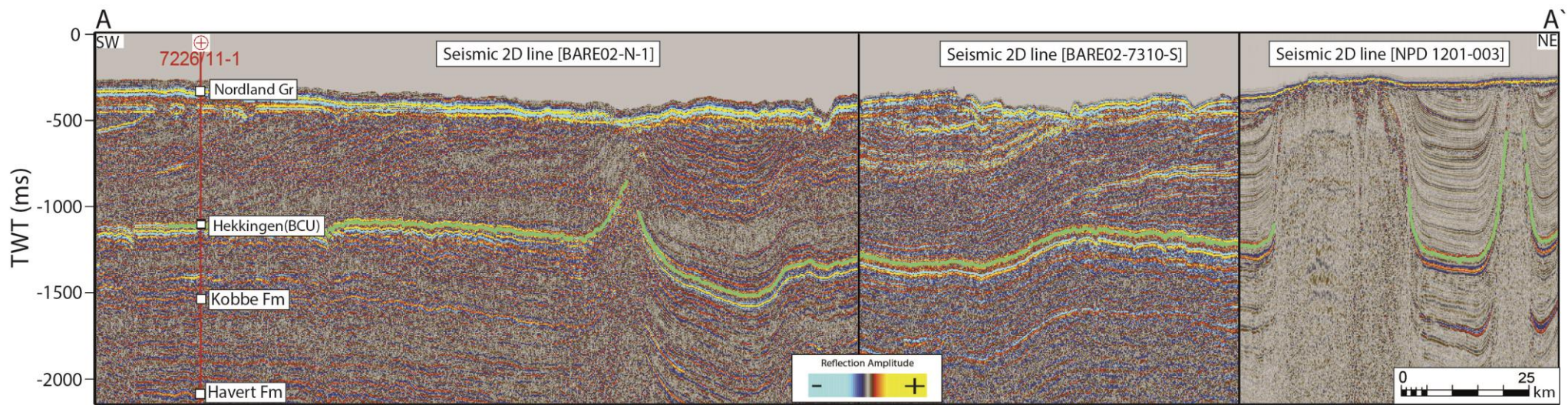
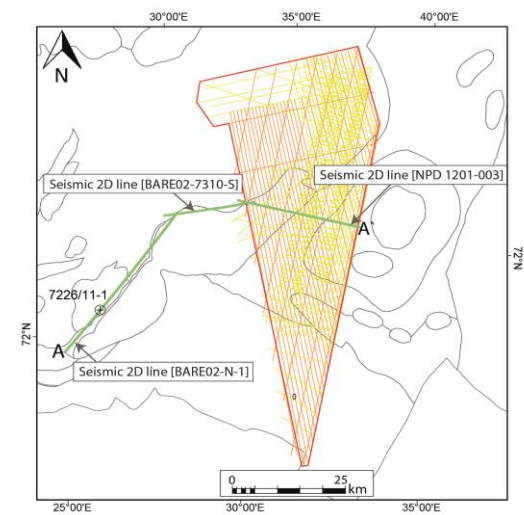


Figure 4-1. Seismic tie from well 7226/11-1. Hekkingen Formation is highlighted in green color.



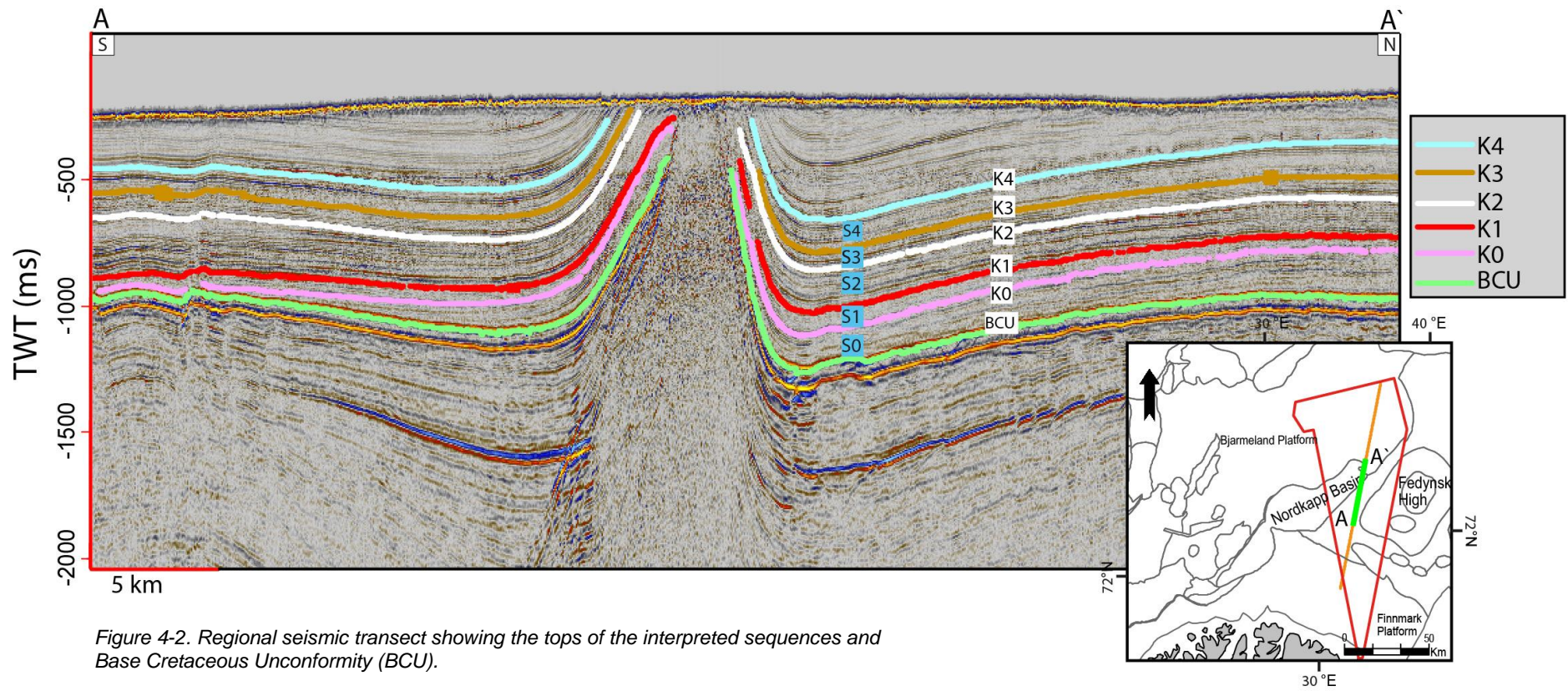


Figure 4-2. Regional seismic transect showing the tops of the interpreted sequences and Base Cretaceous Unconformity (BCU).

Top Hekkingen Formation (BCU) horizon

The top Hekkingen Formation (BCU) horizon represents the boundary between younger overlying Cretaceous sediments and underlying older Jurassic sediments. The BCU horizon is characterized by a high amplitude with a negative reflection coefficient. The horizon is continuous, which enables mapping of the horizon throughout the entire study area. The horizon depth varies between 0 and 1400 ms (TWT). The horizon is intersected by salt diapirs that reach up to the present seafloor in the Nordkapp Basin. Minor faulting on the platform areas affects the horizon, while larger throws are identified adjacent to salt diapirs along the margins of the Nordkapp Basin.

Horizon KO

The KO horizon represents the top of the seismic sequence SO. The horizon has a low- to medium amplitude with a positive reflection coefficient. North of the Nordkapp Basin, the horizon appears as semi-continuous, while it becomes discontinuous further southeast. The horizon depth varies between 200 and 1400 ms (TWT). The horizon onlaps towards salt diapirs within the Nordkapp Basin, and downlaps southeast of the Nordkapp Basin onto the BCU.

Horizon K1

The K1 horizon represents the top of the seismic sequence S1. It is characterized by a medium- to high amplitude, with a negative reflection coefficient. The horizon is generally continuous, while it becomes discontinuous southeast of the Nordkapp Basin. The horizon depth varies between 200 and 1200 milliseconds (TWT). The horizon downlaps onto the BCU near Tiddlybanken Basin in southwest, and onlaps towards salt diapirs in the Nordkapp Basin.

Horizon K2

The K2 horizon represents the top of the seismic sequence S2. It is characterized by a medium-to high amplitude, with a positive reflection coefficient. The horizon pattern is generally continuous from the northern parts of the Nordkapp Basin, while it becomes discontinuous towards platform areas adjacent to the Fedynsky High. The horizon depth varies between 300 and 1200 milliseconds (TWT). The K2 horizon downlaps onto the Hekkingen Formation (BCU) near the margin of the Tiddlybanken Basin, and onlaps onto salt diapirs in the Nordkapp Basin.

Horizon K3

The K3 horizon represents the top of the seismic sequence S3. The horizon displays medium-to high amplitudes, with a negative reflection coefficient. The horizon is continuous, but deviates northwest of the Nordkapp Basin where it appears to be semi-continuous with lower amplitude. The depth of the horizon varies between 200 and 1200 ms (TWT). The horizon downlaps onto the BCU south of the Tiddlybanken Basin, near the Finnmark Platform. Onlap termination towards salt diapirs in the Nordkapp and Tiddlybanken Basins is common.

Horizon K4

The K4 horizon marks the top of the seismic sequence S4, which makes it the shallowest horizon. It is characterized by a medium to high amplitude, with a positive reflection coefficient. The horizon is continuous and varies in depth between 200 and 1100 ms (TWT). The horizon downlaps onto the BCU near the Finnmark Platform, and onlaps onto salt diapirs in the Nordkapp Basin and the Tiddlybanken Basin.

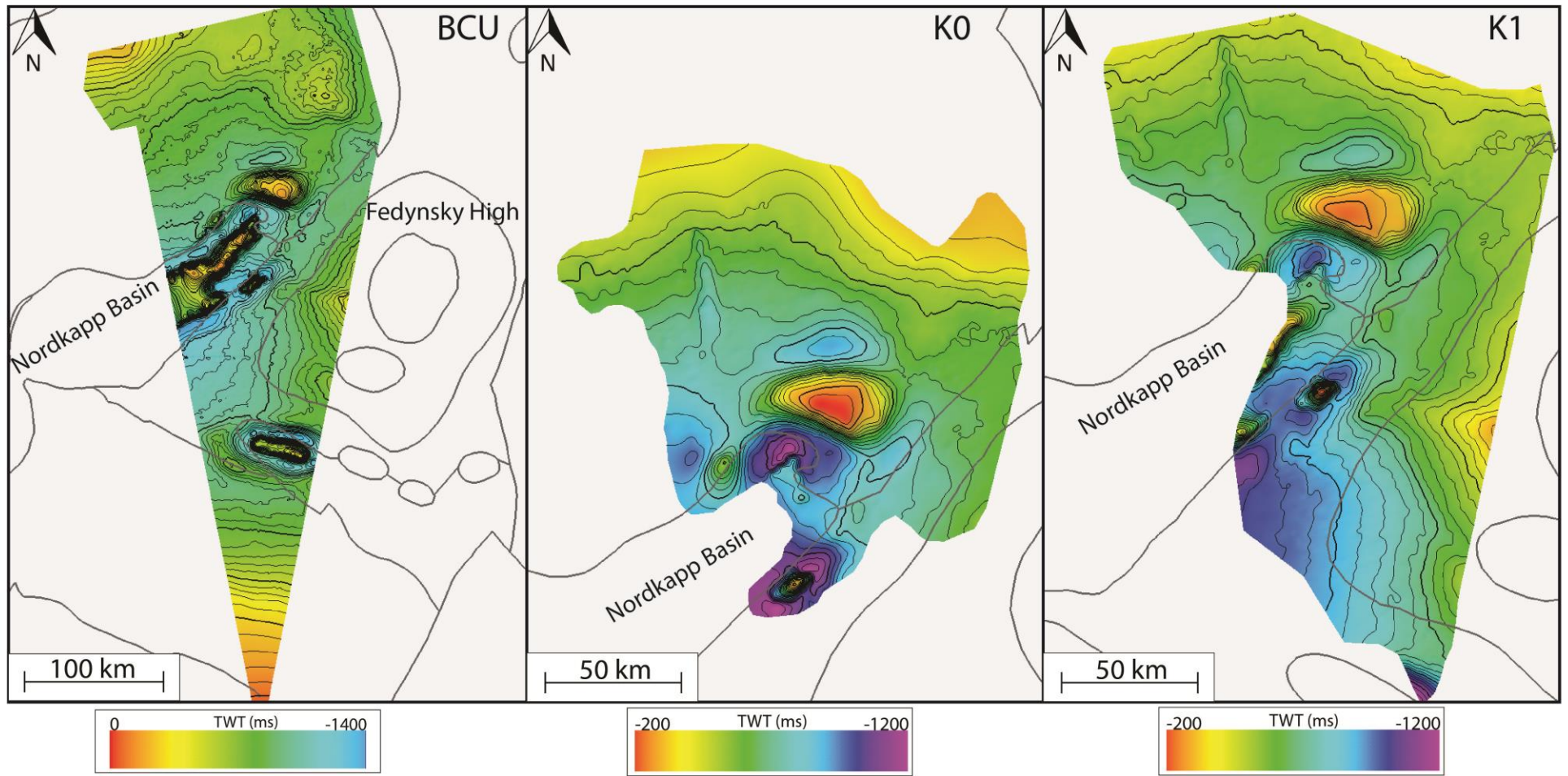


Figure 4-3. Time ms (TWT) maps of the surfaces generated from the interpreted horizons. From left: BCU, K0 and K1

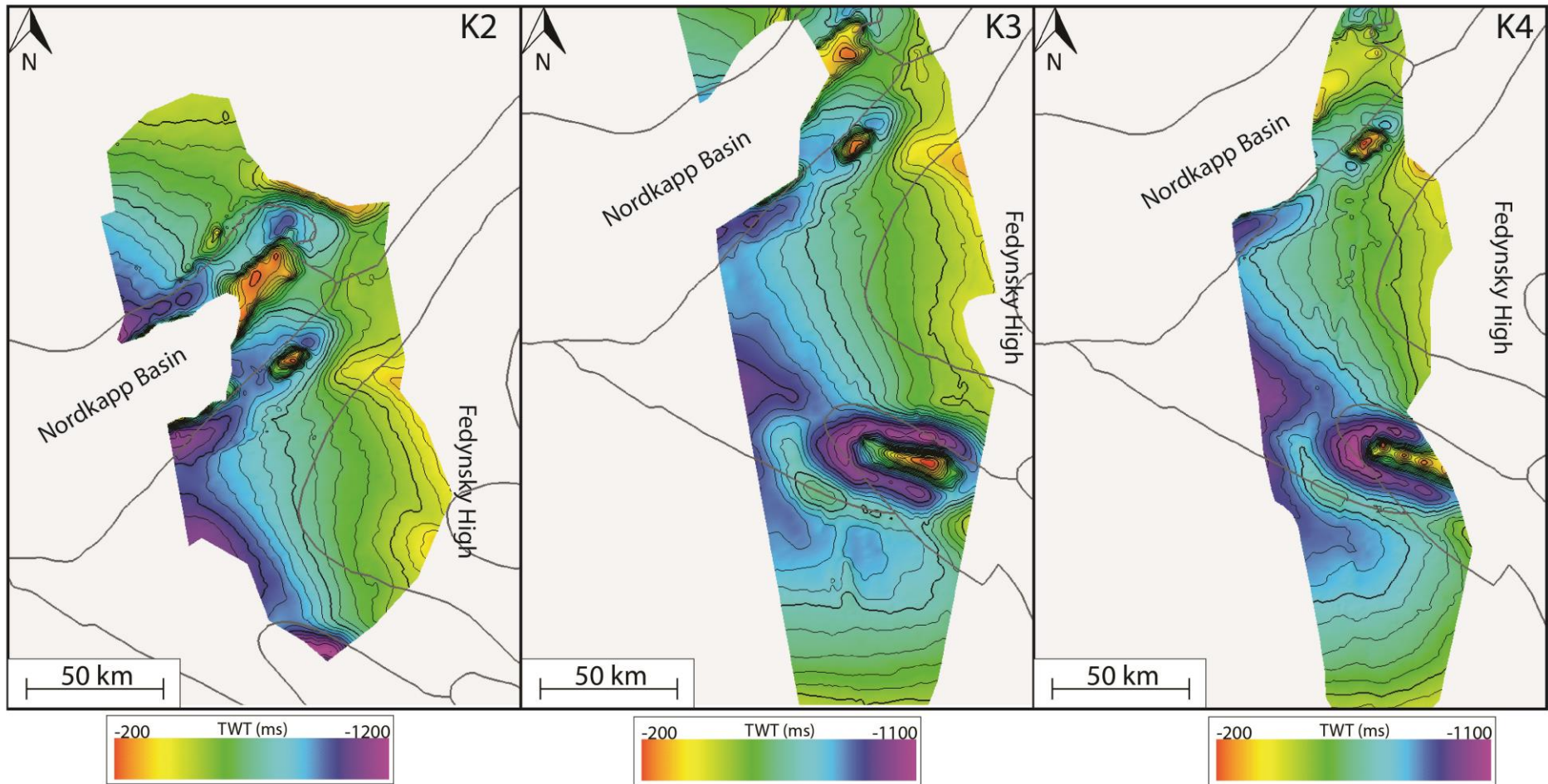


Figure 4-4. Time ms (TWT) maps of the surfaces generated from the interpreted horizons. From left: K2, K3 and K4

4.3 Seismic sequence description

In the following section, a presentation of five thickness maps for the S0-S4 sequences are given, which are bounded by the interpreted horizons (BCU-K4). Clinofolds within each sequence are consecutively described. Lastly, the distributions of the clinofolds within the study area is presented (Figure 4-16).

4.3.1 Sequence 0 (S0)

S0 consists of continuous to semi-continuous internal reflections, characterized by low- to medium amplitudes. Individual chaotic reflections are observed in the northeast. The thickness of this sequence increases northeast towards the Fedynsky High (Figure 4-5). The Polstjerna Fault Complex is located within the sequence around the western margin of the Nordkapp Basin, where a maximal throw of 180 ms (TWT) was observed. The Veslekari Dome truncates the sequence northeast of the Nordkapp Basin. Rim synclines are observed north and southeast of the dome structure. The sequence displays seismic reflections that onlap against dominating salt diapirs in the Nordkapp Basin.

Clinofolds have been identified in two different locations in sequence 0. Clinofolds that prograde from northeast towards southwest are observed north of the margin of Fedynsky High (Figure 4-6), and have been termed S0₁ in Figure 4-16. The clinofolds identified here are characterized as high relief (110-250 ms TWT) sigmoid, with foreset angles of 0.7-1° (Table 4-1). The height of the clinofolds increases southwestwards, reaching a maximum height of approximately 250 ms (TWT), before the clinofolds downlap onto the BCU horizon. The trajectory is flat to slightly ascending (Trajectories chapter 1.2.9).

Clinofolds that prograde from north towards south are identified in the extension of the rim synclines south of the Veslekari Dome structure (Figure 4-7), and have been termed as S0₂ in Figure 4-16. They show high relief (108-170 ms TWT) sigmoid geometries, with foreset angles of 0.9-1.2°. The height of the clinofolds increases southeastwards to a maximum height of approximately 170ms (TWT), before the clinofolds downlap onto the BCU horizon. The trajectory is flat to ascending.

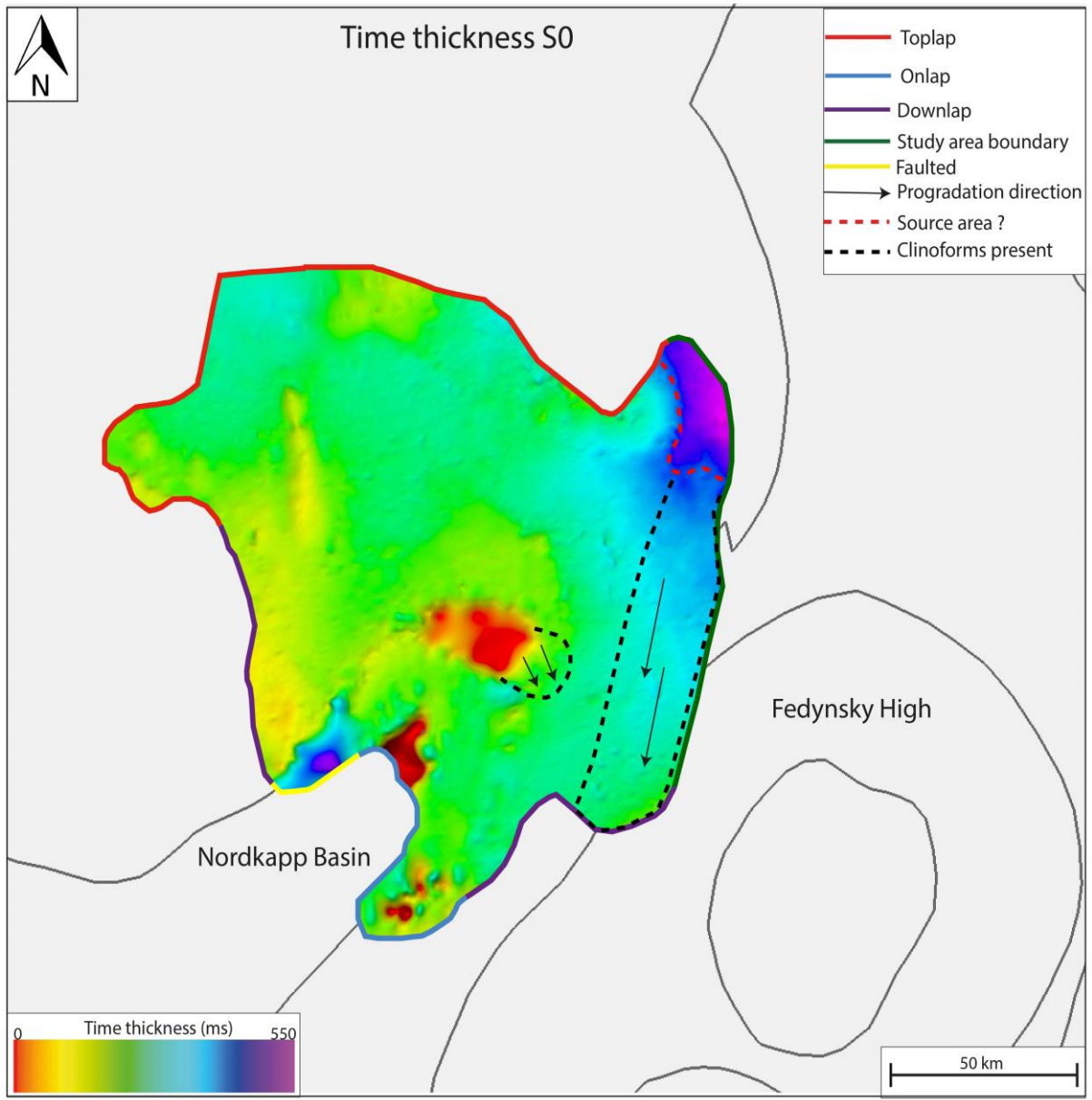


Figure 4-5. Time thickness map of sequence S0. Terminations displayed in different colors. Location of the clinoforms are marked with black dashed line. Red dashed indicate a possible sediment source area. Black arrows indicate progradational direction.

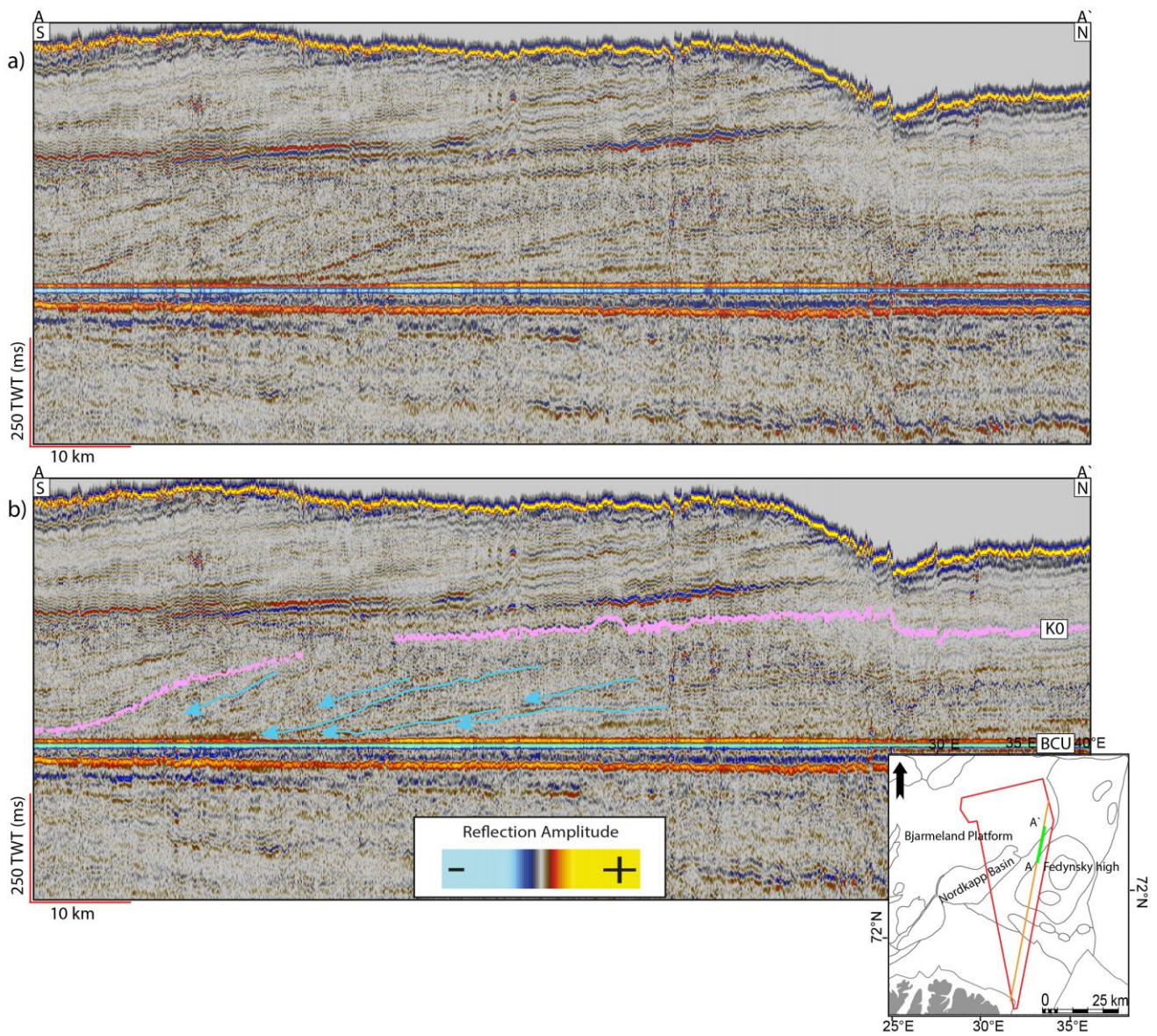


Figure 4-6. a) Uninterpreted seismic section near the margin to Fedynsky High flattened to the BCU. B) Interpreted seismic section showing high-relief sigmoidal clinoforms in sequence S0, with low gradient foresets.

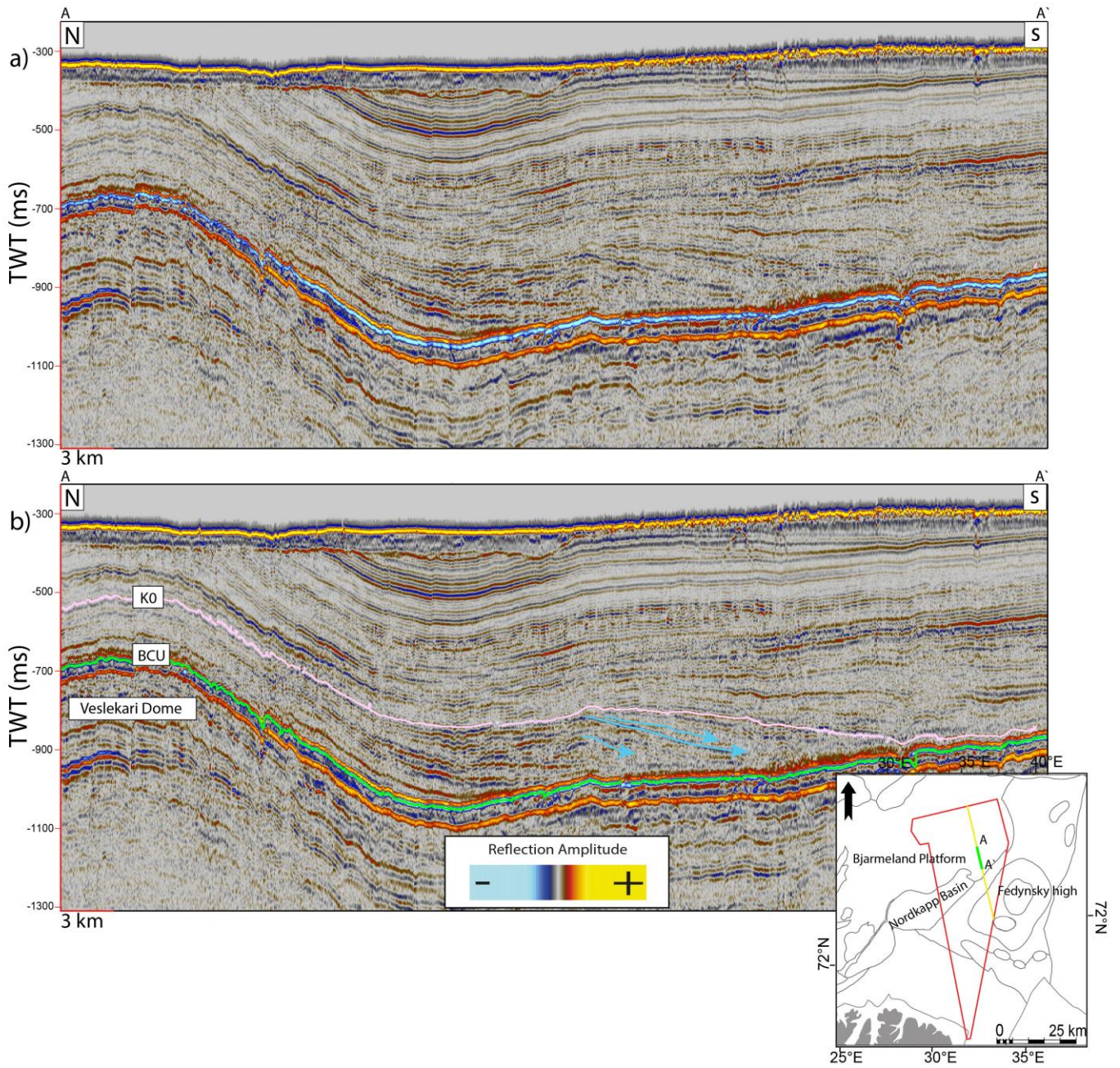


Figure 4-7. a) Uninterpreted seismic section near the Veslekari Dome structure. b) Interpreted seismic section showing high-relief sigmoidal clinoforms in sequence S0, with low gradient foresets.

4.3.2 Sequence 1 (S1)

S1 shows continuous to semi-continuous reflections, characterized by low- to medium amplitudes (Figure 4-9). The sequence has a relatively uniform thickness distribution, but an increase in thickness is observed northwest of the Nordkapp Basin and southeast near the margin of Fedynsky High (Figure 4-8). As for sequence 1, the Veslekari Dome truncates the sequence northeast of the Nordkapp Basin. The Polstjerna Fault Complex cuts through the sequence with significant dip-slip components. The interpreted Upper Regional Unconformity (URU) truncates the northern part of the sequence.

Clinoforms that prograde from northwest towards southeast are identified south of the Veslekari Dome Structure. They have high relief (92-220 ms TWT) sigmoid geometries, with foreset angles of 0.9-1.3° (Table 4-1). The height of the clinoforms increases southeast, before they downlap onto the BCU horizon. The trajectory is hard to estimate, due to the chaotic reflections. However, the trajectory appears to be slightly ascending.

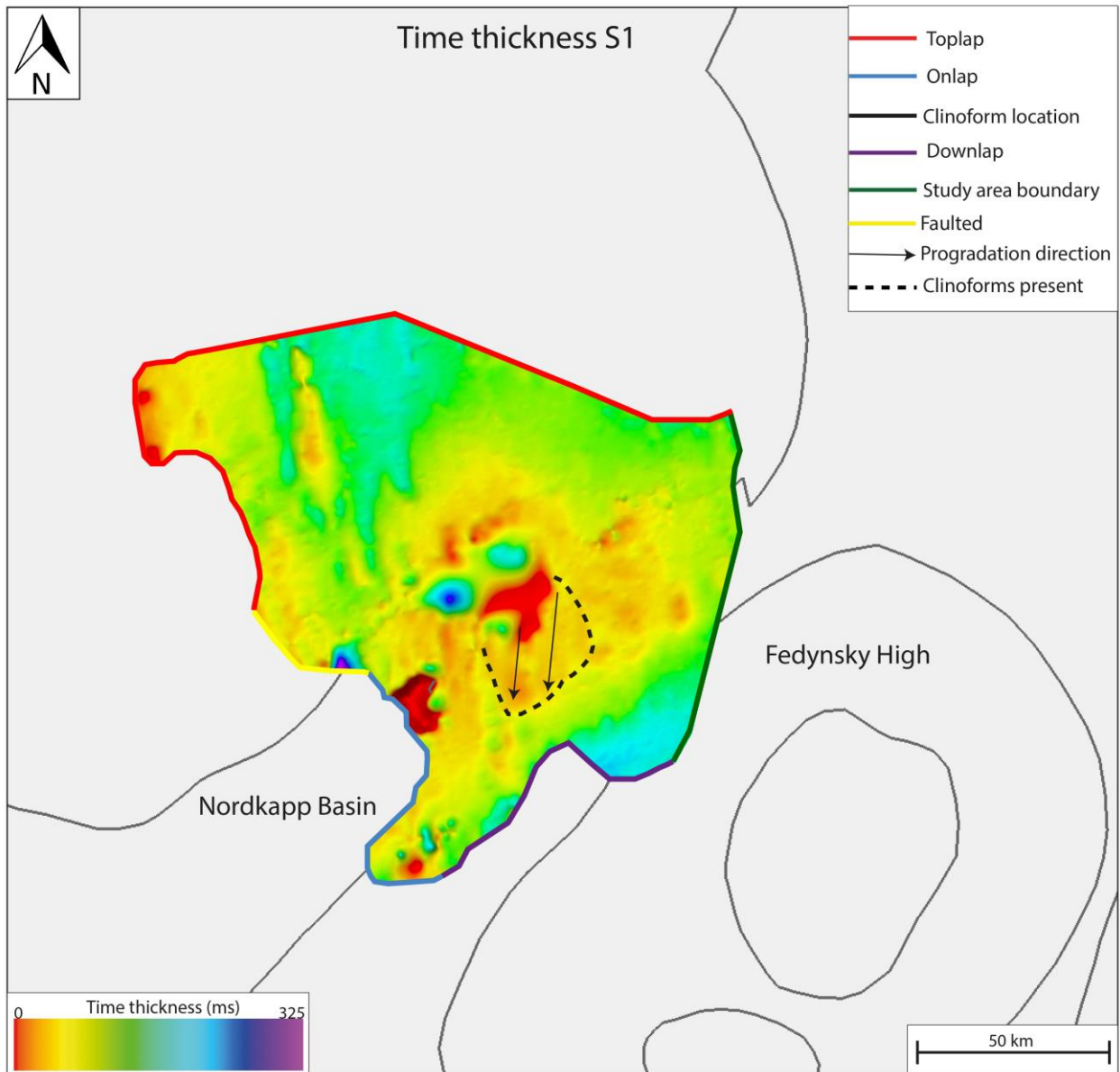


Figure 4-8. Time thickness map of sequence S1. Stratal terminations are illustrated with different colors, and location of clinoforms are marked with black dashed lines

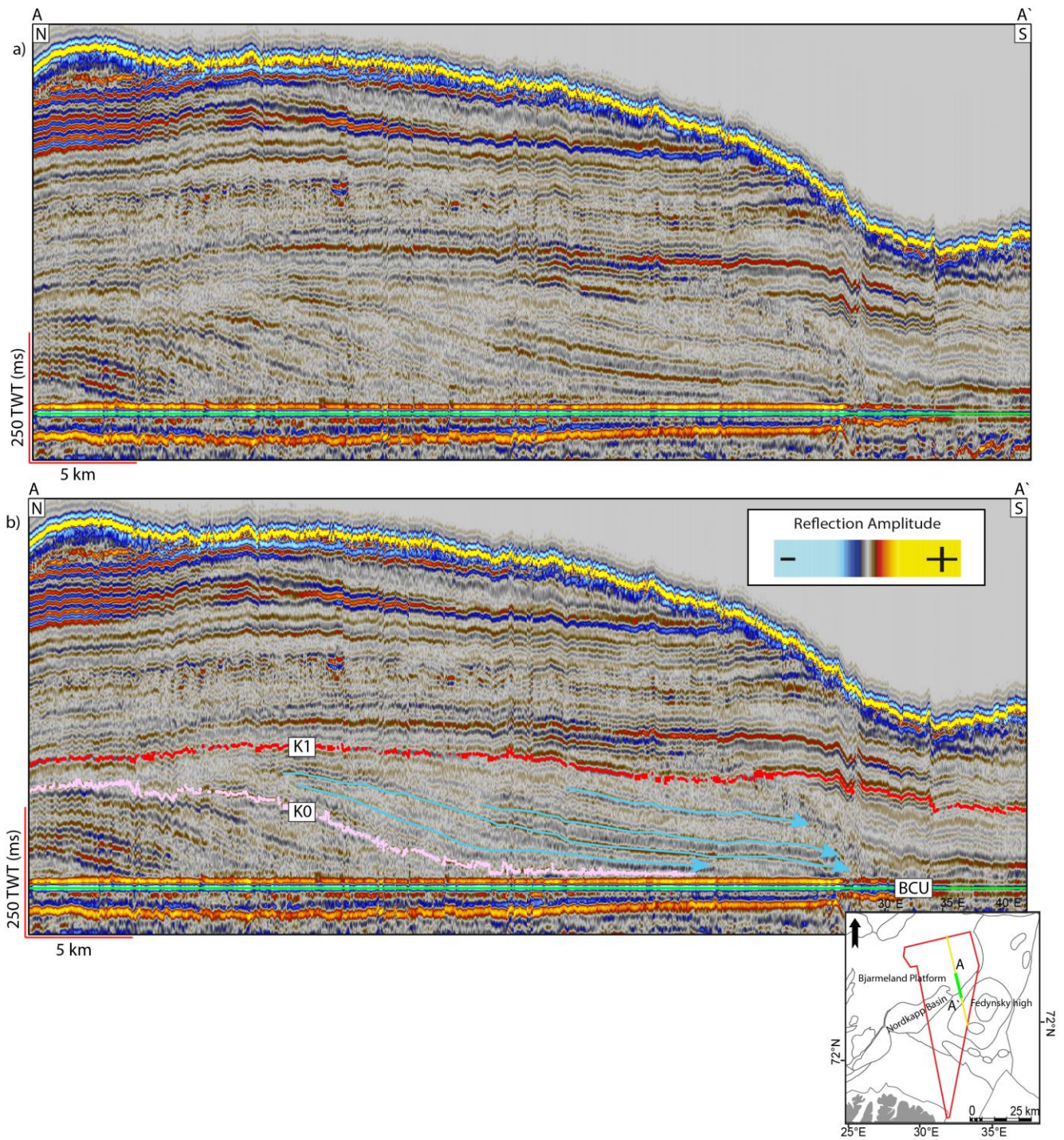


Figure 4-9. a) Uninterpreted seismic section crossing the flank of Fedynsky High flattened to the BCU. b) Interpreted seismic section showing high-relief sigmoidal clinoforms in sequence S1, with low gradient foresets.

4.3.3 Sequence 2 (S2)

S2 shows mainly continuous seismic reflections, characterized by medium- to high amplitudes (Figure 4-11). The sequence displays some semi-continuous reflections associated with salt diapirs in the Nordkapp Basin. The thickness of this sequence increases southwards, towards a possible depocenter located between the Nordkapp Basin and the Fedynsky High (Figure 4-10). The Thor Iversen Fault Complex cuts through the sequence around the eastern margin of the Nordkapp Basin, where throws up to 50 ms (TWT) have been identified. In addition, the Polstjerna Fault Complex is located in the western part of the sequence and the Veslekari Dome structure truncates the sequence northeast of the Nordkapp Basin.

Clinoforms that prograde from northeast towards southwest have been identified north of the Tiddlybanken Basin, between the Nordkapp Basin and the Fedynsky High. The identified clinoforms display high relief clinoforms (50-260 ms TWT). The proximal and northern part of the clinoforms show gentler foresets, with a sigmoid geometry and foreset angles of 0.7-0.8°. The distal and southern part of the clinoforms, display steeper-dipping foresets hence representing an oblique geometry with angles of 0.8-1.1° (Table 4-1). The height of the clinoforms increases southwest, reaching a maximum height close to 260ms (TWT). The trajectory is ascending, and the clinoforms downlap onto the BCU horizon north of the Tiddlybanken Basin.

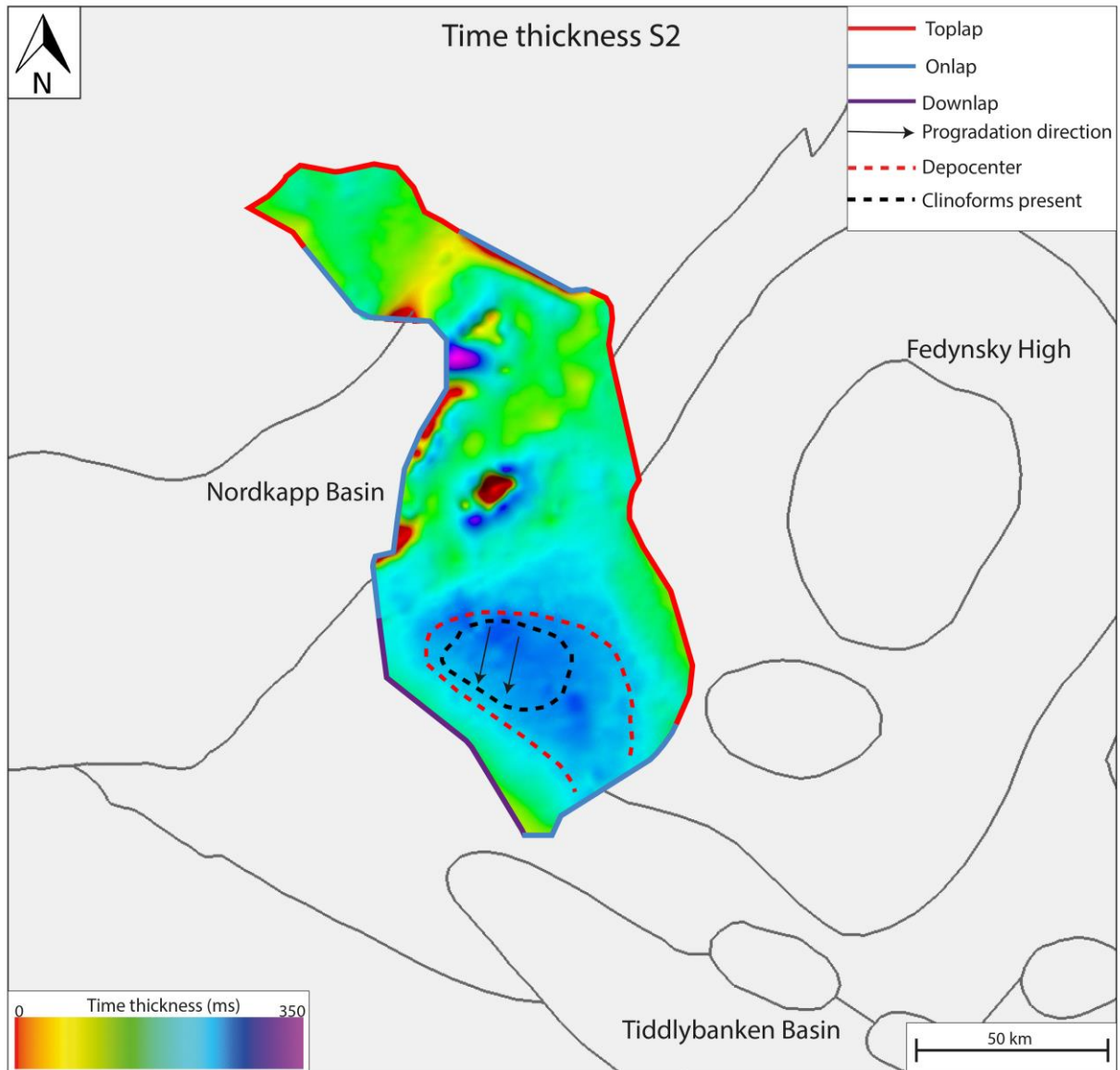


Figure 4-10. Time thickness map of sequence S2. Stratal terminations are illustrated with different colors, and location of clinoforms and depocenter are marked with black and red dashed lines.

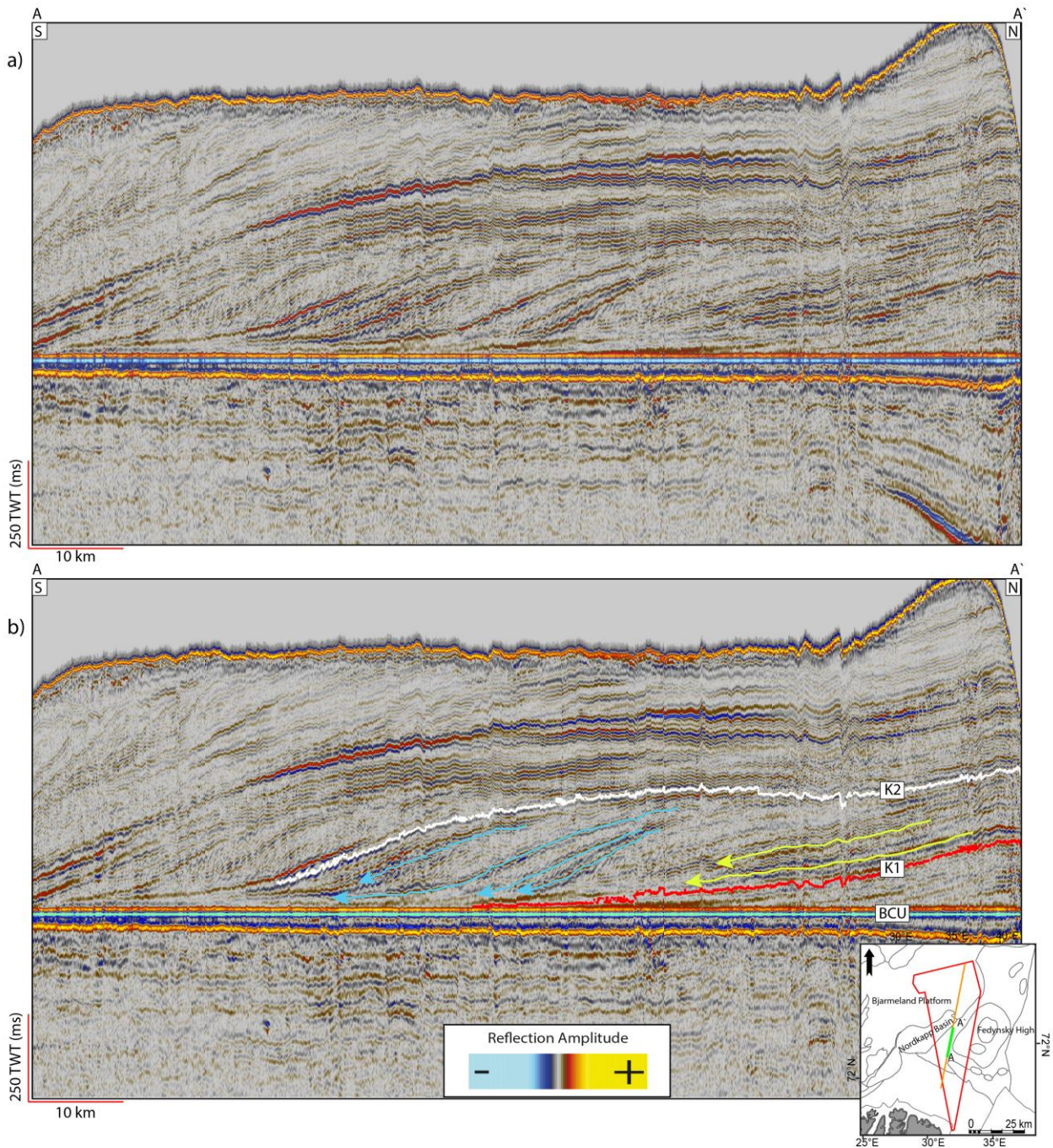


Figure 4-11. a) Uninterpreted seismic section crossing the northeastern margin of the Nordkapp Basin, flattened to the BCU. b) Interpreted seismic section showing high relief sigmoid clinoforms in the northern parts (yellow), and parallel oblique clinoforms towards the south (blue) within the S2 sequence.

4.3.4 Sequence 3 (S3)

S3 shows continuous to semi-continuous reflections characterized by low- to medium amplitudes (Figure 4-13). Some sporadic high amplitude reflections can be observed around the western margin of the Nordkapp Basin and within clinoforms. The thickness of this sequence is relatively homogenous in the eastern part of the study area. However, the sequence displays an increase in thickness southeast and northwest of the Nordkapp Basin (Figure 4-12). The Polstjerna Fault Complex is also present in this sequence around the western margin at the Nordkapp Basin. Additionally, the sequence is truncated by the Veslekari Dome structure. The Upper Regional Unconformity (URU) marks the northern part of the sequence, while the southern part of the sequence onlap onto the Signahornet Dome structure in the Tiddlybanken Basin.

Clinoforms that prograde from northeast towards southwest have been identified north of the Tiddlybanken Basin, between the Nordkapp Basin and the Fedynsky High. Clinoforms in sequence 3 are characterized by high relief (60-180 ms TWT) sigmoid geometries. They display foreset angles of 0.7-0.8° (Table 4-1). The height of the clinoforms increases southwestwards, reaching a maximum height of approximately 250 ms (TWT), before the clinoforms onlap onto the Signahornet Dome structure. The trajectory is ascending.

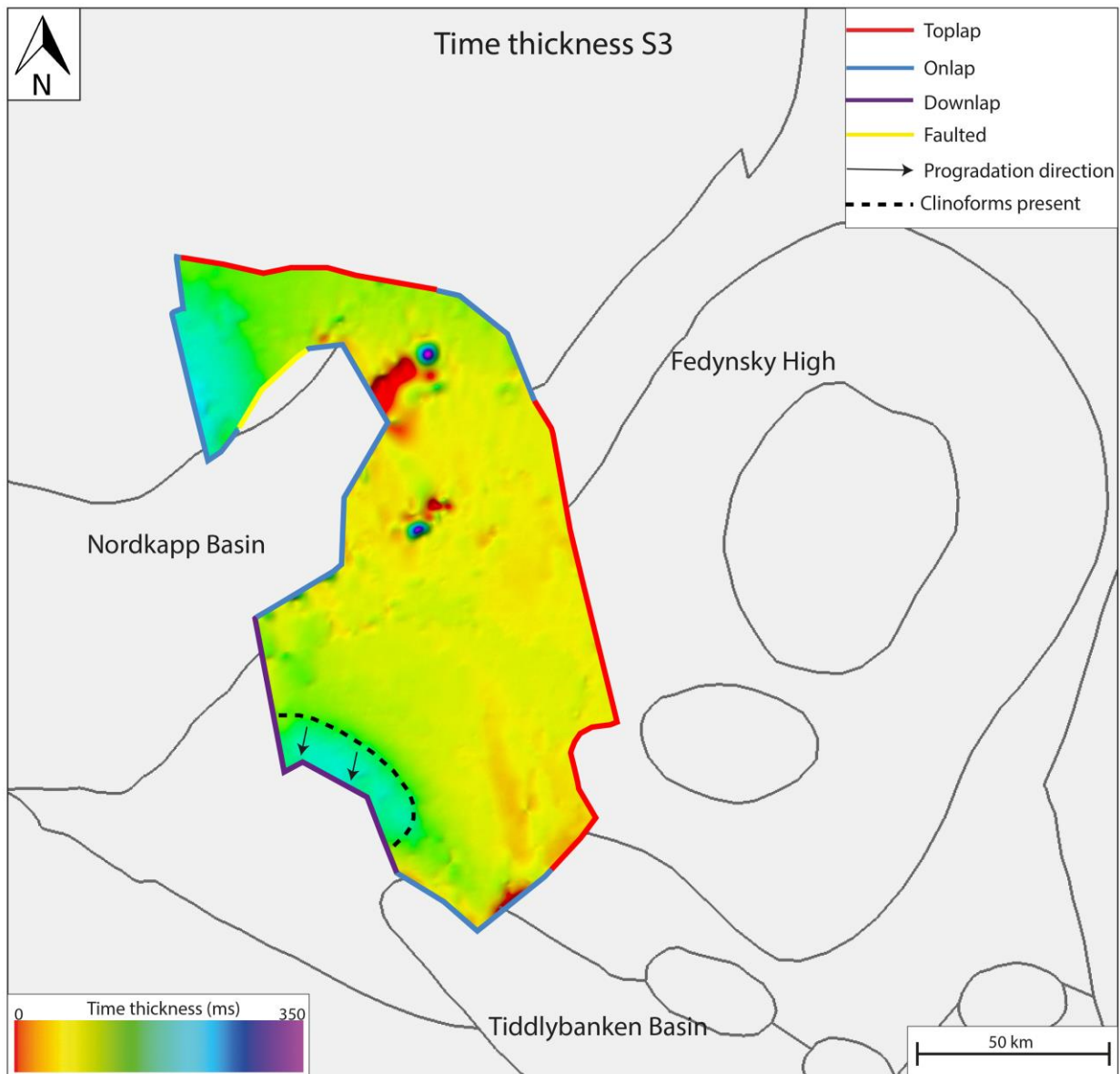


Figure 4-12. Time thickness map of sequence S3. Stratal terminations are illustrated with different colors, and location of clinoforms are marked with black dashed lines.

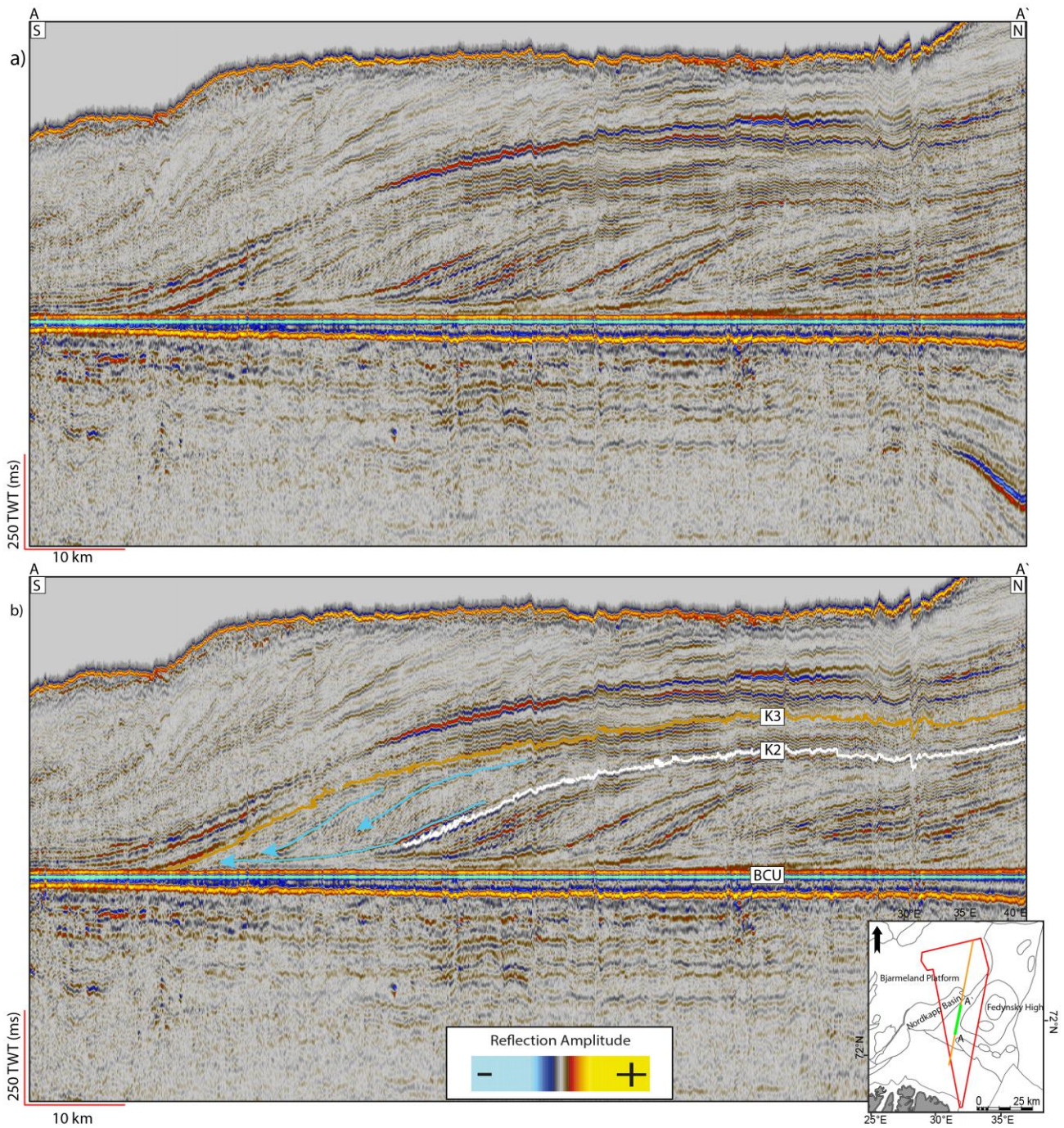


Figure 4-13. a) Uninterpreted seismic section crossing the northeastern margin of Nordkapp Basin, flattened to the BCU. B) Interpreted seismic section of sequence 3 showing high relief, parallel sigmoid clinoforms.

4.3.5 Sequence 4 (S4)

S4 shows continuous to semi-continuous reflections, characterized by medium- to high amplitudes (Figure 4-15). High amplitude reflections are prominent and abundant near the Finnmark Platform and around the southeastern margin of the Nordkapp Basin. The thickness of this sequence is relatively homogenous, but exceptions occur around salt diapirs in the northern part of the Nordkapp Basin and in the northeastern part of the Tiddlybanken Basin (Figure 4-14). The Upper Regional Unconformity (URU) marks the southern and north/northeastern boundaries of the sequence. The Thor Iversen Fault Complex appear to influence the sequence adjacent to salt diapirs at the northeastern margin of the Nordkapp Basin, where throws up to 70 ms (TWT) have been identified.

Clinoforms that prograde from northeast towards southwest were identified north of the Tiddlybanken Basin, between the Nordkapp Basin and the Fedynsky High. These clinoforms display gentler foreset, compared to the southern clinoforms in sequence 3. They have low relief sigmoid (55-102 ms TWT) geometries with foreset angles of 0.2-0.3° (Table 4-1). The height of the clinoforms increases northeastwards, reaching a maximum height of approximately 102 ms (TWT). The clinoforms onlap onto the Signalthornet Dome structure in south. The trajectory is slightly ascending (Table 4-1).

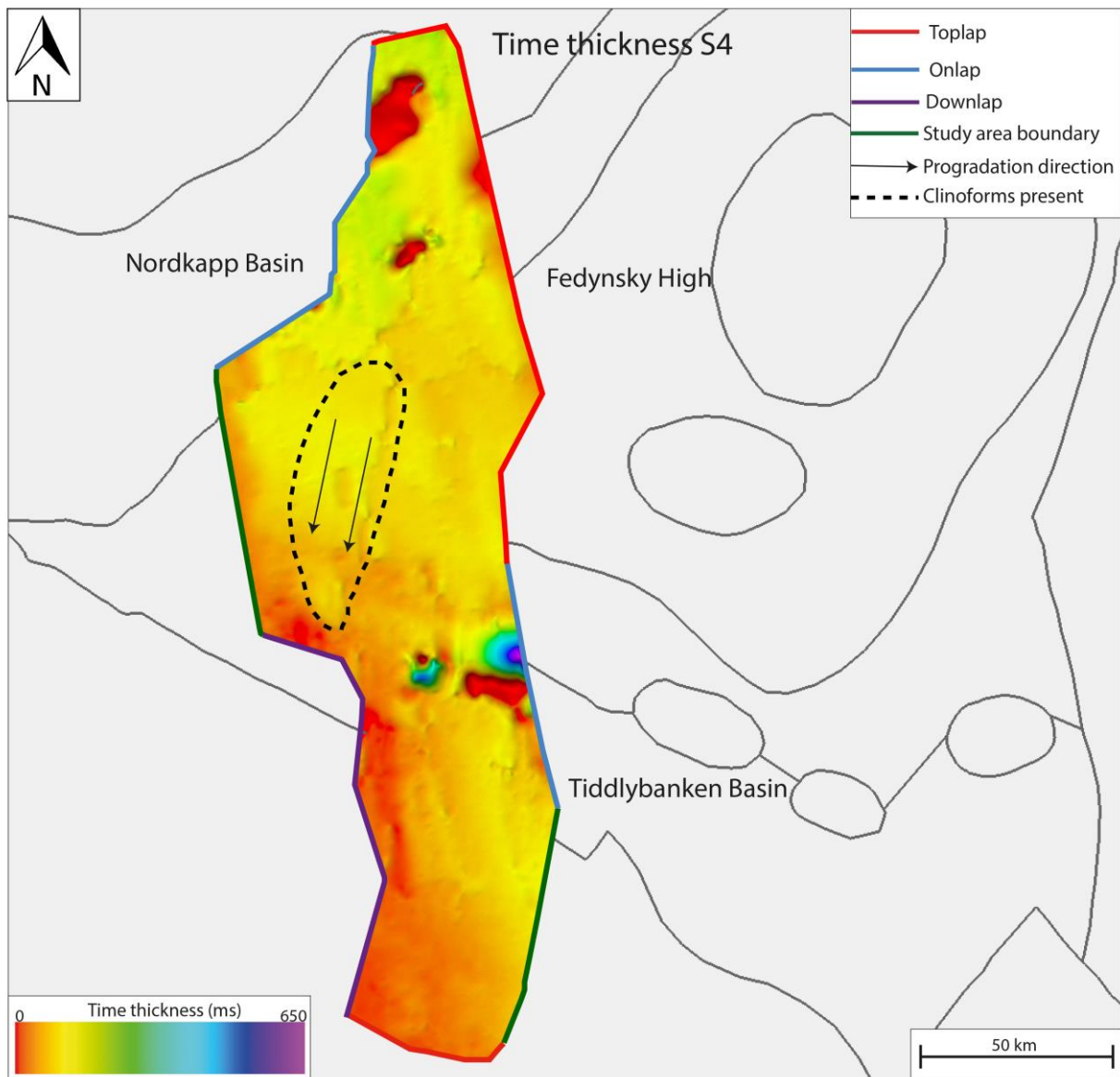


Figure 4-14. Time thickness map of sequence S4. Stratigraphic terminations are illustrated with different colors, and location of clinoforms are marked with black dashed lines.

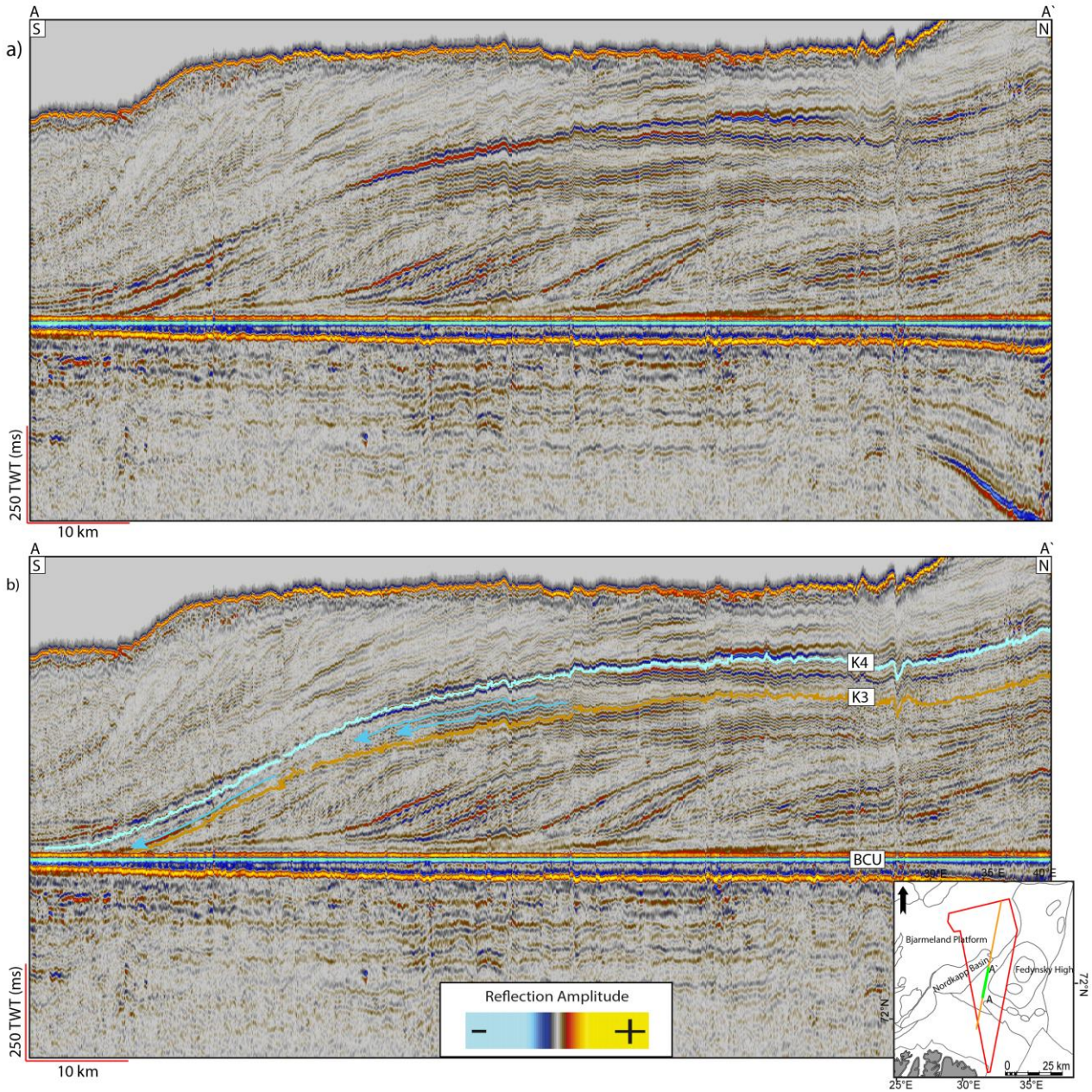


Figure 4-15. a) Uninterpreted seismic section crossing the northeastern margin of Nordkapp Basin, flattened to the BCU. B) Interpreted seismic section of the S4 sequence showing high relief parallel sigmoid clinofolds.

4.4 Clinoform geometry

The calculated estimations of clinoform geometries are presented below (Table 4-1). Followed by an overview showing the distribution of the clinoforms within the study area (Figure 4-16).

Table 4-1. Summary of the geometric parameters for the observed clinoforms, including thickness (R_c = relief clinoforms). The S0 sequence has been divided in two sequences, the S0₁ representing clinoforms in the S0 sequence around the Fedynsky High area, and S0₂ representing clinoforms in the S0 sequence around the Veslekari Dome.

Sequence	Example	R_c <i>ms (twl)</i>	Gradient		Trajectory	Geometry
			$v = 2500 \text{ m/s}$	$v = 3500 \text{ m/s}$		
Sequence 0 ₁	Figure 4-6	110-250	0.5-0.7°	0.7-1°	Ascending	High-relief, low gradient, sigmoidal
Sequence 0 ₂	Figure 4-7	108-170	0.6-0.7°	0.9-1.2°	Ascending	High-relief, low gradient, sigmoidal
Sequence 1	Figure 4-9	92-220	0.7-0.9°	0.9-1.3°	Ascending	High-relief, low gradient, sigmoidal
Sequence 2	Figure 4-11	50-260	0.6-0.8°	0.7-1.1°	Flat (slightly ascending)	High-relief, low gradient, sigmoid and higher gradient oblique
Sequence 3	Figure 4-13	60-180	0.5-0.6°	0.7-0.8°	Ascending	High relief, sigmoidal
Sequence 4	Figure 4-15	55-102	0.1-0.2°	0.2-0.3°	Flat/slightly ascending	Low relief, sigmoid
Post sequence 4	Figure 5-11	>350	0.6-0.9°	0.8-1.2°	Ascending	High relief, sigmoid

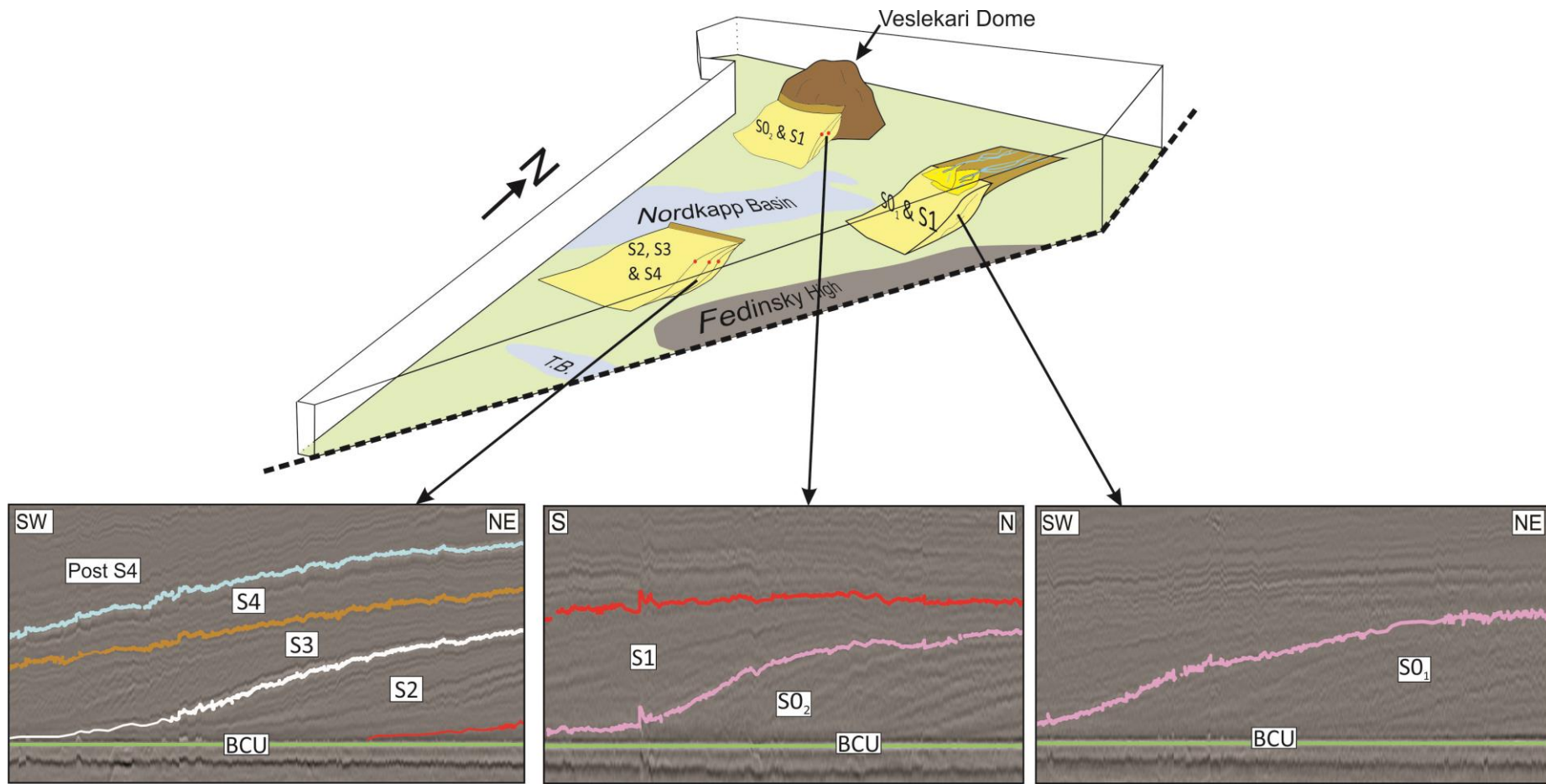


Figure 4-16. 3D-Visualization displaying the distribution of the clinoforms sequences identified within the study area. Seismic sections linked to the highlighted clinoform features are shown in black/white. The S0₁ and S0₂ division correspond to those of Table 4-1. TB = Tiddlybanken Basin.

5 Discussion

Firstly, the suggested timing of deposition is presented as an overview (Figure 5-1). The suggested ages are based on seismic stratigraphic interpretation, which is further discussed, where five sequences are interpreted in order to investigate the regional Cretaceous development in the southeastern Barents Sea. Towards the end of the discussion, a suggested conceptual model for the depositional environments is presented (Figure 5-13). Lastly, post-depositional processes, which have altered the sequences, are proposed.

5.1 Timing of deposition

The timing of deposition for the identified sequences (S0-S4), have been evaluated in light of previous studies done in the Barents Sea (Marin et al., 2016; Grundvåg et al., 2017; Kairanov et al., 2018). The time of deposition for respectively S0 and S1, is proposed to have endured during the Early Barremian-Early Aptian age (Figure 5-1 and Figure 5-2). This correlates respectively with the Kolje Formation (Dalland et al., 1988). This is suggested based on the interpreted northeastern location of the shelf break, which was successively displaced towards the southwest during the deposition of S2, S3 and S4 in Late Aptian/Early Albian times (Figure 5-2) (Grundvåg et al., 2017). This correlates with the suggested shelf break presented by Kairanov et al. (2018). Additionally, Marin et al. (2016) indicated that increasing heights in clinofolds likely were caused due to deposition into deeper waters during Aptian-Albian times (Figure 5-1). The latter sequences (2, 3 and 4) display an increase in clinofold heights, and is therefore suggested to have been deposited during the same time-

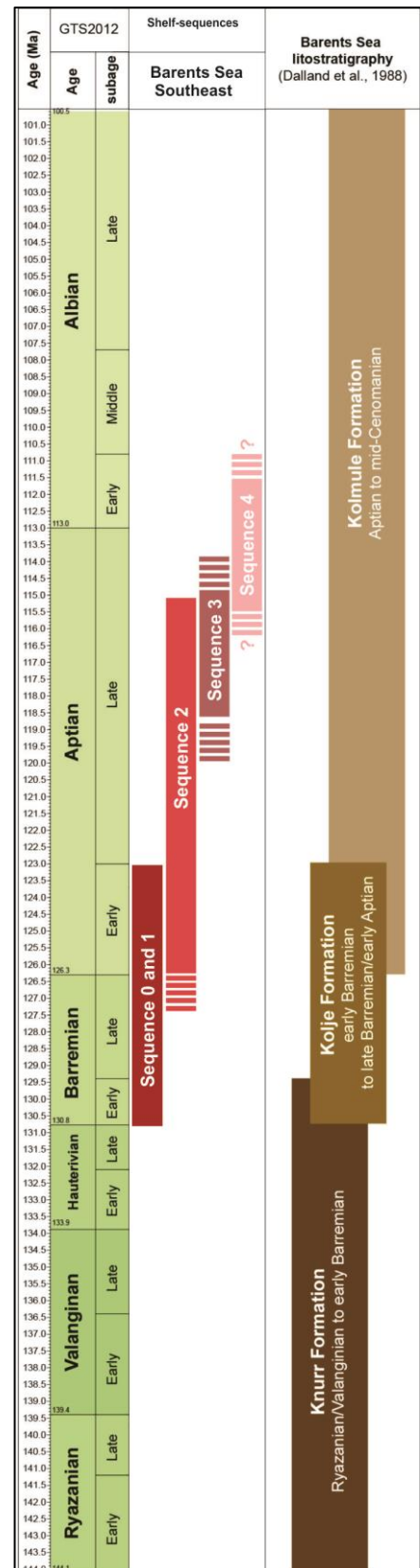


Figure 5-1. Suggested age for the sequences S0-S4. Figure modified after Grundvåg et al. (2017).

interval as discussed by Marin et al. (2016). However, there is a great uncertainty connected to the suggested ages of deposition for the five presented sequences (Figure 5-1). This is due to lack of well-data within the seismic study area, which could have provided a more accurate estimation of the timing of deposition.

A suggested paleogeographic reconstruction map of the Barents Shelf has been compiled to visualize the suggested timing of deposition (Figure 5-2). The paleogeographic reconstruction is generated by modification and correlation of paleomaps, originally suggested by Marin et al. (2016), Grundvåg et al. (2017) and Kairanov et al. (2018). The regional age correlation is suggested by comparing the location of the paleo shelf-edge in the western Barents Sea (Grundvåg et al., 2017) and in the north/east (Kairanov et al., 2018) with the shelf break identified in the Barents Sea southeast within this study.

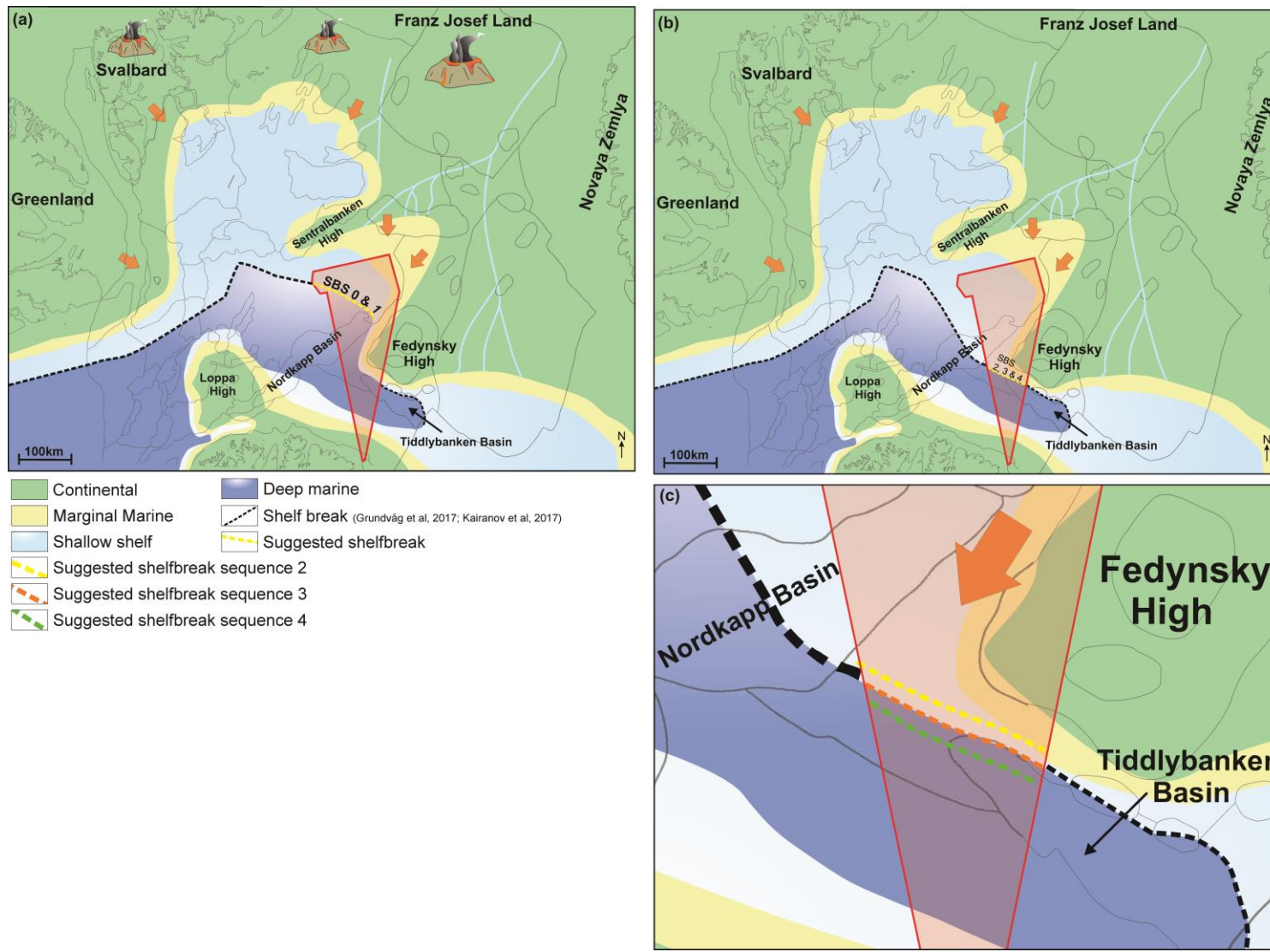


Figure 5-2. Proposed paleogeographic map of the southern Barents Sea, for respectively the sequences S0-S4. a) Early Barremian-Early Aptian. b) Aptian-earliest Albian. Successive displacement of the shelf break characterize the sequences.

5.2 Sequences S0-S4

5.2.1 Sequence 0 and 1

Sequence 0 (S0) and sequence 1 (S1) show several similarities in the reflection configurations in the seismic data. The northern part of S0 has a combination of gently dipping seismic reflections and discontinuous chaotic reflections (Figure 5-3). The southern part of sequence S0 displays more continuous parallel seismic reflections (Figure 5-4), and the same is observed for sequence S1 (Figure 5-5). The discontinuous reflections (northern part) may point to a geological environment with rapid changes in energy regimes (Mitchum et al., 1977). High-energy slope systems are often characterized by deposition of coarser sediments, such as sand and gravel. This type of environment is localized in a proximal area to the sediment source (Nichols, 2009). The dipping and discontinuous seismic reflections may therefore indicate a proximal depositional environment, with successive prograding sand-prone sediments in a continental to shallow marine environment. This type of depositional environment on a shelf could be linked to the regression which prevailed in the transition between Jurassic and Cretaceous times, as suggested by Smelror et al. (2009) (Mesozoic 2.2.2). The northern part represents a smaller interval of the S0 sequence, and is therefore not discussed further. From this point, the southern (parallel, continuous) part of the S0 sequence will be emphasized.

The continuous parallel reflections in the southern study area for S0 and S1 (Figure 5-3, Figure 5-5), could be associated with continuous strata deposited under the same sedimentary conditions (Veeken, 2007). The gently dipping seismic reflections in the study area within these sequences could indicate sediment transport from higher- to lower elevated areas. The reflections in respectively the elevated and lower areas show a shift in reflection configuration. This shift may represent a change in the depositional process and environment. Such large-scale change in the depositional regime may indicate that the sequence prograded from the proximal (high-energy) areas, across the shelf break, towards deep marine distal (low-energy) parts (Veeken, 2007; Nichols, 2009). The shelf break has been defined as the margin separating the shallow-marine (continental) shelf from deeper basins. This is defined irrespective of the basin's tectonic setting (Helland-Hansen et al., 2012). The identified shelf break in this area (S0 and S1 sequences, Figure 5-3 and Figure 5-4) is compliant with the suggested shelf break from Kairanov et al. (2018). Deep-marine environments may therefore have been dominating to the south, whereas shallower- marine environments dominated to the north (Figure 5-6).

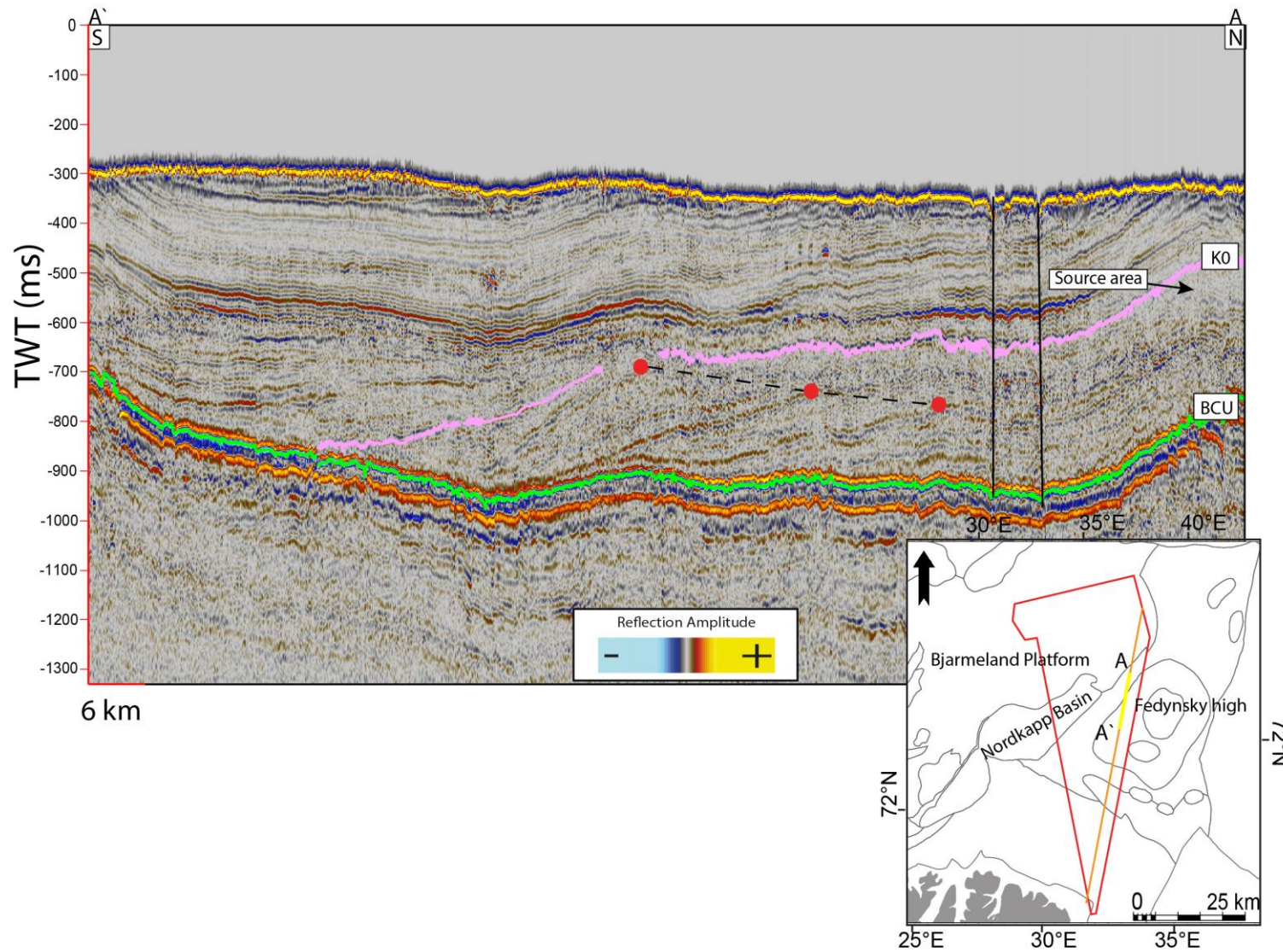


Figure 5-3. Interpreted seismic section in the S0 sequence, near the margin of Fedynsky High in the southeastern Barents Sea. Red points indicates ascending trajectories. Note chaotic reflections to the north. Black lines indicate fault zones.

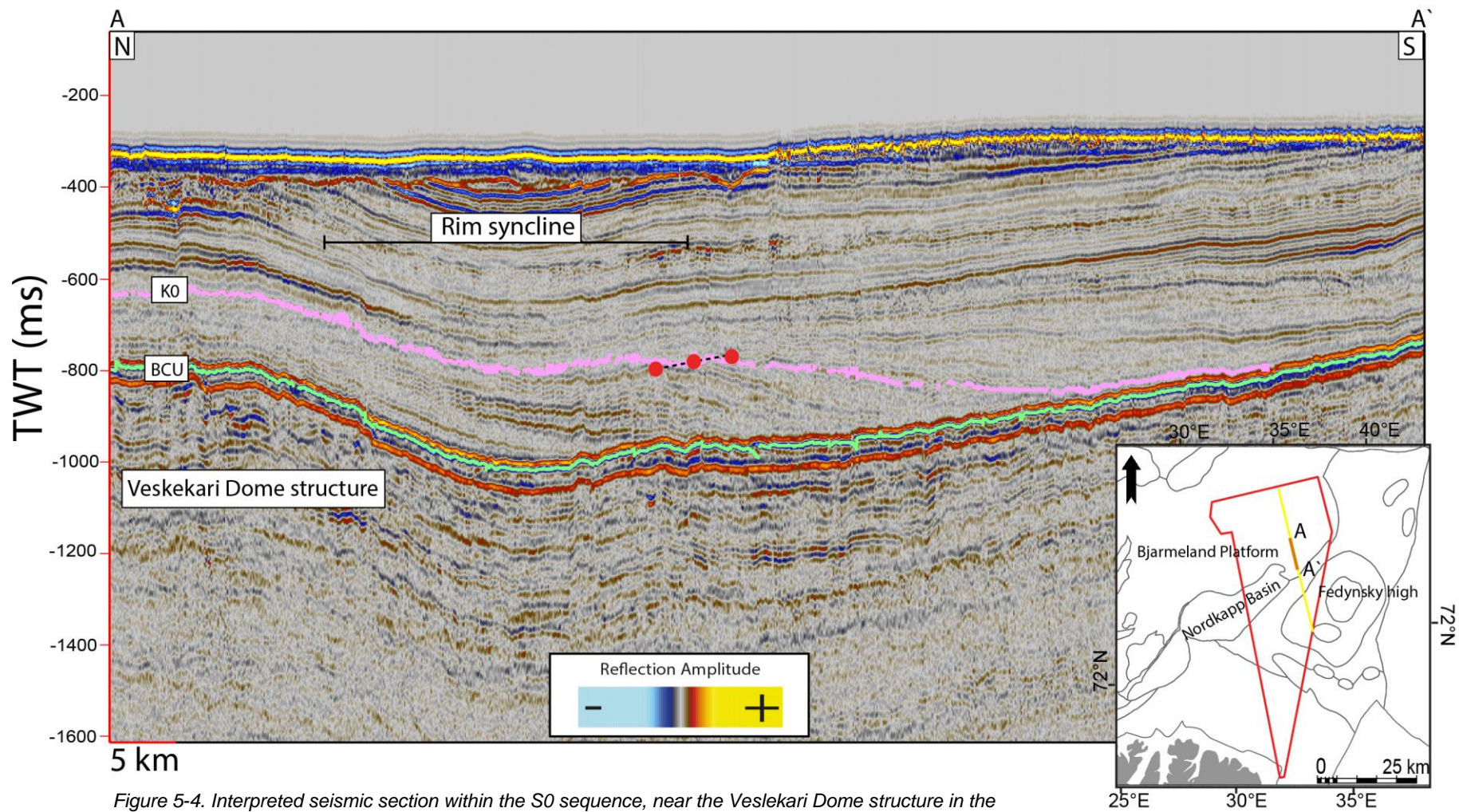


Figure 5-4. Interpreted seismic section within the S0 sequence, near the Veskekari Dome structure in the southeastern Barents Sea. Red points indicate ascending trajectories.

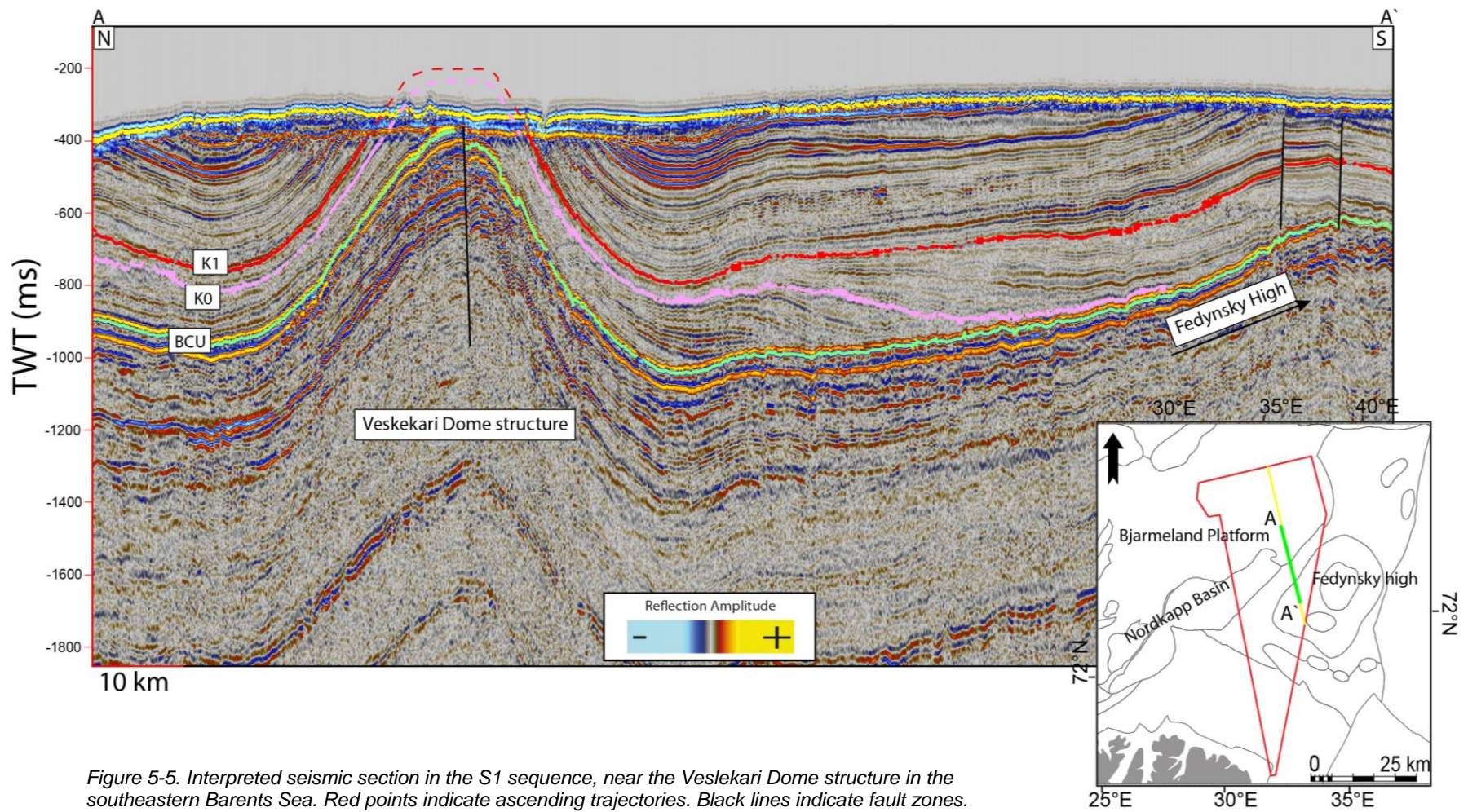


Figure 5-5. Interpreted seismic section in the S1 sequence, near the Veslekari Dome structure in the southeastern Barents Sea. Red points indicate ascending trajectories. Black lines indicate fault zones.

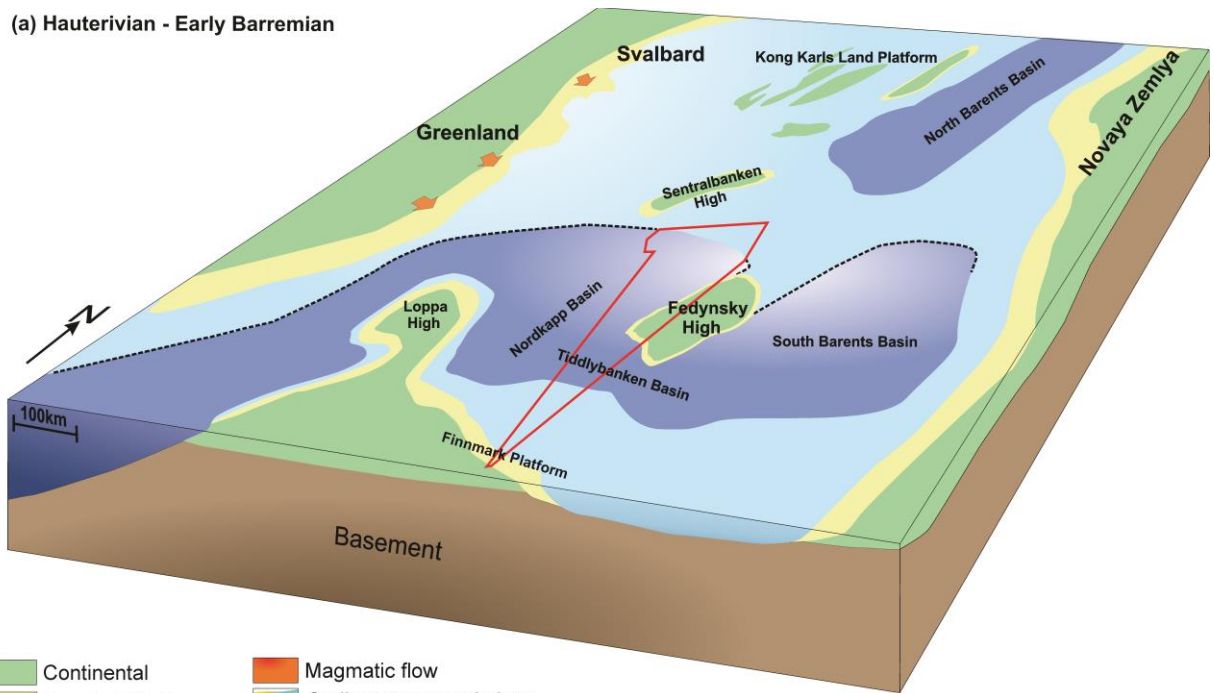
Previous work (Maher, 2001; Worsley, 2008; Corfu et al., 2013; Polteau et al., 2015) suggested that the formation of the High Arctic Large

Igneous Province (HALIP) caused an uplift of the northern Barents Shelf between 125 Ma and 122 Ma. The HALIP represents a period where increased heat flow and magmatism were induced by rifting and seafloor spreading, which covered vast provinces in the Barents Sea region. Eventually, this led to the opening of the Amerasia Basin (Figure 2-2) in the north (Worsley, 2008; Henriksen et al., 2011). The HALIP refers to mafic igneous rocks of Early Cretaceous age scattered around the Arctic Ocean (Polteau et al., 2015). Polteau et al. (2015) pointed out that regional changes in depositional patterns of sedimentary strata on Svalbard are closely associated in time with the HALIP province. Regional uplift of the northern Barents Shelf resulted in deposition of the fluvial/deltaic Helvetiafjellet and Battfjellet Formations on Svalbard and continental-sedimentary accumulations on Franz Josef Land (Steel et al., 2000; Polteau et al., 2015).

The uplifted areas, were according to Kairanov et al. (2018) dominated by continental- to shallow shelf environments during Early Barremian-Early Aptian age. This is also supported by Artyushkov et al. (2014), who suggested that the North Barents Basin was filled with clinoforms up to the paleo sea level in Early Cretaceous times. The North Barents Basin is located north of the study area (Figure 5-6).

The continental-to shallow marine depositional environment which dominated the northern Barents Shelf, was also responsible for providing a major sediment source for the subsiding basins in the southern Barents Sea during this time (Faleide et al., 2015). This hinterland may have been the controlling factor regarding the progradation and position of the shelf break identified within the S0 and S1 sequences. The depositional environment in S0 and S1 could therefore be time-equivalent with the uplift caused by the HALIP during Early Barremian-Early Aptian age (Figure 5-6).

(a) Hauterivian - Early Barremian



(b) Early Barremian - Early Aptian

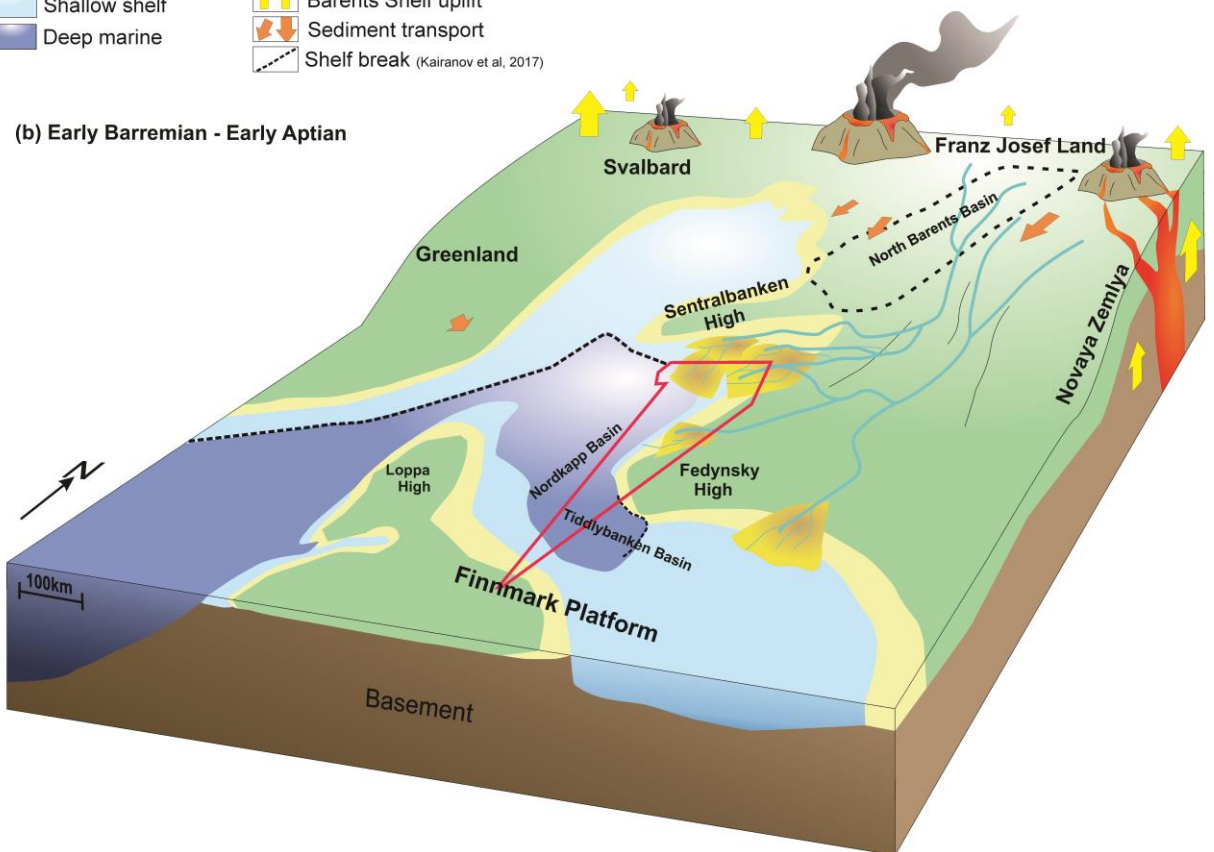


Figure 5-6. Illustration of the northern Barents Sea uplift caused by magmatic activity associated with the HALIP (High Arctic Large Igneous Province) during Early Barremian-Early Aptian times. In the uplifted areas, continental environments dominated. The uplift caused transport of sediments from the north towards the southeastern Barents Shelf. Note the transition from marine to continental environments from (a)-(b) for the North Barents Basin. Red polygon indicates the study area.

Clinoforms identified in sequence 0 north of the Fedynsky High margin (S0₁, Figure 4-16 and Figure 5-3) is suggested to represent low gradient, shelf-edge clinoforms. The most prominent shelf-edge clinoforms are located near the margin of Fedynsky High, while the others are located near the Veslekari Dome structure (S0₂, Figure 4-16 and Figure 5-4). The trajectory represents the prograding shelf-pathway during the development of accreting clinoforms. The flat to slightly ascending trajectory in S0 (Figure 5-3 and Figure 5-4) indicates an overall rise of relative sea level, when the shelf-clinoforms prograded southwards, and caused an accretion of the shelf break. One of the implications from the trajectory of this sequence is that a greater percentage of the sediment budget is stored on the on the contemporary shelf, with little being partitioned into the deep water areas (Johannessen & Steel, 2005). Ascending trajectories is a strong indicator of mud-prone shelves (Steel & Olsen, 2002).

O`Grady et al. (2000) suggested that sigmoid margins are common in depositional environments characterized by high sediment input and few canyons. In contrast to steep and rough margins, which usually have lower sediment input, and are often affected by erosion and the presence of canyons. The abundant appearances of canyons in combination with low sediment input for the latter one may indicate that the rate of sediment input does not exceed the rate of sediment removal caused by mass-wasting processes. For the sigmoid margins, on the other hand, this balance may be reversed, where the sediment supply is high and canyon incisions is low. (O`Grady et al., 2000). This is illustrated later on, in Figure 5-13.

Shelf-edge clinoforms near the Fedynsky High (Figure 5-3) display foresets with gradients of $0.7 - 1^\circ$. This could indicate that shelf-edge clinoforms which developed in sequence 0 are the result of high sediment input from the source area in north/northeast, similarly to the sigmoid margins depositional environment suggested by O`Grady et al. (2000). Mud-rich systems are common in distal areas with high input of sediments (Marin et al., 2016). The presence of mud is likely to represent a long transport of the sediments, hence, the system is suggested to have been located with a significant distance from the sediment source (distal). As the energy level decreases with distance from the sediment source, the transport agents (water/fluvial transport) ability to transport larger grains is weakened. Therefore, only fine-grained particles such as muds may be transported over large distances in form of suspension (Figure 5-13). Suspension is defined as turbulence within the flow, which produces sufficient upward motion. This upward motion keeps the fine-grained particles flowing within the moving fluid (Nichols, 2009), possibly over large distances in low energy environments. Considering this, it may be likely

that the sediments originated from a sediment source in the north, and prograded southwards (Figure 5-6). High amounts of mud, would also be expected since the lithostratigraphic unit of the Nordvestbanken Group (respectively the Knurr, Kolje and Kolmule Formations) corresponding to the Early Cretaceous of the Barents Sea, consists of mudstone with interbeds of other lithologies deposited in a distal environment (Dalland et al., 1988).

The Kolmule Formation is found in Well 7226/11-1, and has an age of Aptian to mid-Cenomanian (Dalland et al., 1988). The well is located on the Norsel High, closed to the southwestern margin of the Nordkapp Basin (NPD, 2011), outside the study area of this thesis. The top Kolmule horizon appear with a severe vertical offset above the top Hekkingen in the well. This vertical time interval represents the Nordvestbanken Group. It is suggested that the S0 and S1 sequences is well within the Nordvestbanken Group within the study area, but this is further discussed in chapter 5.3.4.

Clinoforms within the S0 sequence have also been identified south of the Veslekari Dome structure, north of the Nordkapp Basin, with an overall north-south orientation (Figure 5-4). These clinoforms show high relief, sigmoid geometries, with slightly steeper foreset angles, 0.9-1.2° (Table 4-1), compared to the previously described S0 clinoforms (north of the Fedynsky High). The overlying S1 clinoforms in this area show similar reflection configurations to the S0 clinoforms (Figure 5-5). This could indicate that the S1 clinoforms is a continuation of the depositional pattern dominating the S0 clinoforms. However, the seismic sequence of S1 shows more reflection free zones. This is caused by weak or lacking acoustic impedance contrasts, which implies a rather homogene gross lithology (Mitchum et al., 1977; Veeken, 2007). Such homogeneous lithologies can be thick shales, limestones, large successions of sand, and so on. The clinoforms around the Veslekari Dome have been suggested to consist of fine-grained material, since the seismic reflection pattern shows striking similarities to the clinoforms located around the Fedynsky High. It could be argued that the more mud-prone, homogenous fine-grained, foresets (Steel & Olsen, 2002) are responsible for the reflection free pattern.

Continuous, high amplitude reflections is known to represent a flooding surface in many cases (Veeken, 2007). The flooding surface represents the onset of baselevel fall, meaning the flooding stage determining the start of a seaward movement of the shoreline (Veeken, 2007). The top surface of the S1 sequence (K1-horizon), is characterized by a high amplitude, continuous horizon (Figure 5-12), which is interpreted to mark a regional flooding event.

The height of the clinoforms increase between the S0 and S1 clinoform sequences. This may be explained by increasing paleo water depths in the study area. The paleo water depth can roughly be estimated by measuring the difference in milliseconds between the topset and the bottomset (Veeken, 2007). However, since 2D-data only allows for interpretation in the inline-direction, the recognition of topsets is restricted. A rough estimate between the presumed topset (of S1) and bottomset (towards the BCU) suggests a paleo water depth of approximately 488m (279ms TWT) assuming a seismic velocity of 3500m/s. This could indicate that during the deposition of the S0 and S1 sequences, an overall transgression was in place. A transgression represents a relative rise in sea level (Coe et al., 2003). This may coincide with the regional sea level rise during the Aptian age described by Worsley (2008). Higher resolution seismic data in addition to sedimentary logs/core samples is necessary to confirm this.

The clinoforms of sequence 0 and 1 around the Veslekari Dome structure is present south of the rim syncline associated with the dome. The rim syncline represents semi-circular, curved depressions encircling central domes such as i.e. salt, which developed in relation to doming events (Figure 5-4) (Cita & Aghib, 1991). Erosion along the Veslekari Dome could be suggested to have been a sediment source for the clinoforms. However, this is not likely, considering that the sequences show equal thickness on both sides of the dome. The top of the S0 and S1 sequences show horizons (K0 and K1) which are quite continuous and preserved on both sides and above the dome structure (Figure 5-5). The overlying sediments is interpreted to have been structurally modified into anticlinal structures, which curved the horizons upwards, and has later been eroded along the seafloor. The S0 and S1 sequences shows equal thickness on both sides of the structure, which in combination with the continuous horizons, suggest post-Cretaceous doming of the Veslekari Dome (Mattingsdal et al., 2015). A schematic illustration of this interpretation is presented in Figure 5-7.

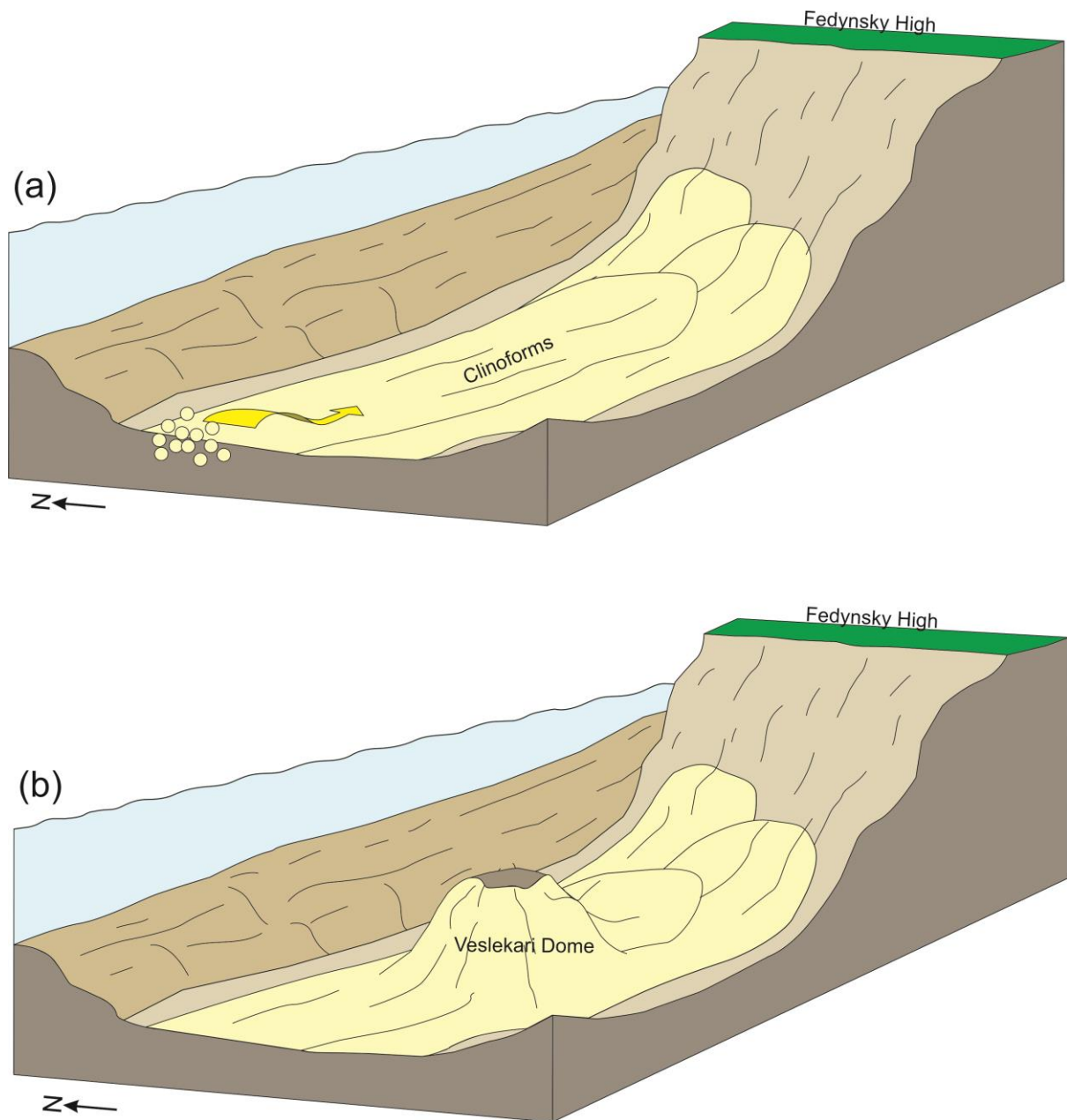


Figure 5-7. Suggested interpretation for clinofolds found in sequence 1. a) Clinofold outbuilding into a basin in front of the Fedynsky High margin, with sediment transport from elevated areas in the further north. b) Post-Cretaceous tectonic doming of the Veslekari Dome, interpreted based on domed Cretaceous strata and equal thickness on both sides of the structure. The top of the sequence has been eroded above the Veslekari Dome.

5.2.2 Sequence 2

The seismic pattern within sequence 2 (S2) shows continuous reflections with medium- to high amplitudes (Figure 5-8), suggesting that the sediments in this sequence were deposited during the same depositional regime (Veeken, 2007).

The sequence displays thickening towards the southwest (Figure 4-10). This increase in thickness differs from the S0 and S1 sequences, where there were only smaller thickness variations (Figure 4-5 and Figure 4-8). It is therefore reasonable to presume that sediments were deposited in a depocenter where more accommodation space was available. This suggests that the shelf-edge had prograded i.e. towards a deep-marine basin or abyssal plain, and that the depocenter was displaced from the northeastern part of the study area (Figure 5-9) towards the southwest. The depocenter represents an area where sediments can accumulate, since accommodation space is available (Coe et al., 2003).

The location of the shelf break for sequence 2, which is displaced towards the southwest relative to the S0 and S1 sequences, is interpreted to be representative for the Latest Aptian to the Earliest/Middle Albian age. This is suggested based on previous work which showed a shelf break located further southwest (Grundvåg et al., 2017). The distance from the location of the former shelf break in S0 and S1, to the location of the shelf break in S2, was measured to be approximately 155km in Petrel.

Kairanov et al. (2018) suggested that the northeast-southwest progradation of the shelf could be controlled by subaerially exposed structural highs. The positive relief highs acted as bounding structures and altered the routing pattern of the paleodrainage-system. The Fedynsky High is the most prominent structural high within the study area. The Fedynsky High was uplifted and partly eroded during the Kimmerian movements (Smelror et al., 2009), but remained as a positive feature during the Early Cretaceous. It could be suggested that the Fedynsky High contributed to the southwestwards progradation of the shelf, by routing the sediments into a paleodrainage system (Figure 5-9).

The internal reflections of S2 show a shift in dipping geometries, between the northern and southern areas (Figure 5-8). The clinoforms identified show high relief (50-260 ms TWT). The northern part of the clinoforms show gentle foresets, with a sigmoid geometry and foreset angles of 0.7-0.8° (Table 4-1). The southern part, displays steeper-dipping foresets, hence representing an oblique geometry with foreset angles of 0.8-1.1°.

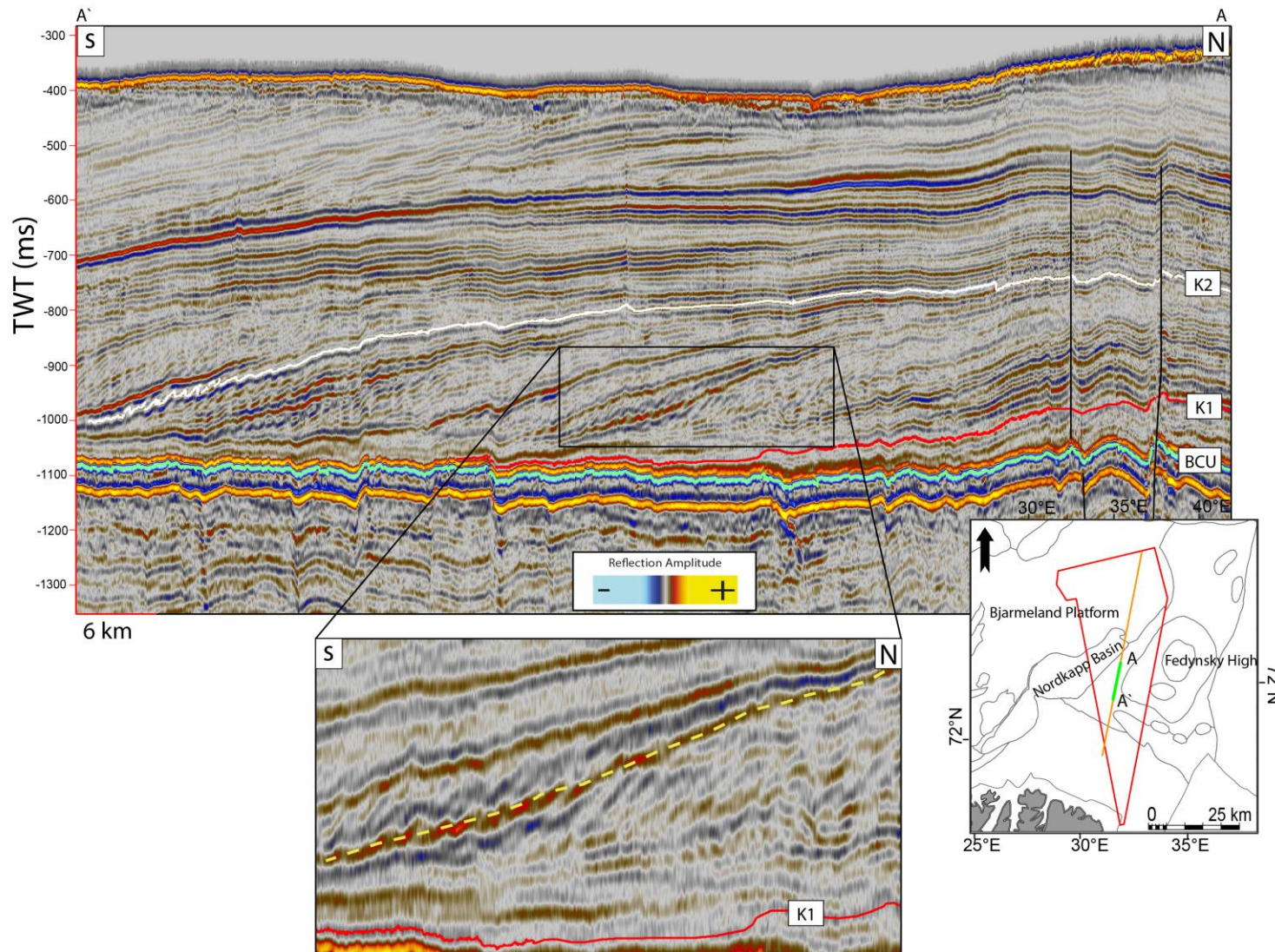


Figure 5-8. Interpreted seismic section in the S2 sequence, east of the Nordkapp Basin in the southeastern Barents Sea. Red points indicate flat trajectories. The square (yellow dotted line) shows the suggested shift from mud-prone to sand-prone foresets.

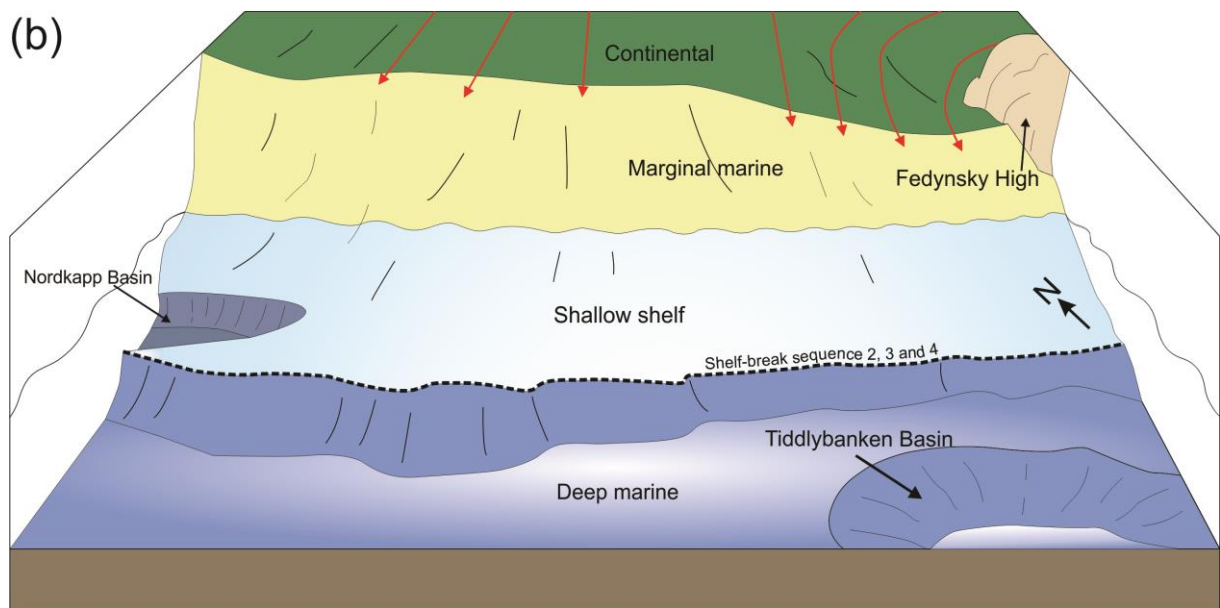
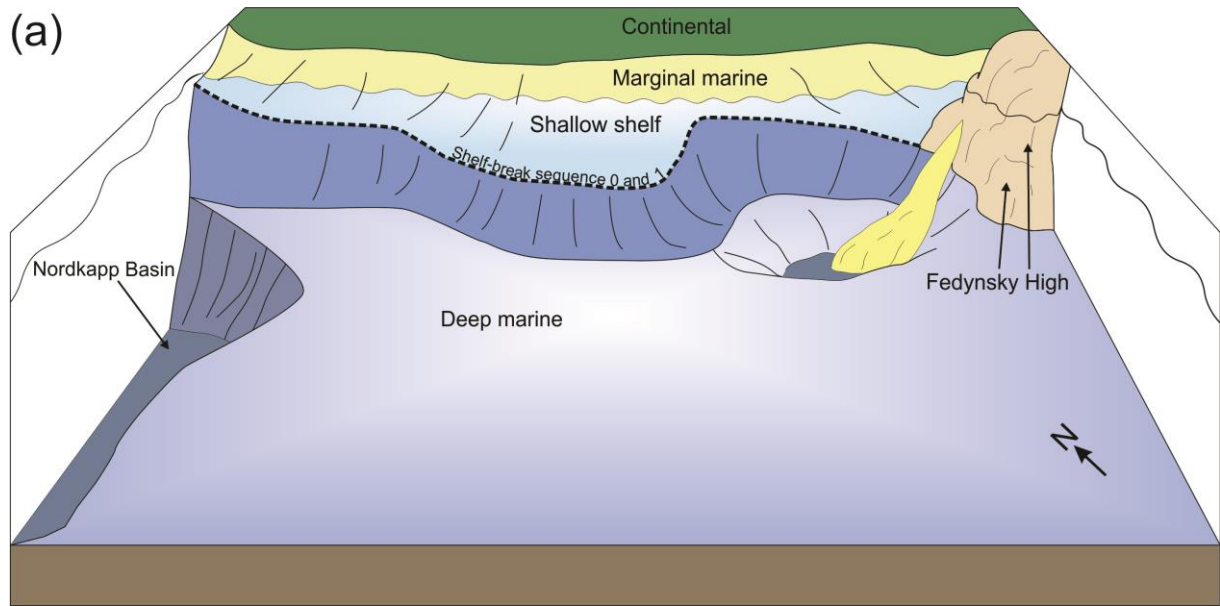


Figure 5-9. Suggested interpretation for the depositional environment during Early Cretaceous. The shelf break indicates where maximum progradation of clinoforms have taken place during the different sequences. For simplification, the shelf break in sequence 2, 3 and 4 are merged together since there are small paleo-geographic differences between them. a) Deposition in the north/northeast dominated by fluvial material, sourced from elevated areas. Red arrows indicate paleodrainage system. b) Displacement of the shelf break towards south/southwest, which could have been triggered by tectonic subsidence in the Nordkapp Basin and Tiddlybanken Basin, and/or cyclic variations in relative sea level.

To the south, sequence S2 shows higher amplitudes compared to the northern parts (Figure 5-8). The high amplitude reflections, generally points to vertical alternation of contrasting lithologies, whereas low amplitude often reflects lithologies which are of similar properties (Veeken, 2007). The shifting foreset geometries between the northern and southern (Figure 5-8) areas are suggested to mark a shift in lithological properties (Mitchum et al., 1977; Veeken, 2007), and are here suggested to be attributed to alternations between mud- and sand-prone deposits. The mud-prone deposits are represented by gentler foresets, whereas the sand-prone are represented by steeper-dipping foresets.

As mentioned, the foresets in the southern part of S2 display an oblique geometry. The oblique progradational geometry is a strong indicator of high-energy slope system, where coarser deposits may be incorporated (Figure 5-13) (Veeken, 2007).

The clinoforms to the north show a dip towards the southwest within S2, and are suggested to have prograded in the same direction. This dip orientation coincides with those observed within the S0 and S1 clinoforms, and thus suggests that the sediment source has been roughly the same throughout the deposition of S0, S1 and S2 clinoforms. The progradational orientation (northeast towards southwest) is also the same for the three sequences. Hence, the sediment source was still located towards the north/northeast. The sediments are therefore suggested to have been transported from the uplifted hinterland in the north and across the shallow shelf towards the southwest (Figure 5-6), as discussed for S0 and S1.

The oblique clinoforms in the distal parts of S2, display relatively flat to slightly ascending trajectories. This supports that sandy-lithologies dominate within these clinoforms, due to the fact that flat-trajectories is typically sand-prone (Johannessen & Steel, 2005; Helland-Hansen & Hampson, 2009; Helland-Hansen et al., 2012). In other words, the shelf prograded basinwards where sand was portioned into deep water, which indicate less storage potential on the shelf-edge, and significantly more sediment bypass onto the slope and basin floor (Figure 5-13) (Johannessen & Steel, 2005).

An important aspect which influence both the shelf regime and the sediment available at the shelf break involves the changing balance between accommodation on the shelf and the sediment supply across the shelf (Steel et al., 2000). In order for sandy sediments to deposit along or below the shelf break, high sediment input in combination with a high-energy environment has to be in place across the shelf. A regression is defined as a relative fall in sea level (Coe et al., 2003). Migration of deltas as a response to a regression is the main mechanism

by which shelf accrete into deeper water with sand-prone sediments (Johannessen & Steel, 2005). During times of relative sea level lowstand, the shelf is more likely to be incised by developing river systems (Steel & Olsen, 2002). The slopes become channelized, and these channels contribute to sediment transport of coarser material towards deeper marine environments (Figure 5-13). However, storm wave processes may influence the sediment transport on shelves by eroding sediments that aggrade above the shelf equilibrium profile (Grundvåg et al., 2017). Furthermore, sand-prone slopes usually occur where the sediment flux from the shelf break is high (Johannessen & Steel, 2005). The sand-prone foresets within S2 is suggested to have been deposited due to a relative fall in sea level, where deltaic and fluvial systems transported sediments from the hinterland in the north/northeast towards a southwestern deep marine environment (Figure 5-13).

The heights of the clinoforms in sequence 2 show an increase relative to the heights of S0 and S1 clinoforms (Table 4-1). Marin et al. (2016) suggested that large-scale tectonics influenced the development of clinoform accretion in the eastern Barents Sea during Aptian-Albian times. Tectonic subsidence could have been initiated due to fault activity or movement of salt, especially in the Nordkapp Basin, but also in the Tiddlybanken Basin. The subsidence pattern within the Nordkapp Basin varied considerably during Cretaceous time and the process is suggested by Gabrielsen et al. (1992) to have lasted well into the end of Albian. The height of the clinoforms in sequence 2 is suggested to have increased due to one of the two processes suggested by Marin et al. (2016): 1) they prograded into a deeper marine area during the deposition of S2; 2) increase in tectonic subsidence within the Nordkapp Basin created more accommodation space.

5.2.3 Sequence 3 and 4

Sequence 3 shows increasing thickness towards the west and southwest in the study area (Figure 4-12). The seismic pattern within sequence 3 in the southwestern part displays in general medium- to low amplitudes, with some reflection free zones (Figure 5-10). This reflection configuration suggest homogenous lithologies within the sequence, as discussed for sequence S1 (Mitchum et al., 1977). Furthermore, the S3 sequence in the southwest display an apparent continued progradational shelf from the S2 sequence. The clinoform foresets within sequence S3 show rising trajectories, which in combination with the homogenous lithologies suggest mud-prone foresets (Steel & Olsen, 2002; Helland-Hansen et al., 2012). The geometries of the clinoforms are sigmoidal, with gently dipping foreset angles of 0.7-0.8° (Table 4-1). The sigmoid geometry is typically reflecting a low energy depositional environment (Veeken, 2007). The ascending trajectory, in combination with the sigmoidal geometry and homogenous lithology, could indicate a transgression. The depositional regime of these foresets is suggested to have been similar to those of S0 and S1, in a low-energy environment. The transition from oblique geometries in S2, which is suggested to represent sand-prone foresets (Steel & Olsen, 2002) towards sigmoid geometry in S3, could indicate a shift in depositional environment caused by a change in sea level (Figure 5-12 and Figure 5-13).

The seismic shows that within the thicker succession of sequence 3 in the western part of the study area, sporadic high amplitudes appear in the otherwise reflection-free pattern (Figure 5-10). This suggest that small changes in lithologies are present (Veeken, 2007). The main lithology is interpreted to consist of fine-grained sediments deposited during a transgression, similar to the southwestern part as discussed above, however with interbedded sand deposits. In general, where the shelf-edge shows a record of basinward migration, sand is likely be deposited to and beyond the shelf break for smaller periods, irrespective of the shelf-edge trajectory geometries (Helland-Hansen & Hampson, 2009). Such small occurrences of sand within mud-prone foresets, as observed within this sequence, may be caused by i.e. increase in sediment input.

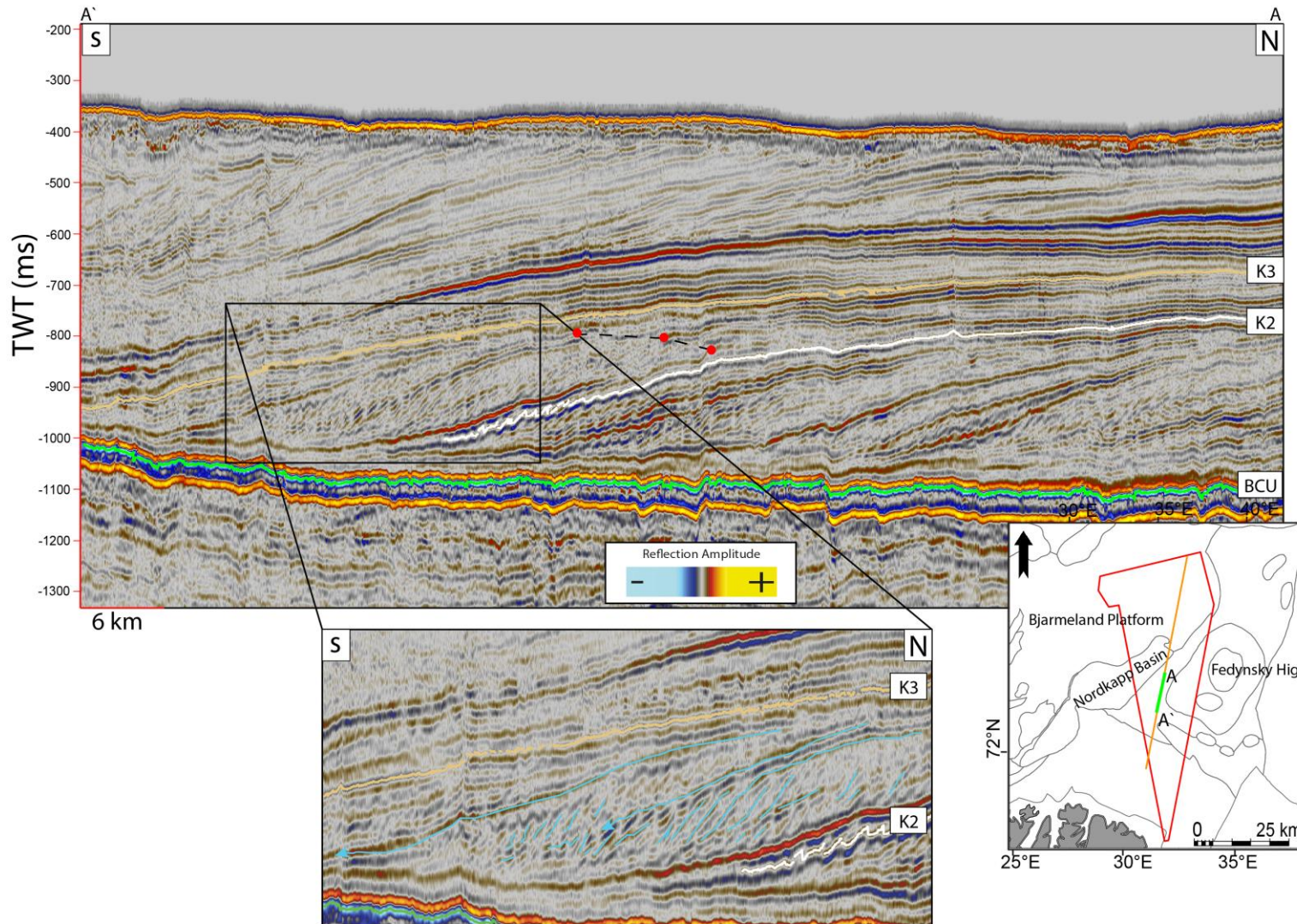


Figure 5-10. Interpreted seismic section in the S3 sequence, east of the Nordkapp Basin in the southeastern Barents Sea. Red points indicate the slightly ascending trajectories, whereas highlighted square shows generally low amplitude reflections.

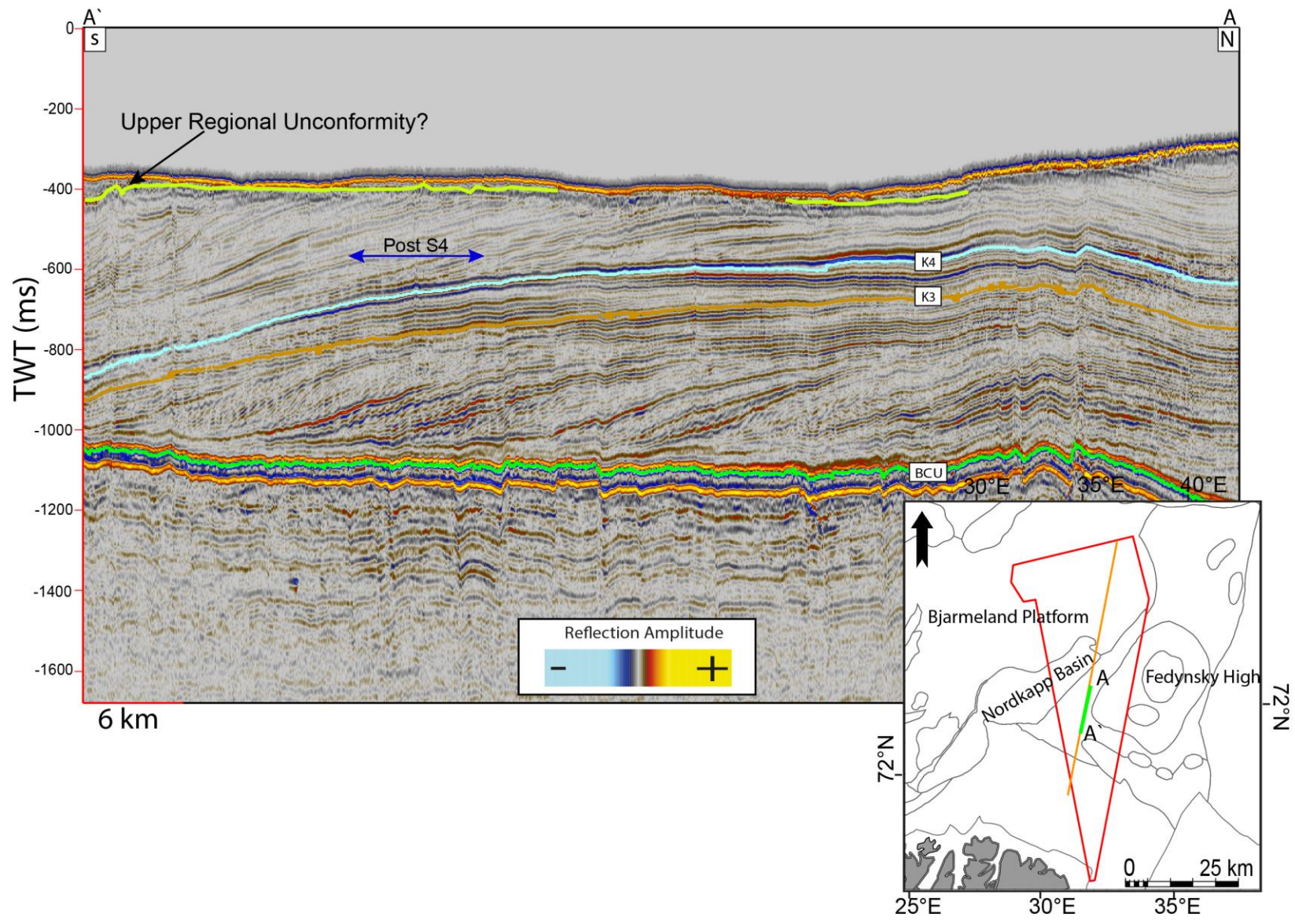


Figure 5-11. Interpreted seismic section in the S4 sequence, east of the Nordkapp Basin in the southeastern Barents Sea. Post S4 reflects a continuation of the S3 and S4 sequences, and is truncated by the Upper Regional Unconformity.

Sequence S4 shows similar reflection patterns compared to the S3 sequence (Figure 5-11), and is suggested to represent a continuation of the depositional pattern observed in S3. The suggested transgression continued during the deposition of these two sequences, with fine-grained sediments dominating (Figure 5-13). The top horizon (K4) of the S4 sequence displays a high amplitude, and can be tracked across large distances in the study area, which suggests that marine environments covered great distances during deposition of S4. The horizon is suggested to represent a flooding event, based on its high continuity, amplitude and horizontal extent (Veeken, 2007). Above S4 (post-S4, Figure 5-11), the reflections display ascending trajectories (Table 4-1), and is suggested to be a continuation of the depositional pattern from S3 and S4. The reflections are eventually truncated by the Upper Regional Unconformity (URU, Figure 5-11). The URU marks the boundary which separates glacial sediments from pre-glacial older sediments (Richardson et al., 1993).

As previously discussed, the seismic sequences show variations in reflection configurations, which is interpreted to reflect cyclic changes in the lithological properties. The cyclic pattern is characterized by firstly, fine-grained material (S0 and S1), subsequently underlain by sandy-material (S2), followed by fine-grained materials once again (S3 and S4). Similar cyclic stratigraphic successions of Barremian age has previously been observed on Spitsbergen (Steel et al., 2000). Such cycles were suggested to reflect changes in relative sea level during the time of deposition, where the accommodation space and sediment supply on the shelf varied. Based on the previous study done by Steel et al. (2000), it is likely that such cycles, as those suggested within this study, occur on a shelf over time.

Figure 5-12 shows the proposed cycles of transgressions and regressions. The overall discussed and suggested depositional regimes, dominating on the shelves for respectively the transgressions and regressions, is presented in Figure 5-13.

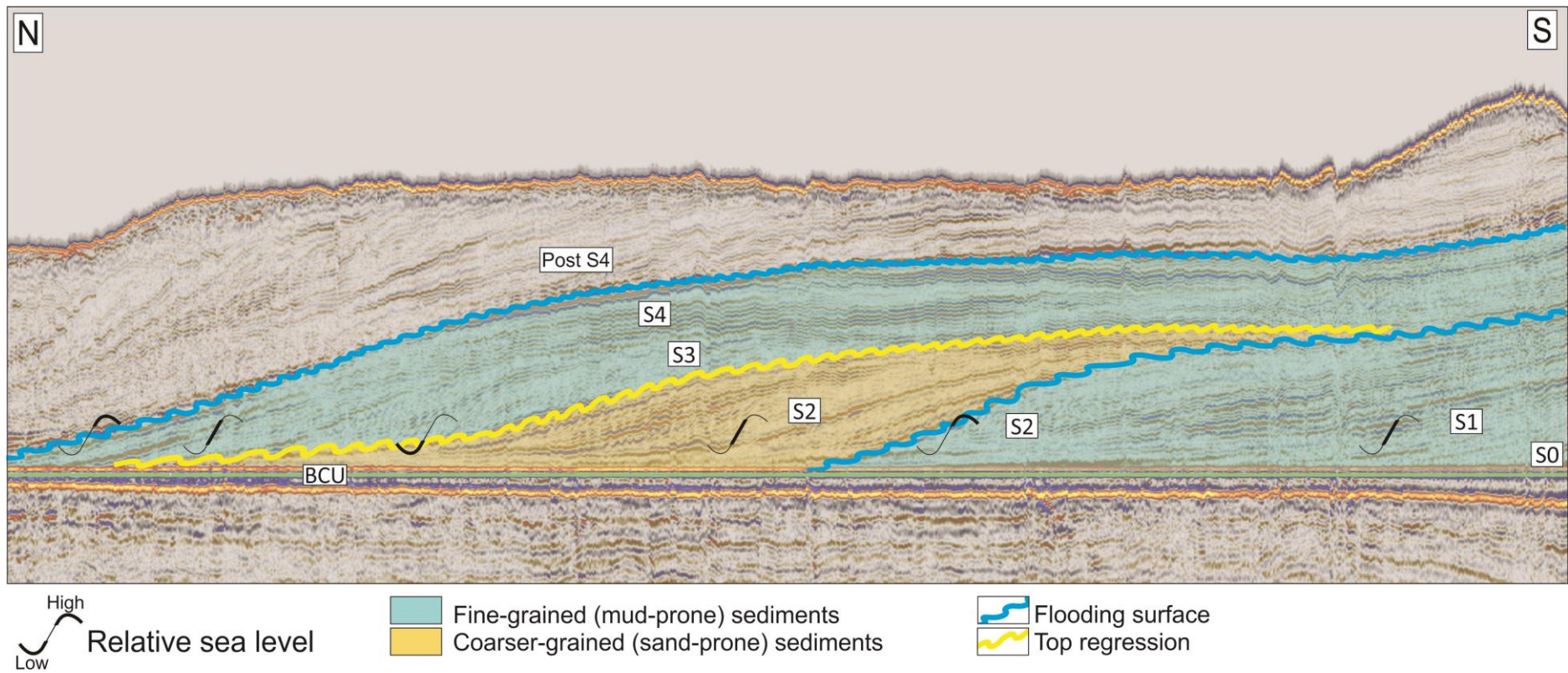


Figure 5-12. Overview of the interpreted cyclic variations in relative sea level for the S0-S4 sequences. S2 displays more sand-prone foresets, compared to the remaining mud-dominated sequences.

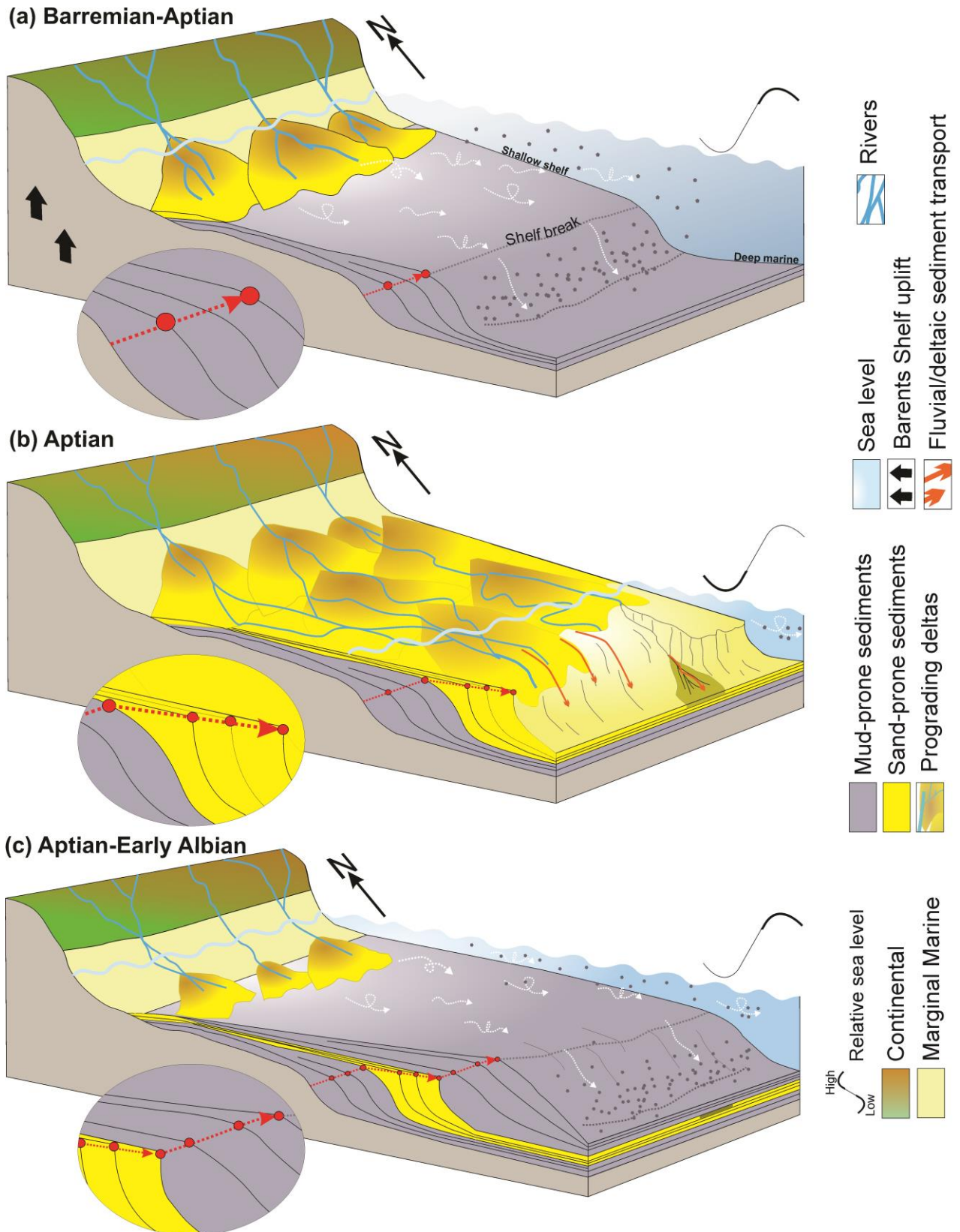


Figure 5-13. Conceptual model, showing the suggested depositional environments during deposition of a) S0 and S1 during Barremian-Aptian times, b) channelized slope during S2, Aptian, c) S3 and S4 during Aptian-Early Albian. Red arrows and circles in highlighted ellipse show the interpreted trajectories, respectively; a) ascending, b) flat, c) ascending. The internal geometries of the sequences are a) sigmoid, b) oblique, c) sigmoid. The white arrows indicate sediment transport from suspension. Note the sand-prone sediments in (b), in times of flat/descending trajectories.

5.3 Post-depositional processes

The following sections describes processes which have altered the sediments within the study area, after deposition.

5.3.1 Salt

Shelf-edge clinoforms in sequence 2, 3 and 4 are located adjacent to salt diapirs in the Nordkapp Basin (Figure 5-15). The Nordkapp Basin is known for active salt tectonics (Nilsen et al., 1995; Smelror et al., 2009). The salt was initially deposited during Late Carboniferous-Early Permian times (Nilsen et al., 1995), but have been locally mobilized several times (Smelror et al., 2009). Movement of salt bodies (halokinetic processes) is normally triggered by density differences between salt-layers and overlying sediments in the sub-surface, but may also occur as a response to tectonic events (Selley, 1997). The activation of salt movement within the Nordkapp Basin occurred in Triassic, and was triggered by basement-involved regional extension and normal faulting (Nilsen et al., 1995). Cretaceous sediments were subsequently deposited above the diapiric salt, and a new episode of halokinetic movement took place during the Late Cretaceous (Nilsen et al., 1995). The latter halokinetic movement was caused by a Late Cretaceous episode of regional extension (Nilsen et al., 1995).

The constant thickness of the S2, S3 and S4 on both sides of salt diapirs in the Nordkapp Basin, indicate that sedimentary wedges prograded and deposited without any influence from halokinetic movements (Figure 5-14). If salt diapirs had been active during deposition in Early Cretaceous, the seafloor reflector would be expected to appear as deformed in the seismic (Nilsen et al., 1995). This suggest that salt diapirs in the Nordkapp Basin were not active during deposition of the sequences. The observed salt bodies most likely intruded the Lower Cretaceous sediments (S2, S3 and S4) during the Late Cretaceous episode of regional extension (Figure 5-16) (Nilsen et al., 1995).

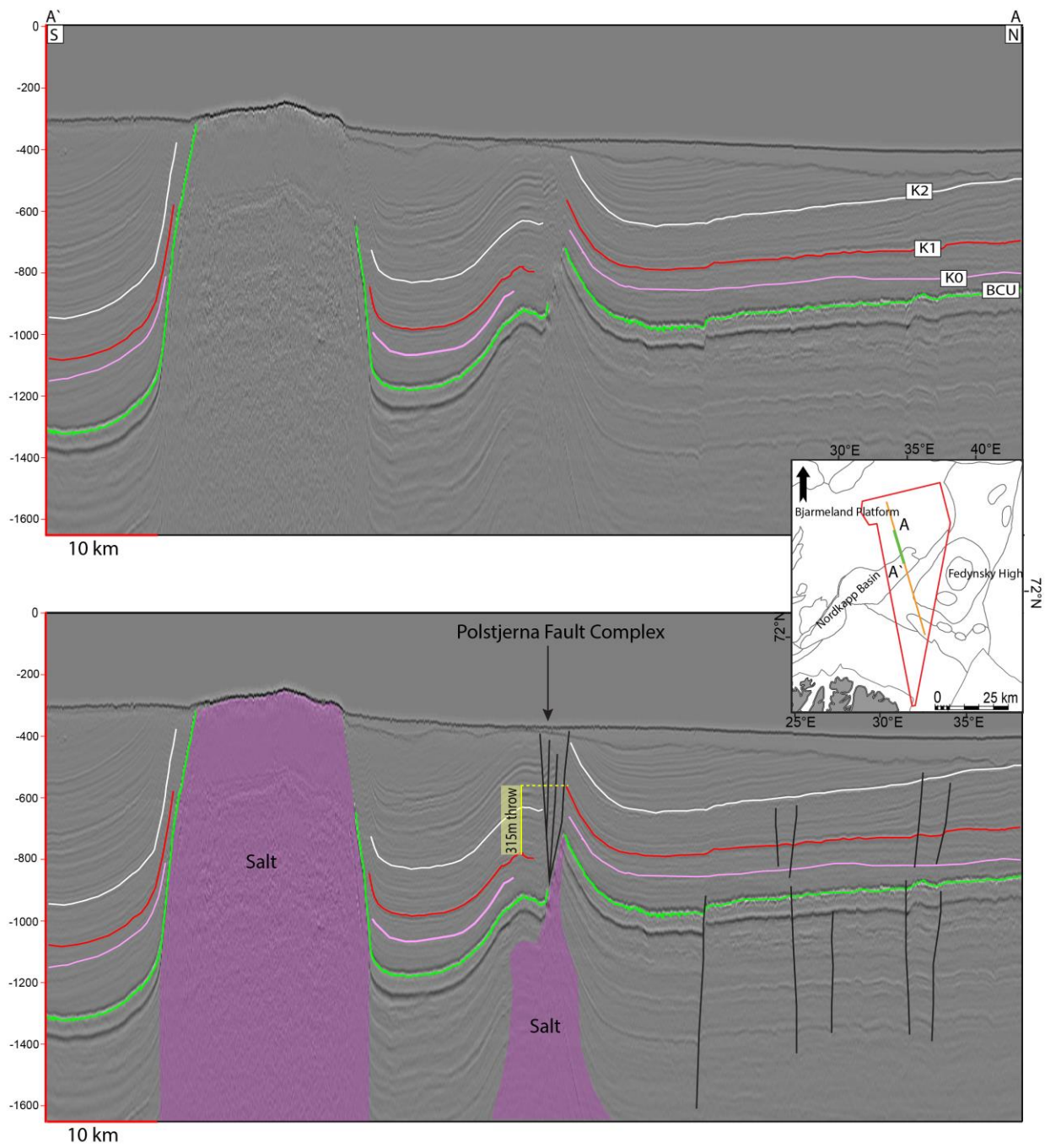


Figure 5-14. Black/white seismic section showing the Polstjerna Fault Complex along the northwestern margin of the Nordkapp Basin, and additionally smaller faults in the Cretaceous package above the BCU. The vertical throw of the K1 horizon is indicated in yellow. Black lines indicate faults.

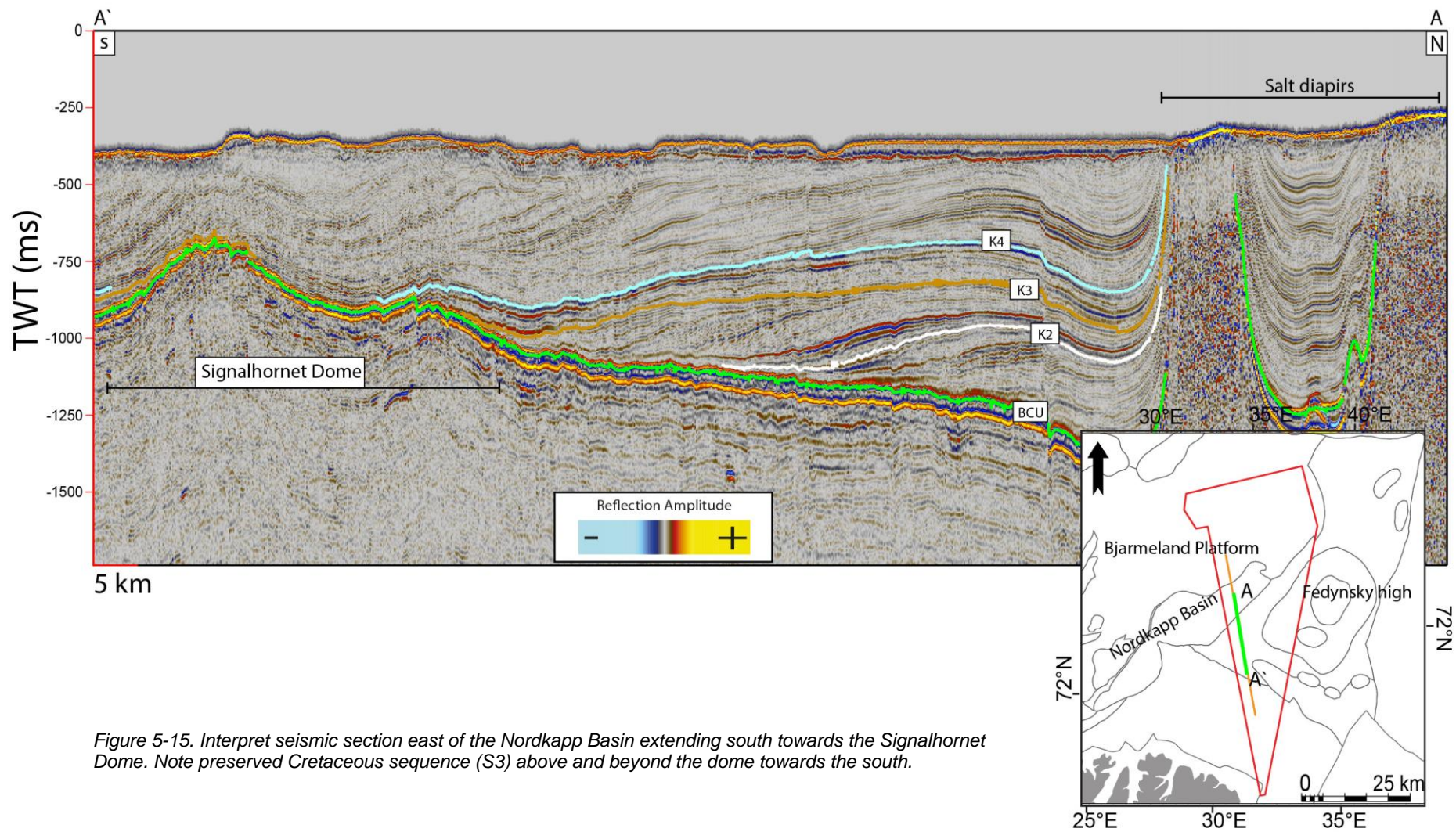


Figure 5-15. Interpret seismic section east of the Nordkapp Basin extending south towards the Signalhornet Dome. Note preserved Cretaceous sequence (S3) above and beyond the dome towards the south.

5.3.2 Signalhornet Dome

The Signalhornet Dome is a structural high located at the western and southwestern rim of the Tiddlybanken Basin (Figure 2-5a) (Mattingsdal et al., 2015). The structure is suggested to be salt-related and has a core formed by a salt pillow (Figure 5-16). The dome probably started to slightly develop in response to salt movement during Triassic and Late Cretaceous times, as for the Nordkapp Basin (Nilsen et al., 1995; Mattingsdal et al., 2015). The main doming was probably related to tectonic events in Paleogene. As seen from Figure 5-15, the sequence 3 and 4 reflections, which were deposited during Early Cretaceous, appears to be uplifted in today's seismic data. This indicates that the doming occurred after Early Cretaceous times. The shelf-edge clinoforms most likely prograded without any dome-structures present, which could if present, have altered the drainage pattern and sediment transport (Figure 5-15 and Figure 5-16).

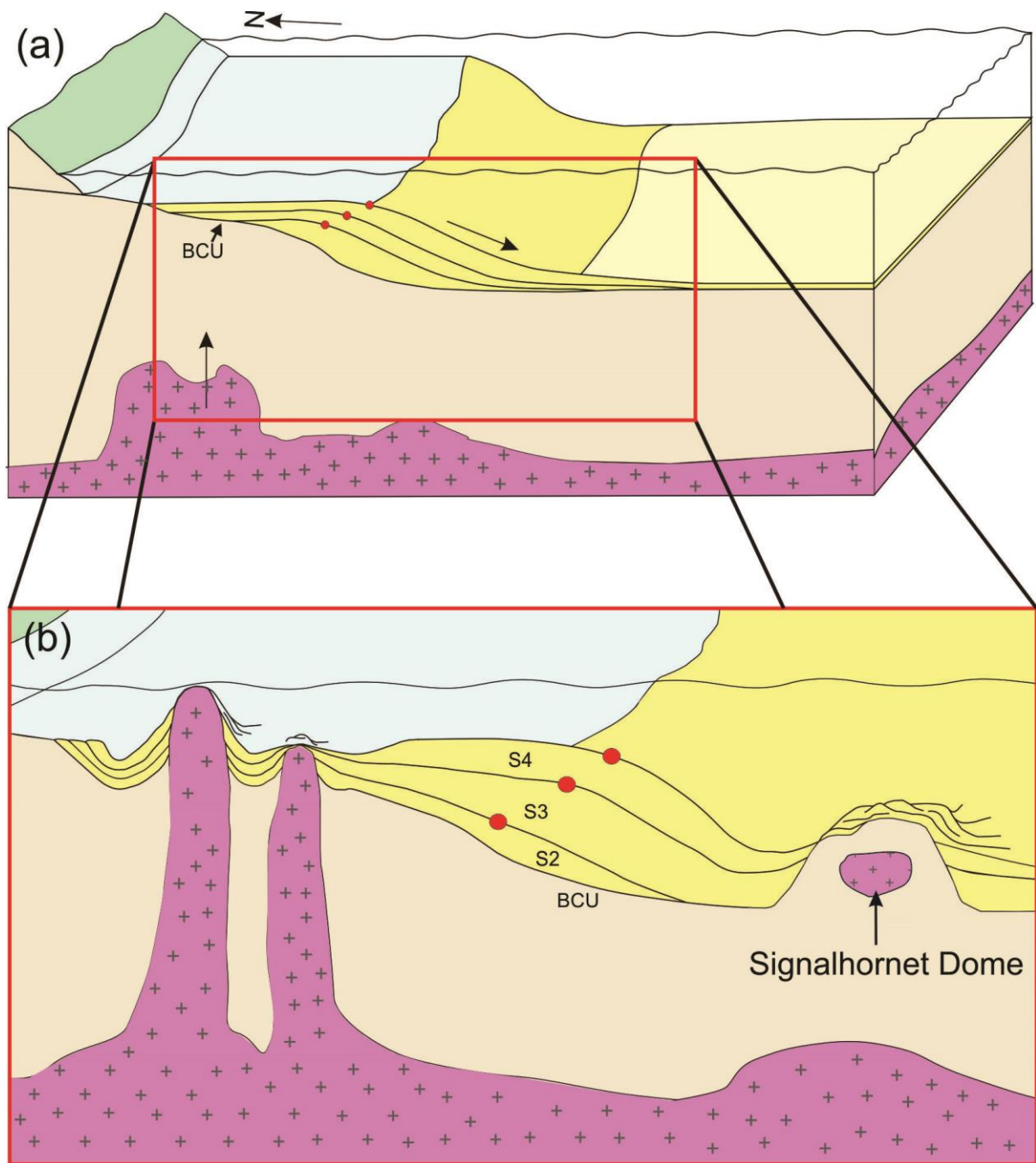


Figure 5-16. Suggested interpretation of a) Shelf-edge clinoforms prograding into deep-water, without any disturbance from salt diapirs or domes. b) Suggested interpretation showing preserved Cretaceous strata above salt diapirs in the Nordkapp Basin and above the Signalhornet Dome structure adjacent to the Tiddlybanken Basin.

5.3.3 Faults

Small-scale faults, which terminate near the BCU horizon, are recognized within the Cretaceous package (Figure 5-14). The small scale faults, may be related to halokinetic movements during the Cenozoic era, as suggested by Richardsen et al. (1993).

In addition, two major fault complexes; the Thor Iversen and the Polstjerna Fault Complexes, are identified respectively northeast and northwest of the Nordkapp Basin (Figure 2-5). These faults, cut vertically through both Cretaceous and underlying older sequences in the seismic sections. The Thor Iversen Fault Complex, is suggested to have formed in Early Carboniferous with reactivations during Mesozoic and Cenozoic times (Gabrielsen et al., 1990b). However, the vertical extent of Cretaceous sediments is equal on both sides of the two fault zones. This may indicate that fault activity prevailed after the sediments were deposited.

The Polstjerna Fault Complex occur along a smaller salt diapir along the northwestern margin of the Nordkapp Basin (Figure 5-14). Salt migration towards the fault complex is suggested to have played an important role in the development and reactivation of the fault zone (Mattingsdal et al., 2015). The observed vertical displacement of Cretaceous sequences along the Polstjerna Fault Complex shows a throw of approximately 315m, assuming a velocity of 3500m/s (Figure 5-14). The fault is suggested to have displaced the sediments during reactivation caused by halokinetic movements during Late Cretaceous (Mattingsdal et al., 2015).

In general, all the observed faults within the study area (both small-scale and Polstjerna/Thor Iversen Fault Complexes), is suggested to have influenced the area after deposition of the units discussed above. Hence, faults did not play an active role in controlling the sedimentary pattern of deposition along the shelves. By contrast, sedimentary shelves does not depend on tectonic processes other than requiring long-term accommodation provided by basin subsidence (Helland-Hansen et al., 2012). The identified shelves in this study are interpreted to represent sedimentary shelves.

6 Conclusions

Regional development of the Early Cretaceous in the southeastern Barents Sea:

- At the onset of the Cretaceous period, an ongoing regression, which began in the Late Jurassic, prevailed in the study area for a short period. This is suggested based on the steep, discontinuous reflections within the northern part of the S0 sequence.
- The uplift of the northern Barents Shelf during Early Barremian-Early Aptian has contributed to a southwestern progradation of the shelf break in the southeastern Barents Sea.
- The successive prograding shelf break during Early Cretaceous is represented by well defined shelf-edge clinoforms.
- The clinoforms identified within this study are characterized by mainly two types of foreset angles and geometries. 1) Sigmoid geometry, with gently dipping foresets which suggest mud-prone lithologies (S0, S1, S3, S4), 2) Oblique geometry with steeper dipping foresets, which could suggest sand-prone lithologies (S2).
- Cyclic variations in the suggested lithologies, may propose fluctuating sea level changes throughout the Early Cretaceous (Figure 5-12 and Figure 5-13).
- An overall transgression is suggested to have been in place during the Early Barremian to Aptian age (S0 and S1), where fine-grained sediments were transported from suspension to the shelf break and accumulated on the shelf slope. The end of the first transgressional event was identified as a flooding surface.
- The transgression was followed by a smaller regression (S2) during the Aptian, which indicates a relative fall in sea level, where sandy sediments deposited out to and beyond the shelf break. The sandy sediments may have reached out to the shelf break by prograding deltas and fluvial systems.
- Lastly, a new transgressive period prevailed (S3 and S4), where fine grained sediments dominated in the study area.
- The S2, S3 and S4 clinoforms showed an increase in thickness, which is suggested to have been caused either by subsidence within the Nordkapp Basin, or deposition into deeper marine environments where more accommodation space was available.

Post-depositional processes affecting the Lower Cretaceous sequences in the southeastern Barents Sea:

- Doming processes, which formed the Veslekari and Signalthornet Domes, along with diapiric growth of salt bodies, is proposed to have occurred during post-depositional times, of the Late Cretaceous and Paleogene.
- Two major fault complexes, respectively the Polstjerna and Thor Iversen, is suggested to have formed in pre-Cretaceous times, with reactivation in the Late Cretaceous, but after deposition of the S0-S4 sequences.
- Smaller-scale faults were additionally identified within the dataset. Both the larger- and smaller fault complexes were probably caused as a response to salt movement in Late Cretaceous.

7 References

- Artyushkov, E. V., Belyaev, I. V., Kazanin, G. S., Pavlov, S. P., Chekhovich, P. A., & Shkarubo, S. I. (2014). Formation mechanisms of ultradeep sedimentary basins: the North Barents basin. Petroleum potential implications. *Russian Geology and Geophysics*, 55(5), 649-667. doi:<https://doi.org/10.1016/j.rgg.2014.05.009>
- Brown, A. R. (1999). *Interpretation of three-dimensional seismic data* (5th ed. ed. Vol. 42). Tulsa, Okla: American Association of Petroleum Geologists.
- Brønner, M., Gernigon, L., Pascal, C., Koziel, J., & Marello, L. (2009). *Barents Sea Aeromagnetic Remapping 2009 Acquisition and processing report and preliminary interpretation of the SW Barents Sea*. Retrieved from
- Bugge, T., Elvebakk, G., Fanavoll, S., Mangerud, G., Smelror, M., Weiss, H. M., . . . Nilsen, K. (2002). Shallow stratigraphic drilling applied in hydrocarbon exploration of the Nordkapp Basin, Barents Sea
- Catuneanu, O. (2006). *Principles of Sequence Stratigraphy*: Elsevier Science.
- Catuneanu, O., Abreu, V., Bhattacharya, J. P., Blum, M. D., Dalrymple, R. W., Eriksson, P. G., . . . Winker, C. (2008). Towards the standardization of sequence stratigraphy. *Earth-Science Reviews*, 92(1), 1-33. doi:<https://doi.org/10.1016/j.earscirev.2008.10.003>
- Cita, M. B., & Aghib, F. S. (1991). Evidence of relief inversion from the rim-syncline of Bannock Basin. *Marine Geology*, 100(1), 67-81. doi:[https://doi.org/10.1016/0025-3227\(91\)90225-S](https://doi.org/10.1016/0025-3227(91)90225-S)
- Coe, A. L., Bosence, D. W. J., Church, K. D., Flint, S. S., Howell, J. A., & Wilson, C. L. (2003). The Sedimentary Record of Sea-Level Change In (pp. 288).
- Corfu, F., Polteau, S., Planke, S., Faleide, J. I., Svensen, H., Zayoncheck, A., & Stolbov, N. (2013). U–Pb geochronology of Cretaceous magmatism on Svalbard and Franz Josef Land, Barents Sea Large Igneous Province. *Geological Magazine, Cambridge University Press*, 150(6), 1127-1135. doi:<https://doi.org/10.1017/S0016756813000162>
- Dalland, A., Worsley, D., & Ofstad, K. (1988). A lithostratigraphic scheme for the Mesozoic and Cenozoic suvversion offshore mid- and northern Norway 254 *Bulletin 4*.
- Dorè, A. G. (1995). Barents Sea Geology, Petroleum Resources and Commercial Potential. *Arctic*, 48(3), 207-221.
- Ehrenberg, S. N., Nielsen, E. B., Svånå, T. A., Stemmerik, L., & (1998). Depositional evolution of the Finnmark carbonate platform, Barents Sea: .results from wells 7128/6-1 and 7128/4-1 *Norsk Geologisk Tidsskrift*, 78, 185-224.
- Faleide, J. I., Bjørlykke, K., & Gabrielsen, R. H. (2015). *Geology of the Norwegian Continental Shelf*: Springer, Berlin, Heidelberg.
- Faleide, J. I., Gudlaugsson, S. T., & Jacquart, G. (1984). Evolution of the western Barents Sea. *Marine and Petroleum Geology*, 1, 123-150.
- Faleide, J. I., Solheim, A., Fiedler, A., Hjelstuen, B. O., Andersen, E. S., & Vanneste, K. (1996). Late Cenozoic evolution of the western Barents Sea-Svalbard continental margin. *Global and Planetary Change*, 12(1-4), 53-74.
- Gabrielsen, R. H., Færseth, R. B., Jensen, L. N., Kalheim, J. E., & Riis, F. (1990a). NPD-BULLETIN NO 6
- Gabrielsen, R. H., Færseth, R. B., Jensen, L. N., Kalheim, J. E., & Riis, F. (1990b). Structural Elements of the Norwegian continental shelf, Part 1: The Barents Sea Region. *NPD-Bulletin no 6*.
- Gabrielsen, R. H., Rasmussen, K. A., & Stølan, T. (1992). Interaction between halokinesis and faulting: structuring of the margins of the Nordkapp Basin, Barents Sea region In B. T. Larsen & E. Talleraas (Eds.), (Vol. Norwegian Petroleum Society (NPF) 1992, pp. 121-131): Elsevier, Amsterdam.
- Gee, D., G., & Pease, V. (2004). The Neoproterozoic Timanide Orogen of eastern Baltica: Introduction *Geological Society, London*, 1-3. doi: <https://doi.org/10.1144/GSL.MEM.2004.030.01.01>
- Geldand, I. M., & Saul, M. (2001). Trigonometry

- Gernigon, L., Brönnert, M., Roberts, D., Olesen, O., Nasuti, A., & Yamasaki, T. (2014). Crustal and basin evolution of the southwestern Barents Sea: From Caledonian orogeny to continental breakup. *AGU Publications: Tectonics*, 33(4), 347-373. doi:10.1002/2013TC003439
- Glørstad-Clark, E., Faleide, J. I., Lundschiene, B. A., & Nystuen, J. P. (2010). Triassic seismic sequence stratigraphy and paleogeography of the western Barents Sea area. *Marine and Petroleum Geology*, 27(7), 1448-1475. doi:10.1016/j.marpetgeo.2010.02.008
- Grundvåg, S. A., Marin, D., Kairanov, B., Śliwińska, K. K., Nøhr-Hansen, H., Jelby, M. E., . . . Olausson, S. (2017). The Lower Cretaceous succession of the northwestern Barents Shelf: Onshore and offshore correlations. *Marine and Petroleum Geology*, 86, 834-857. doi:<https://doi.org/10.1016/j.marpetgeo.2017.06.036>
- Helland-Hansen, W., & Hampson, G. J. (2009). Trajectory analysis: concepts and applications *Basin Research*, 21, 454-483. doi:10.1111/j.3656-2117.2009.00425.x
- Helland-Hansen, W., Steel, R. J., & Sømme, T. O. (2012). Shelf genesis revisited. *Journal of Sedimentary Research*, 82(3), 133-148. doi:10.2110/jsr.2012.15
- Henriksen, E., Ryseth, A. E., Larssen, G. B., Heide, T., Rønning, K., Sollid, K., & Stoupakova, A. V. (2011). Chapter 10 Tectonostratigraphy of the greater Barents Sea: implications for petroleum systems. *Geological Society, London, Memoirs*, 35(1), 163-195. doi:10.1144/m35.10
- Johannessen, E. P., & Steel, R. J. (2005). Shelf-margin clinoforms and prediction of deepwater sands. *Basin Research*, 521-550. doi:10.1111/j. 1336-2117-2005-00278.x
- Johansen, S. E., Ostistiy, B. K., Birkeland, Ø., Fedorovsky, Y. F., V.N, M., Bruun Christensen, O., . . . Margulis, L. S. (1992). Hydrocarbon potential in the Barents Sea region: play distribution and potential In T. Vorren, E. Bergsager, Ø. A. Dahl-Stamnes, E. Holter, B. Johansen, E. Lie, & T. B. Lund (Eds.), *Arctic Geology and Petroleum Potential* Elsevier Science Publishers B.V
- Kairanov, B., Escalona, A., Mordasova, A., Śliwińska, K., & Suslova, A. (2018). Lower Cretaceous tectonostratigraphic evolution of the northcentral Barents Sea. *Journal of Geodynamics*. doi:<https://doi.org/10.1016/j.jog.2018.02.009>
- Kearey, P., Brooks, M., & Hill, I. (2002). *An Introduction to Geophysical Exploration* (Third Edition ed.): Blackwell Science Ltd.
- Klitzke, P., Faleide, J. I., Scheck-Wenderoth, M., & Sippel, J. (2014). A lithosphere-scale structural model of the Barents Sea and Kara Sea region. *Solid earth discussions*, 6, 1579-1624. doi:10.5194/se-6-153-2015
- Larssen, G. B., Elvebakk, G., Henriksen, L. B., Kristensen, S.-E., Nillson, I., Samuelsen, T. J., . . . Worsley, D. (2002). Upper Palaeozoic lithostratigraphy of the Southern Norwegian Barents Sea 77.
- Maher, H. D. (2001). Manifestations of the Cretaceous High Arctic Large Igneous Province in Svalbard.
- Marin, D., Alejandro, E., Śliwińska, K. K., Nøhr-Hansen, H., & Mordasova, A. (2016). Sequence stratigraphy and lateral variability of Lower Cretaceous clinoforms in the southwestern Barents Sea *The American Association of Petroleum Geologist*, 1487-1517.
- Mattingsdal, R., Høy, T., Simonstad, E., & Brekke, H. (2015). An updated map of structural elements in the southern Barents Sea. ----.
- Mitchum, R. M., Vail, P. R., & Sangree, J. B. (1977). Seismic Stratigraphy and Global Changes of Sea Level: Part 6. Stratigraphic Interpretation of Seismic Reflection Patterns in Depositional Sequences: Section 2. Application of Seismic Reflection Configuration to Stratigraphic Interpretation. In *Seismic Stratigraphy--Applications to Hydrocarbon Exploration* (pp. 117-133).
- Nejbert, K., Krajewski, K. P., Dubinska, E., & Pécskay, Z. (2011). Dolerites of Svalbard, north-west Barents Sea Shelf: age, tectonic setting and significance for geotectonic interpretation of the High-Arctic Large Igneous Province. *Polar Research*, 30(1), 7306. doi:10.3402/polar.v30i0.7306
- Nichols, G. (2009). *Sedimentology and Stratigraphy - second edition* Wiley -Blackwell
- Nilsen, K. T., Johansen, J. T., & Vendeville, B. C. (1995). Influence of Regional Tectonics on Halokinesis in the Nordkapp Basin, Barents Sea. *AAPG Memoir, Journal Issue 65* 413-436.

- NPD. (2011). Factpages NPD Retrieved from <http://factpages.npd.no/factpages/Default.aspx?culture=en&nav1=survey>
- NPD. (2013). Barents Sea South-East. Retrieved from <http://www.npd.no/en/Publications/Resource-Reports/2013/Chapter-6/>
- NPD. (2014a). The 2014 NPD lithostratigraphic charts.
- NPD. (2014b). Compiled CO₂ atlas for the Norwegian Continental Shelf
- O'Grady, D. B., Syvitski, J. P. M., Pratson, L. F., & Sarg, J. F. (2000). Categorizing the morphologic variability of siliciclastic passive continental margins. *Geology*, 28(3), 207-210. doi:10.1130/0091-7613(2000)28<207:CTMVOS>2.0.CO;2
- Petrov, O. V., Sobolev, N. N., Koren, T. N., Vasiliev, V. E., Petrov, E. O., Larssen, G. B., & Smelror, M. (2008). Palaeozoic and Early Mesozoic evolution of the East Barents and Kara Seas sedimentary basins. *Norwegian Journal of Geology*, 88, 227-234.
- Polteau, S., Hendriks, B. W. H., Planke, S., Ganerød, M., Corfu, F., Faleide, J. I., . . . Myklebust, R. (2015). The Early Cretaceous Barents Sea Sill Complex: Distribution, 40Ar/39Ar geochronology, and implications for carbon gas *Palaeogeography, Palaeoclimatology, Palaeoecology*, 441, 83-95.
- Ramberg, I. B., Bryhni, I., Arvid, N., & Kristin, R. (2008). *The Making of a Land - Geology Of Norway*
- Reynolds, J. M. (2011). *An Introduction to Applied and Environmental Geophysics* John Wiley & Sons, Ltd
- Rich, J. L. (1951). THREE CRITICAL ENVIRONMENTS OF DEPOSITION, AND CRITERIA FOR RECOGNITION OF ROCKS DEPOSITED IN EACH OF THEM. *GSA Bulletin*, 62(1), 1-20. doi:10.1130/0016-7606(1951)62[1:TCEODA]2.0.CO;2
- Richardson, G., Vorren, T. O., & Torudbankken, B. O. (1993). Post-Early Cretaceous uplift and erosion in the southern Barents Sea: A discussion based on analysis of seismic interval velocities *Norsk Geologisk Tidsskrift*, 73, 3-20.
- Ripington, S., Poujardieu, R., Liszczyk, A.-M., & Dyer, N. (2015). Regional Structure of the Southeast Barents Sea - Applying FTG to Exploration Challenges in Frontier Areas. doi:10.3997/2214-4609.201413284
- Ritzmann, O., & Faleide, J. I. (2007). Caledonian basement of the western Barents Sea. *Tectonics*, 26(5). doi:10.1029/2006TC002059
- Ritzmann, O., & Faleide, J. I. (2009). The crust and mantle lithosphere in the Barents Sea/Kara Sea region. 470, 89-104. doi:<https://doi.org/10.1016/j.tecto.2008.06.018>
- Ryseth, A. (2014). Sedimentation at the Jurassic–Triassic boundary, south-west Barents Sea: indication of climate change. *Int. Assoc. Sedimentol. Spec. Publ*, 187-214.
- Rønnevik, H., Beskow, B., & Jacobsen, H. P. (1982). Structural and Stratigraphic Evolution of the Barents Sea *Arctic Geology and Geophysics: Proceedings of the Thrid International Symposium on Arctic Geology - Memoir* 8, 431-440.
- Schuck, A., & Lange, G. (2007). Seismic Methods. In: *Environmental Geology*. 337-402. doi:https://doi.org/10.1007/978-3-540-74671-3_11
- Selley, R. C. (1997). *Elements of Petroleum Geology* (Second edition ed.): Academic Press
- Sheriff, R. E. (1985). Aspects of Seismic Resolution: Chapter 1. In *Seismic Stratigraphy II: An Integrated Approach to Hydrocarbon Exploration* (pp. 1-10): AAPG.
- Smelror, M., Petrov, O. V., Larssen, G. B., & Werner, S. C. (2009). *Geological History of the Barents Sea*. Trondheim: Geological Survey of Norway.
- Steel, R. J., Mellere, D., Plink-Bjorklund, P., Deibert, J., & Loeseth, T. (2000). Deltas vs. Rivers on the Shelf Edge: Their Relative Contributions to the Growth of Shelf-Margins and Basin-Floor Fans (Barremian and Eocene, Spitsbergen). doi:10.5724/gcs.00.15.0981
- Steel, R. J., & Olsen, T. (2002). Clinoforms, Clinoform Trajectories and Deepwater Sands. *ResearchGate*. doi:10.5724/gcs.02.22.0367
- Vail, P. R. (1987). Seismic stratigraphy interpretation using sequence stratigraphy. In A. W. Bally (Ed.), *Atlas of Seismic Stratigraphy: AAPG Studies in Geology* (Vol. 1, pp. 1-10).

- Veeken, P. C. H. (2007). *Seismic stratigraphy, basin analysis and reservoir characterisation* (Vol. 37): Elsevier
- Vorren, T. O., Richardsen, G., Knutsen, S. M., & Henriksen, E. (1991). Cenozoic erosion and sedimentation in the western Barents Sea. *Marine and Petroleum Geology*, 8, 317-340.
- Worsley, D. (2008). The post-Caledonian development of Svalbard and the western Barents Sea. *Polar Research*, 27(3), 298-317.